SAND REPORT
SAND2001-2950
Unlimited Release
Printed September 2001

Useful Equations for Calculating the Induced Voltage Inside a Faraday Cage that has been Struck by Lightning

Roy E. Jorgenson and Larry K. Warne

Prepared by
Sandia National Laboratories
Albuquerque, New Mexico 87185 and Livermore, California 94550

Sandia is a multiprogram laboratory operated by Sandia Corporation, a Lockheed Martin Company, for the United States Department of Energy under Contract DE-AC04-94AL85000.

Sandia National Laboratories

Issued by Sandia National Laboratories, operated for the United States Department of Energy by Sandia Corporation.

Available to DOE and DOE contractors from
U.S. Department of Energy
Office of Scientific and Technical Information
P.O. Box 62
Oak Ridge, TN 37831

Telephone: (865)576-8401
Facsimile: (865)576-5728
E-Mail: reports@adonis.osti.gov
Online ordering: http://www.doe.gov/bridge

Available to the public from
U.S. Department of Commerce
National Technical Information Service
5285 Port Royal Rd
Springfield, VA 22161

Telephone: (800)553-6847
Facsimile: (703)605-6900
E-Mail: orders@ntis.fedworld.gov
Online order: http://www.ntis.gov/ordering.htm

SAND2001-2950
Unlimited Release
Printed September 2001

Useful Equations for Calculating the Induced Voltage Inside a Faraday Cage that has been Struck by Lightning

Roy E. Jorgenson and Larry K. Warne
Electromagnetics and Plasma Physics Analysis Dept.
Sandia National Laboratories
P. O. Box 5800
Albuquerque, NM 87185-1152

Abstract

One of the tasks performed routinely by the Electromagnetics and Plasma Physics Analysis Department at Sandia National Laboratories is analyzing the effects of direct-strike lightning on Faraday cages that protect sensitive items. The Faraday cages analyzed thus far have many features in common. This report is an attempt to collect equations and other information that have been routinely used in the past in order to facilitate future analysis.

Intentionally Left Blank

Contents

Figures

Useful Equations for Calculating the Induced Voltage Inside a Faraday Cage that has been Struck by Lightning

1 Introduction

This report contains a collection of equations and other information used to analyze the protection provided by a Faraday cage against the effects of worst-case, direct-strike lightning. There are three characteristics of the lightning waveform that are of importance in the analysis: the peak current, the maximum rate of current rise and the continuing current. Worst-case lightning (one percentile) has a peak current (I) of 200 kA, a maximum rate of current rise ($\partial I/\partial t$) of 400 kA/μs and a continuing current of 800 A that lasts for 0.5 seconds [1].

The Faraday cages that we have analyzed do not consist of a continuous metallic shell surrounding sensitive contents. Rather, they consist of separate, individual metal pieces that are attached to one another in some manner to enclose the contents. One example of a Faraday cage is shown in Figure 1. The sensitive contents are placed on a metal platform and a metal cover is placed over them. The cover is attached to the platform by bolts that pass through a flange welded to the cover's bottom. In the Faraday cage example shown in Figure 2, the contents are placed inside an open metal can, which is then covered by a metal lid. In the third example, shown in Figure 3, for ease of handling, the metal cover from the first example is made of two halves that are attached to each other in some manner. Instead of using bolts to hold the cover to the platform, metal pieces that rotate over the flange are used. The Faraday cages that we have observed usually have a mechanism that indicates if the cage has content, or if it is empty. This mechanism could be as simple as the viewing port, shown in Figure 1, or could be more complex, like the plunger shown in Figure 2. (The contents push the plunger so that it protrudes from the top of the Faraday cage, indicating that something is inside.)

When designing a Faraday cage to protect sensitive contents, the presence of any metallic penetration that is surrounded by insulation as it passes through the wall of the Faraday cage, is strongly discouraged for the following reason. Lightning could attach to the metallic penetration and drive a high current through the Faraday cage onto the contents until the voltage on the penetration becomes so high that breakdown occurs across the surrounding insulation to the cage. The high current and subsequent high voltage on sensitive contents is a situation that must be avoided. Therefore, as an example, we must ensure that the plunger shown in Figure 2 is an insulator and not made of metal. Once metallic penetrations have been eliminated from the design, the possibility of lightning penetrating the Faraday cage directly is not of concern. Voltages due to lightning can still be induced inside the Faraday cage, however, if conductor loops inside link magnetic flux, which penetrates the cage through its various joints and apertures. The derivative of linked magnetic flux with respect to time causes a voltage to develop between various conductors within the cage. In the following sections we will find expressions for this voltage due to different types of apertures. Determining the inside voltage is a necessary step in determining if the contents are protected sufficiently by the Faraday cage.

2 Long Slots

2.1 PEC Walls

One type of aperture commonly found in a Faraday cage, particularly where the various metal pieces

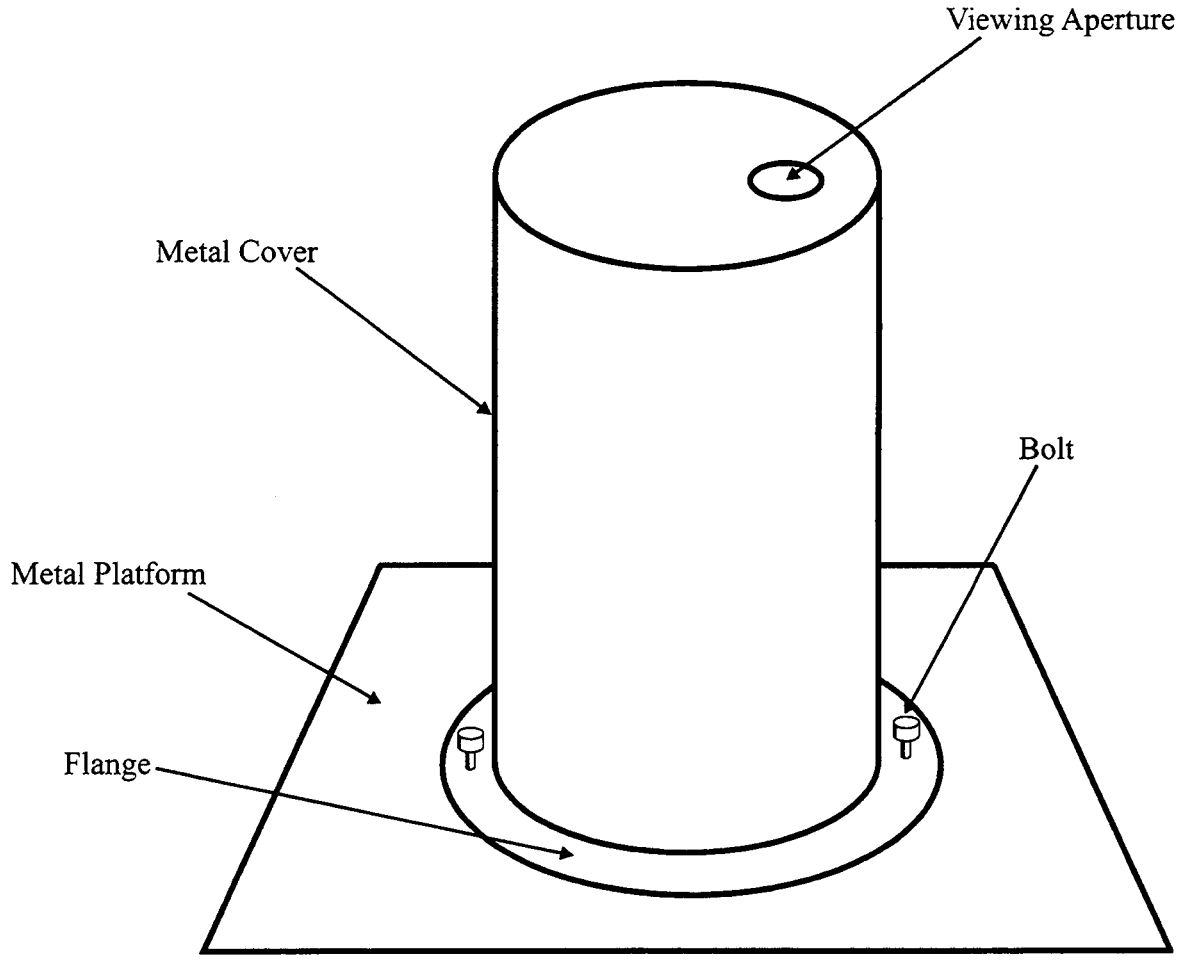

Figure 1. Example Faraday Cage

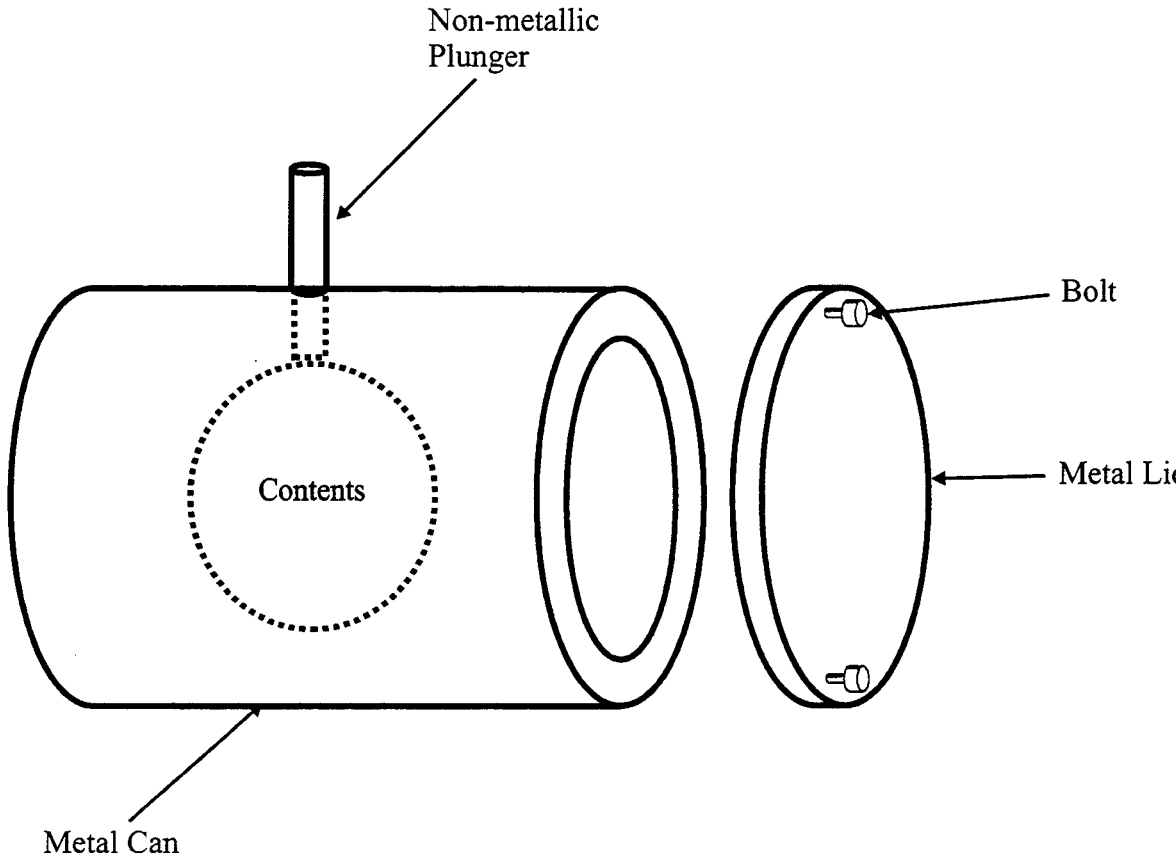

Figure 2. Example Faraday Cage

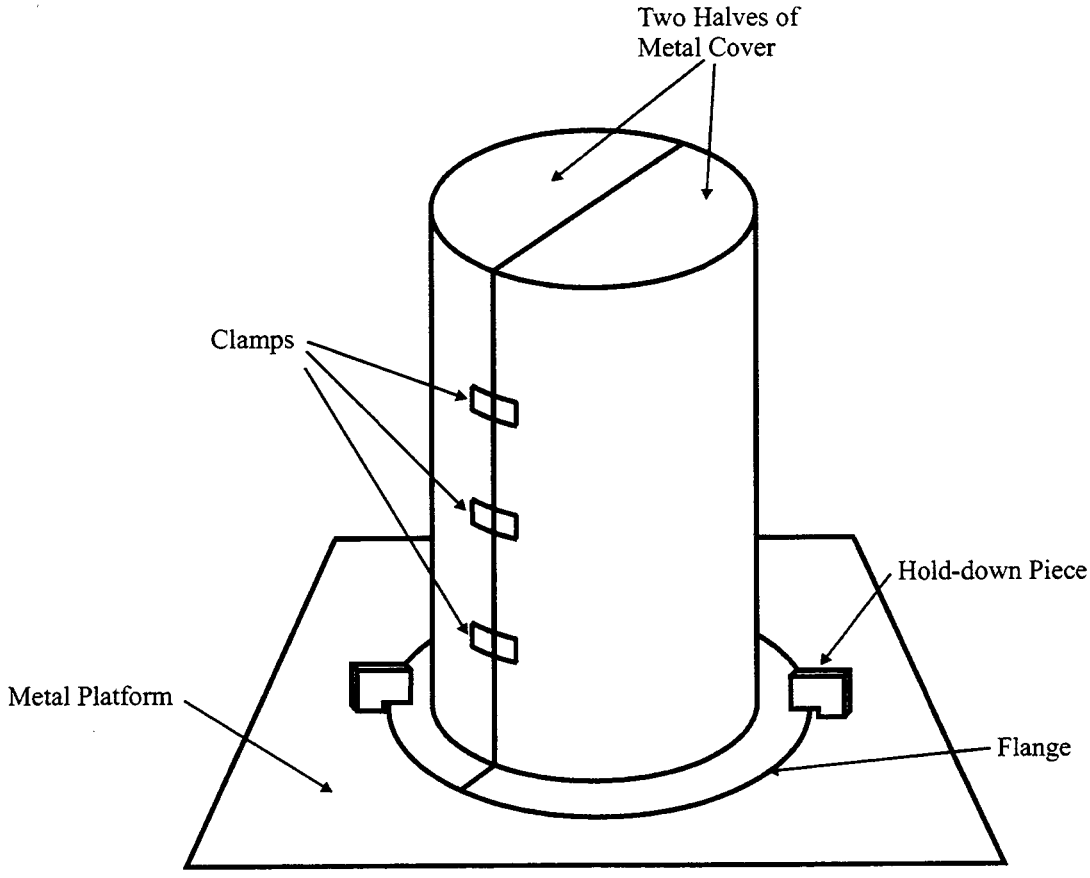

Figure 3. Example Faraday Cage

that make up the cage attach to one another, is a long slot, an example of which is the bolted joint shown in Figure 4. The physical characteristics of the slot are its length ($2h$), which in a bolted joint is the bolt-to-bolt spacing, its depth (d), and its width (w), which is usually caused by imperfections in mating between the two surfaces of the joint. For the following analysis to hold, the length of the slot must be large compared to its depth and (for the finitely-conducting wall and conducting gasket cases) the width must be small compared to its depth. Initially, we assume that the walls of the slot are perfect conductors, that there is no gasket material in the slot and that the bolts at the end of the slot have a negligible inductance (so the voltage across them is zero – they can be modeled as short-circuits). As a worst-case we assume that lightning current attaches to one side of the slot, centered between the two terminating bolts and the return is on the opposite side of the slot. Also as a worst-case, we do not allow breakdown to occur across the slot, which would clamp the maximum voltage available to be the voltage at which the breakdown occurs.

First let us look at Figures 5 and 6 to understand what is happening physically. As the current divides and flows along the top of the slot, through the bolts and back along the bottom of the slot, it generates a magnetic field in accordance with a right-hand rule as shown in Figure 5. Note that in the figure the magnetic field flows into the right half of the slot and out the left half. Figure 6 shows a top view of the slot and magnetic field. If we think of the slot itself as a conducting loop, as we increase the area of the loop by moving our observation point from the right-hand wall toward the slot center, we will increase the amount of magnetic flux that we intercept and, therefore, increase the voltage seen across the slot. This trend continues until we reach the center of the slot; then, as we continue increasing the area of the loop, moving past the center toward the left-hand wall, we begin to intercept magnetic flux flowing out of the slot, decreasing the net flux flowing across the loop surface. This causes the voltage seen across the slot to decrease until it reaches zero at the left-hand wall (the net flux flowing across the entire slot is zero). Thus, the voltage at the center of the slot is the maximum voltage seen along the length of the slot. It is also the maximum voltage seen inside the Faraday cage due to flux entering this particular slot. Since the loop formed by half the slot intercepts all of the flux flowing through it, a single-turn conducting loop, like the one shown in Figure 6, can generate the same maximum voltage as the slot (if it intercepts all of the flux), but will never exceed it. Thus, we can use the maximum slot voltage as an upper voltage bound of the Faraday cage.

The slot can be modeled in terms of an inductance per unit length, which is the parallel combination of the gap inductance per unit length L_{gap} and the external inductance per unit length L_{extr} [3, 4]. These quantities are expressed in terms of the physical slot parameters as

$$L_{gap} = \mu_0 \frac{w}{d} \tag{1}$$

$$L_{extr} = \mu_0 \frac{\pi}{\Omega_0} \tag{2}$$

where

$$\Omega_0 = 2\ln\left(\frac{8h}{w}\right) + 2\left(\ln 2 - \frac{7}{3}\right)$$

is the antenna fatness parameter, and μ_0 is the permeability of free space ($4\pi \times 10^{-7}$ H/m). The total inductance per unit length is

$$L_{tot} = \frac{L_{gap} L_{extr}}{L_{gap} + L_{extr}} \tag{3}$$

which leads to the simplified transmission line model of the slot shown in Figure 7 (Δ represents a small distance along the transmission line). The standard transmission line model could be simplified by neglecting the distributed capacitance and using a lumped circuit approximation since the lightning waveform has such low frequency content (see Appendix A for more details). An observer at the center of the slot would see two inductances $L_{tot}h$ in parallel, or a total slot inductance of

$$L_{slot} = \frac{1}{2} L_{tot} h \tag{4}$$

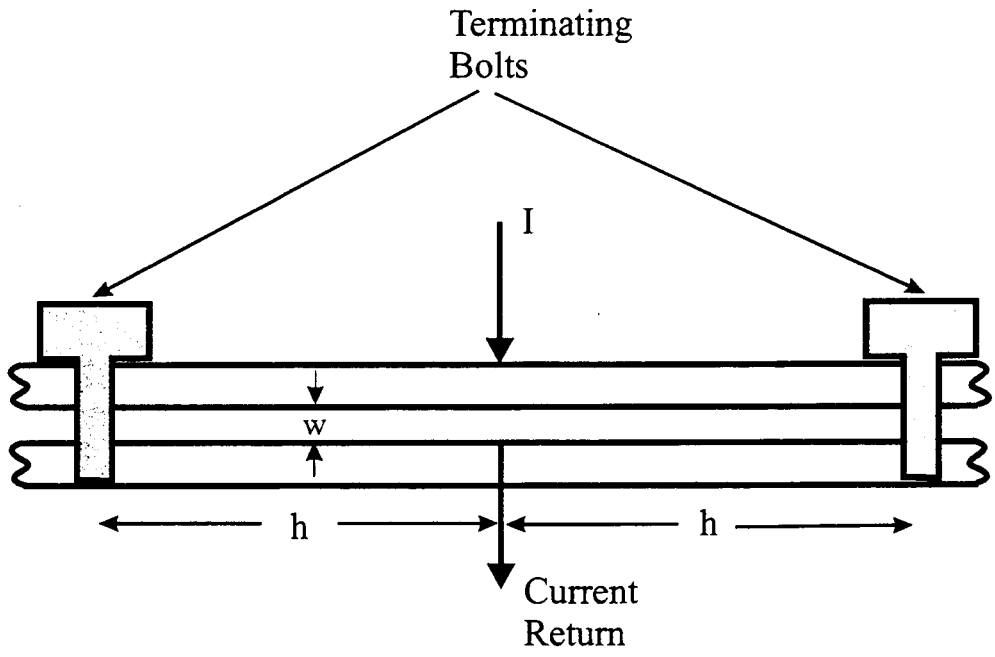

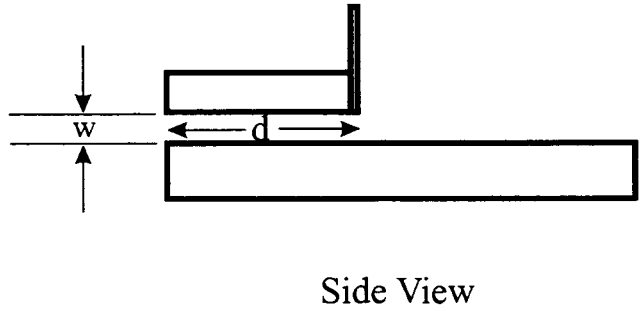

Figure 4. Characteristics of Slot Formed by Bolted Joints

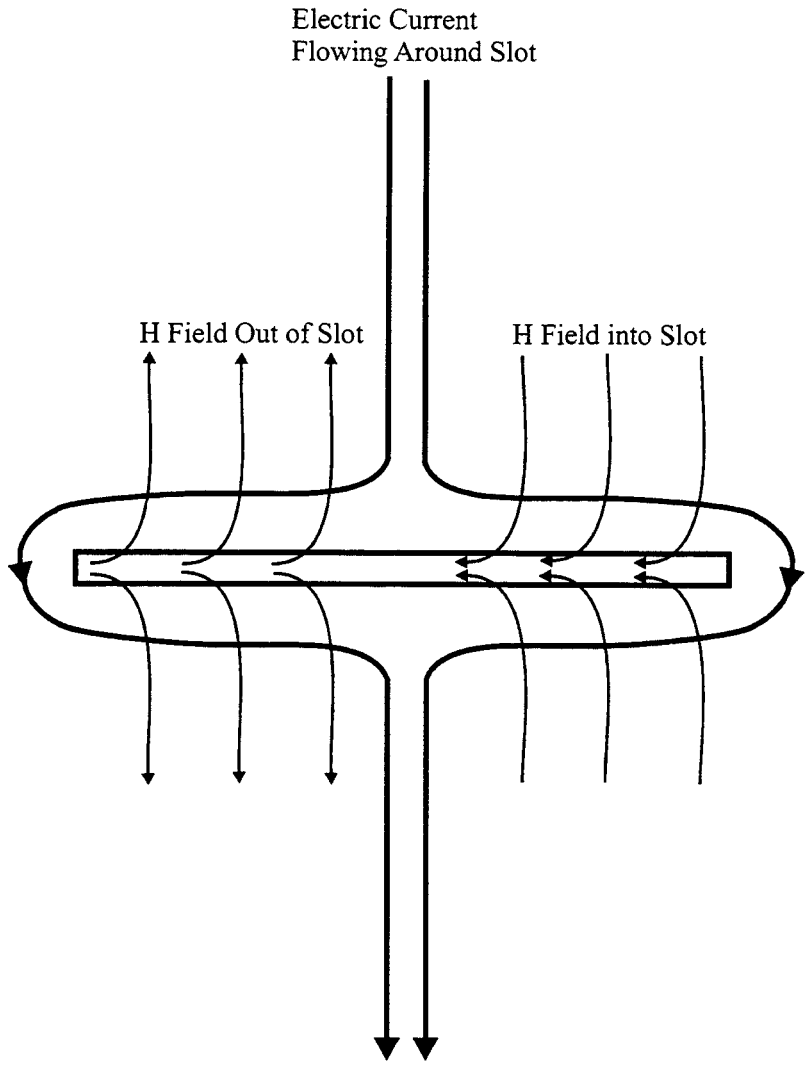

Figure 5. Physical Picture of H Field Entering and Leaving the Slot (Front View)

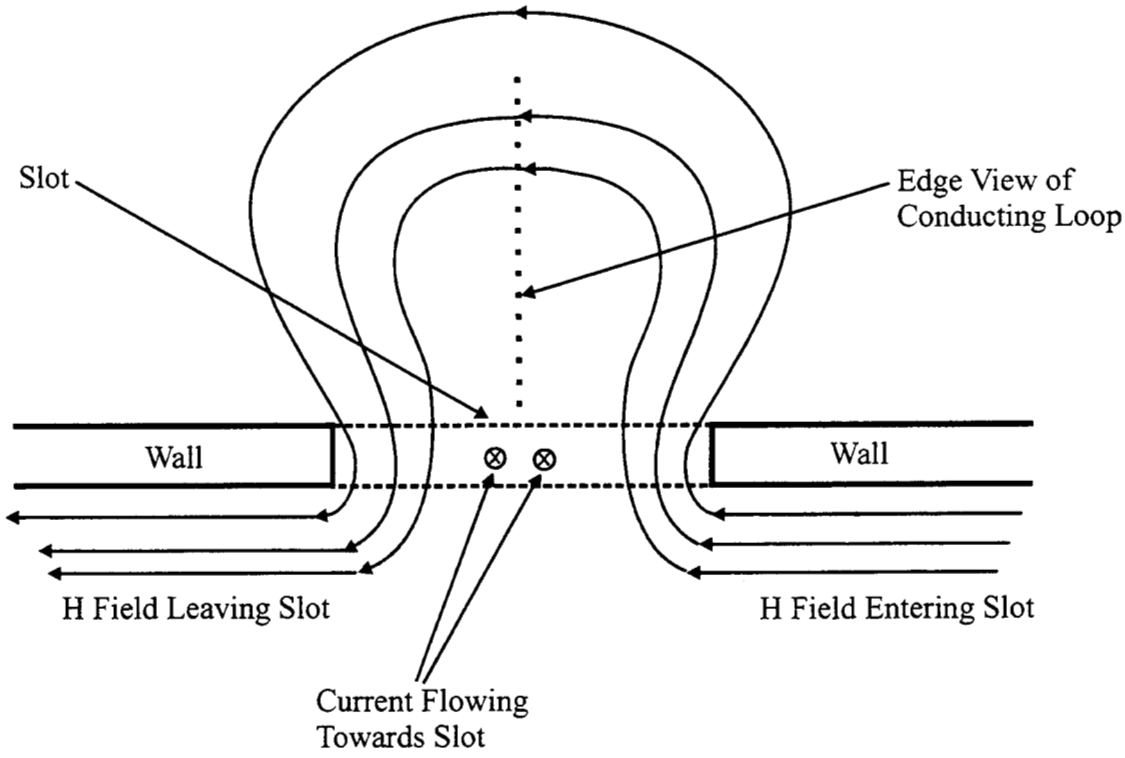

Figure 6. Physical Picture of H Field Entering and Leaving Slot (Top View)

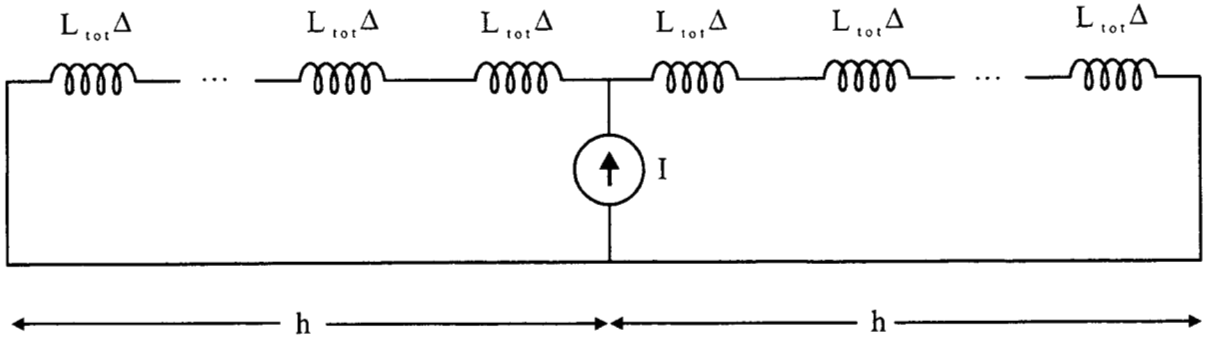

Figure 7. Equivalent Transmission Line Circuit for Slot

If lightning attaches to the center point of the slot, the peak voltage at the center of the slot can be related to the lightning current by

$$V_{pec} = L_{slot}\frac{\partial I}{\partial t} \tag{5}$$

As an example, and one that we will build on throughout this section, we will find the maximum voltage inside the Faraday cage due to a slot having a width of $w = 1.0$ mm, a depth of $d = 25.0$ mm and a bolt spacing of $2h = 500.0$ mm (these are typical dimensions in the Faraday cages encountered thus far). With these slot parameters, $L_{gap} = 50.3$ nH/m, $\Omega_0 = 11.9$ and $L_{extr} = 331$ nH/m. The parallel combination of L_{gap} and L_{extr} gives a total inductance per unit length of $L_{tot} = 43.6$ nH/m, a total slot inductance of $L_{slot} = 5.45$ nH and a maximum voltage of $V_{pec} = 2.2$ kV.

2.2 Finite Conducting Walls

Next, we will relax the assumption that the walls of the slot are perfect electric conductors. Therefore, the current flowing on the walls of the slot is no longer constrained to remain on the surface, but can penetrate some depth into the wall. This allows more magnetic field to penetrate the slot and increases V_{pec} calculated above by an additional term V_{int}. Let us again assume that worst-case lightning current attaches to the center of a slot whose walls now have a finite conductivity. Assume that the current rises linearly in time (t) from 0 kA at $t = 0$ to 200 kA at $t = \tau_r$. If the slot is symmetrical about the current source, as is the case here, the incident current will divide evenly between the two legs of the slot with half flowing in the slot to the right of the current source ($I_0^+ = 100$ kA) and half flowing in the slot to the left of the current source ($I_0^- = 100$ kA). The magnetic field on the walls as a function of time is

$$H_0(t) = h_0^+\frac{t}{\tau_r}$$

where $h_0^+ = I_0^+/d$ (recall that d is the slot depth).

If a wall of the slot is made of magnetic material, such as carbon steel, the voltage evaluated at the time $t = \tau_r$ due to the magnetic material characteristics of the wall is [5]

$$V_{int}^m = hB_s\frac{z_0}{\tau_r}\left(1 - \frac{\tau_0}{\tau_r}\right) + h\mu_0 h_0^+\frac{z_0}{\tau_r}\left(1 - \frac{\tau_0}{2\tau_r}\right) \tag{6}$$

where

$$\frac{z_0}{\tau_r} = \sqrt{\frac{h_0^+/(\tau_r\sigma)}{B_s + \frac{1}{3}\mu_0 h_0^+}}$$

and

$$\frac{\tau_0}{\tau_r} = \tau_r\frac{1}{6}\mu_0\sigma\left(\frac{z_0}{\tau_r}\right)^2$$

V_{int}^m accounts for two facts related to the permeability of the wall material, namely that it has a high permeability at low values of H_0 and the permeability of free space at high values of H_0, after the material has saturated. B_s is the value of magnetic flux density where saturation occurs and is approximately 2.0 Tesla for most materials of interest. σ is the conductivity of the walls. The risetime of the current pulse (τ_r) is taken to be 0.5×10^{-6} seconds in order to remain consistent with the stated worst-case lightning rise rate of 400 kA/μs. Again, h is the half-length of the slot. If both walls of the slot are made of this material, $V_{int} = 2V_{int}^m$.

If a wall of the slot is made of a nonmagnetic material, such as aluminum or stainless steel, the voltage evaluated at the time $t = \tau_r$ due to the nonmagnetic material characteristics of the wall is [5]

$$V_{int}^{nm} = hh_0^+\sqrt{\frac{4\mu_0}{\pi\tau_r\sigma}} \tag{7}$$

Again if both walls are made of this material, $V_{int} = 2V_{int}^{nm}$. If one of the walls is made of magnetic material and the other of nonmagnetic material, $V_{int} = V_{int}^{m} + V_{int}^{nm}$.

Although the voltage waveforms associated with V_{int} and V_{pec} do not crest precisely at the same time, a bound on the total voltage in the center of the slot ($V_{\max}$) may be taken as the sum of V_{int} and V_{pec}. Let us continue with our example from the previous section ($h_0^+ = 100$ kA/0.025 m $= 4.0 \times 10^6$ A/m) and assume that one wall of the slot is made of aluminum (6061), which has a conductivity of $2.6 \times 10^7\ (\Omega - m)^{-1}$ and the other is made of carbon steel, which has a conductivity of $4 \times 10^6\ (\Omega - m)^{-1}$. For the carbon steel wall

$$\frac{z_0}{\tau_r} = \sqrt{\frac{4.0 \times 10^6 / (0.5 \times 10^{-6} \times 4.0 \times 10^6)}{2.0 + \frac{1}{3}\mu_0 4.0 \times 10^6}} = 738 \text{ m/s}$$

and

$$\frac{\tau_0}{\tau_r} = 0.5 \times 10^{-6} \times \frac{1}{6}\mu_0 \times 4.0 \times 10^6\,(738)^2 = 0.228$$

Therefore,

$$\begin{aligned} V_{int}^{m} &= 0.25 \times 2.0 \times 738\ (0.772) + 0.25 \times \mu_0 \times 4.0 \times 10^6 \times 738 \times (0.886) \\ &= 285 + 821 = 1.1 \text{ kV} \end{aligned}$$

For the aluminum wall

$$V_{int}^{nm} = 0.25 \times 4.0 \times 10^6 \sqrt{\frac{4\mu_0}{\pi \times 0.5 \times 10^{-6} \times 2.6 \times 10^7}} = 0.35 \text{ kV}$$

The voltage bound is then $V_{\max} \leq V_{pec} + V_{int}^{m} + V_{int}^{nm} = 3.65$ kV.

2.3 Conductive Gasket

Next we will look at the effect of including a conductive gasket in the slot. Let us assume that the gasket fills the entire region between the two slot walls so that it will have a length of $2h$, a width of w and a depth of d, the conductivity of the gasket is assumed to be σ_g. The total conductance per unit length then is

$$G = \sigma_g \frac{d}{w} \tag{8}$$

The transmission line model of the gasketed slot is shown in Figure 8. Note that the gasket causes current to be shunted across the slot as it travels toward the bolts. In the analysis of Section 2.1, the current was constant along the length of the transmission line, which allowed us to reduce the transmission line to a simple inductive circuit, but this is no longer the case.

Let us first calculate the propagation constant γ of this transmission line.

$$\gamma = \sqrt{j\omega L_{gap} G}$$

where $j = \sqrt{-1}$ and ω is the angular frequency (the time convention is assumed to be $e^{+j\omega t}$). We ignore L_{extr} in this section to make the definition of γ consistent with the transverse electromagnetic (TEM) propagation constant. The presence of a gasket usually physically increases the width of the slot, which tends to increase the slot voltage. This effect is offset by the fact that a conductive gasket changes the current distribution along the length of the transmission line. Continuing with our example from above ($d = 25$ mm), but allowing w to increase to 3.0 mm to accommodate the width of the assumed gasket and using a typical value of $\sigma_g = 10^3\ (\Omega\text{–m})^{-1}$ for gasket conductivity, we obtain $G = 8.33 \times 10^3\ (\Omega\text{–m})^{-1}$. Because of the assumed increase in w, L_{gap} increases to 151 nH/m. The induced voltages that we are

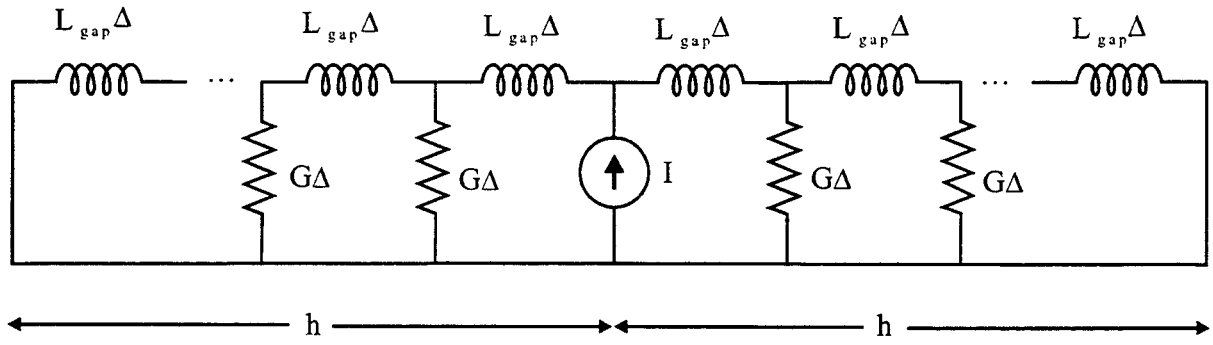

Figure 8. Equivalent Transmission Line Model for Gasketed Slot

calculating arise from a rapidly changing magnetic flux. This, in turn, implies that the highest frequencies of the lightning spectrum, which are due to the risetime of the lightning waveform will contribute most to the voltage. A reasonable high-frequency limit is when $\omega = 1/\tau_r = 2 \times 10^6$ radians/second [2]. At this frequency $\gamma = \sqrt{j\omega L_{gap} G} = \sqrt{j2.52 \times 10^3} = (35.5 + j35.5)\ \mathrm{m}^{-1}$, which means that the magnitude of the current falls exponentially ($e^{-\gamma z}$) as we travel from the source towards the bolt.

Since γ is large for a reasonably conducting gasket, the current will have fallen to nearly zero for a typical slot before it reaches the bolt ($e^{-8.9}$ for our example), so there will be negligible reflection from the short circuit formed by the bolt. At high frequencies, therefore, the transmission line appears to the current source as though it is infinitely long and the maximum voltage is

$$V_{\max} = \frac{Z_0 I}{2} \tag{9}$$

where Z_0 is the characteristic impedance of the transmission line:

$$Z_0 = \sqrt{\frac{j\omega L_{gap}}{G}}$$

In our example, $Z_0 = (4.26 \times 10^{-3} + j4.26 \times 10^{-3})\ \Omega$ so $V_{\max} = 426\ (1 + j)$ kV – a significant change from what V_{pec} would be.

If the gasket becomes more conductive, we may account for exponential decay in the depth direction that reduces the voltage even more as shown in equation B-1.

$$V_{\max} = \frac{I}{2}\omega w \mu_g \left[\frac{1}{k_g d} + 2\sum_{n=1}^{\infty} (-1)^n \left\{ \frac{1}{\sqrt{k_g^2 d^2 - n^2\pi^2}} - \frac{1}{(-jn\pi)} \right\} - j\frac{2}{\pi} \ln 2 \right] \tag{10}$$

where

$$k_g^2 = -j\omega\mu_g (\sigma_g + j\omega\varepsilon_g)$$

and μ_g and ε_g are respectively, the permeability and permittivity of the gasket material.

One note of caution: a conductive gasket can be rendered less effective if there is a nonconductive coating, such as anodization, on the metal where the gasket is attached. Nonconductive coatings must be scraped off before the gasket is applied.

2.4 Inductive Slot Terminations

Thus far in our analysis we have ignored the slot terminations and have modeled them as short circuits. We will now examine the validity of this approximation for various types of terminations. We will confine our discussion to slots without conducting gaskets because, as noted above, if a proper conducting gasket is used, the current waveform attenuates before it reaches the terminations, rendering them unimportant. We will also assume, as an upper bound, that all of the current flows on the walls of the slot under consideration and through its terminations and that none of the current flows on the walls of adjacent slots.

A bolt termination has the same configuration as a section of coaxial transmission line as seen in Figure 9. The inductance of the coaxial section is

$$L_{bolt} = \frac{\Delta_f \mu_0}{2\pi} \ln\left(\frac{r_{out}}{r_{in}}\right) \tag{11}$$

where r_{in}, r_{out} and Δ_f are defined in Figure 9, and μ_0 is the permeability of free space. Typical dimensions are $r_{in} = 5$ mm, $r_{out} = 5.5$ mm and $\Delta_f = 15$ mm, yielding $L_{bolt} = 0.29$ nH. This inductance replaces the

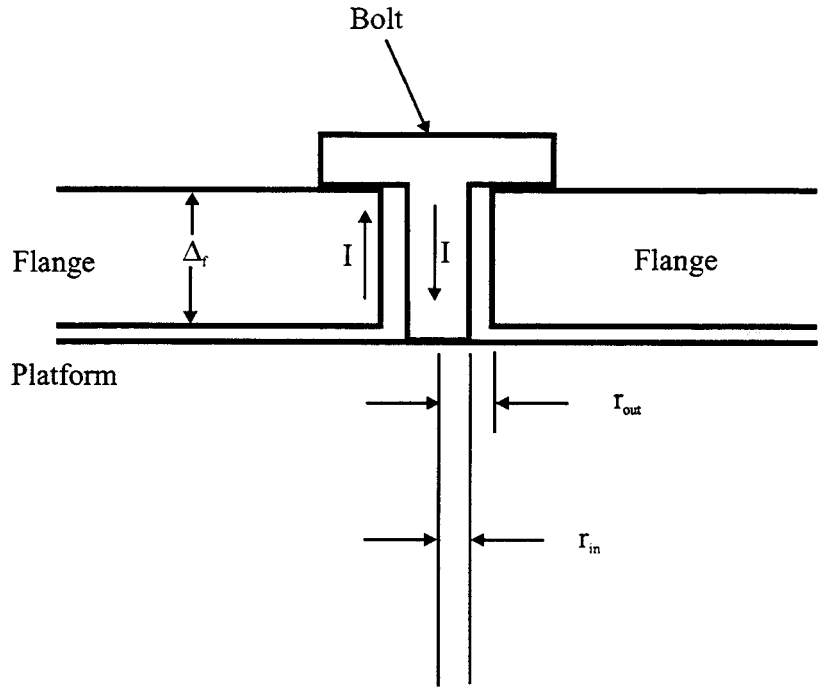

Figure 9. Bolt Termination Detail

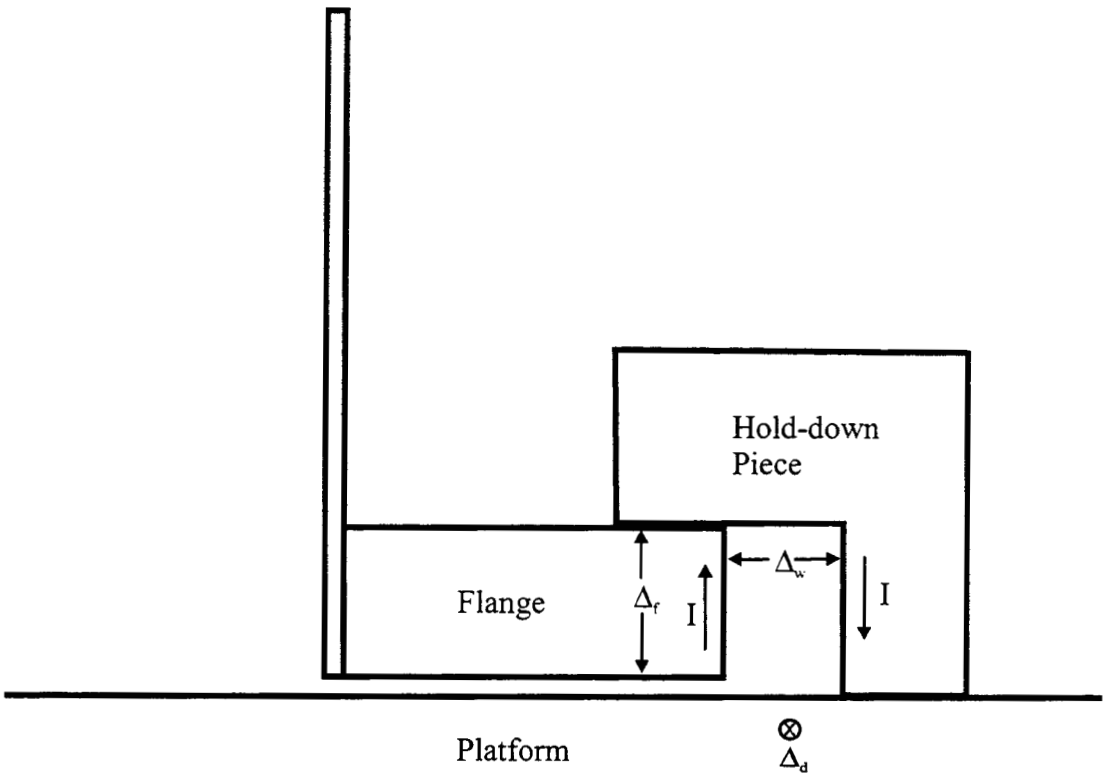

Figure 10. Hold-down Termination Detail

short circuit at the ends of the slots in Figure 7. Equation 4 now becomes

$$L_{slot} = \frac{1}{2}(L_{tot}h + L_{bolt}) \tag{12}$$

and we see that ignoring the bolt inductance in our example underestimates the voltage across the slot by approximately 3%.

Another type of device used to hold the cover onto the platform is the one shown in Figure 3 and shown in cross-section in Figure 10. It consists of a metal piece that rotates over the flange once the cover is in place. It is often used in place of bolts because there is no need to align the flange bolt holes with the tapped holes in the platform and therefore, the Faraday cage is simpler to assemble. The inductance of such a termination is

$$L_{hd} = \mu_0 \frac{\Delta_f \Delta_w}{\Delta_d} \tag{13}$$

Where Δ_f, Δ_w, and Δ_d are defined in Figure 10 (Δ_d is the thickness of the hold-down piece measured into the plane of the drawing). Typical dimensions of such hold-down pieces are $\Delta_f = 15$ mm, $\Delta_w = 10$ mm, and $\Delta_d = 30$ mm, yielding $L_{hd} = 6.3$ nH, which may be a significant contributor to the slot inductance. We can add the effect of finite conductivity of the hold-down device by using equation 6 or 7 and substituting Δ_d for d and Δ_f for h. The voltage due to L_{hd} is expected to dominate in this case, however.

The last type of slot-terminating device that we will examine, is exemplified by the clamps shown in Figure 3, which are used to hold two halves of a cover together. A clamp consists of a wire bail attached to a lever arm, which is, in turn, attached to one half-cover. The wire bail passes over a hook attached to the other half-cover. Action of the lever arm draws the two halves together in a manner very much like a ski boot buckle. A detail of the clamp is shown in Figure 11.

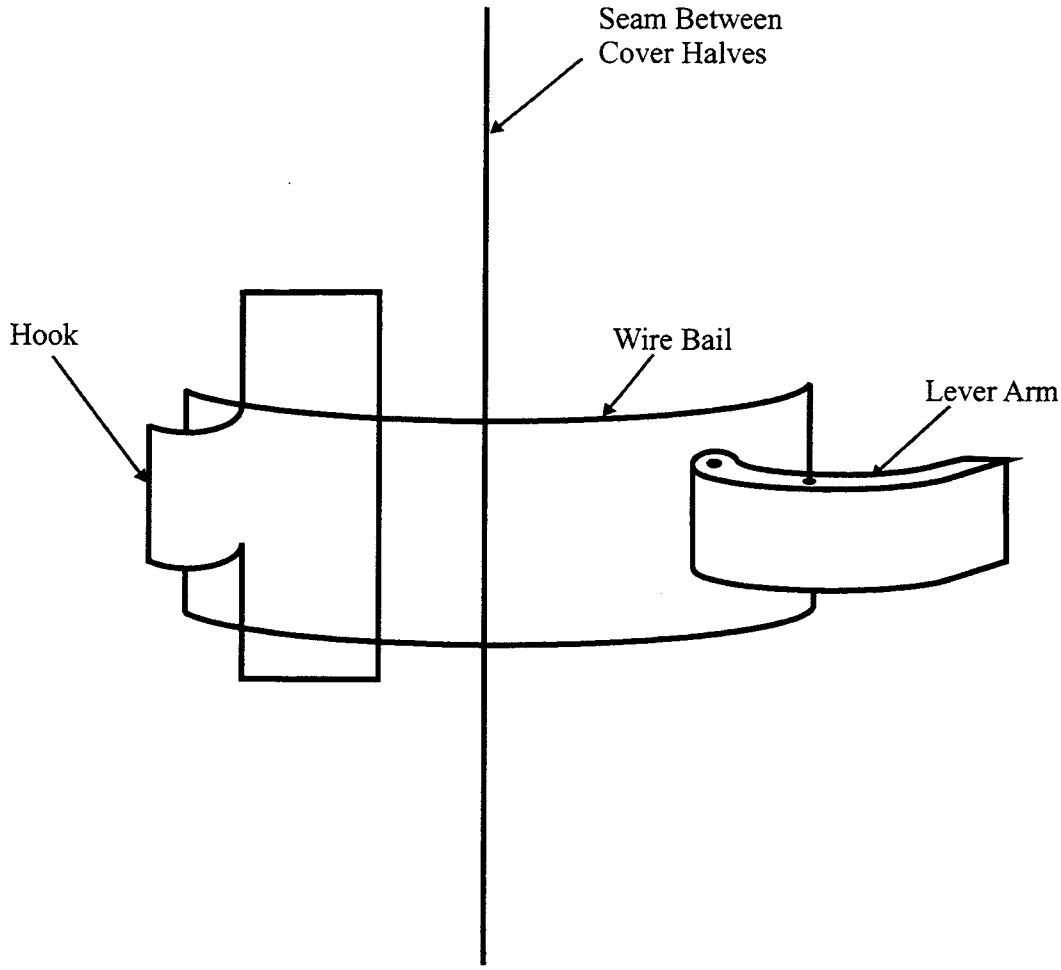

Figure 11. Clamp Detail

Figure 12 shows an end view of the two wires that form the bail. The wires have a radius of r_w, are separated from each other by $2s$ and are a distance h_w above the metal cover. Approximating the wires as being infinite in $\hat{z}$ and neglecting the curvature of the metal cover we find an expression for the $\hat{z}$ directed magnetic vector potential at any observation point in the $z = 0$ plane:

$$A_z = -\frac{\mu_0 I_0}{2\pi} \left[\ln \sqrt{(x+s)^2 + (y-h_w)^2} + \ln \sqrt{(x-s)^2 + (y-h_w)^2} - \ln \sqrt{(x+s)^2 + (y+h_w)^2} - \ln \sqrt{(x-s)^2 + (y+h_w)^2} \right] \tag{14}$$

The inductance per unit length of the clamp can be calculated by the formula

$$L = \frac{1}{2I_0} \oint_l \vec{A} \cdot d\vec{l}$$

where the factor of $1/2$ accounts for the two wires in parallel, and where $\vec{l}$ is the rectangular contour shown in Figure 12 that travels along the wire surface for one meter in the $\hat{z}$ direction; to the surface of the metal cover in the $-\hat{y}$ direction; along the metal surface for one meter in the $-\hat{z}$ direction; and finally back to the wire surface in the $\hat{y}$ direction. This contour was chosen over a contour between the two wires because, since the two wires forming the bail are connected to each other at their ends, the net flux linking them will be zero. All contributions to the integral over the chosen contour are zero, (either because A_z itself is zero at $y = 0$, or because the dot product is zero) except for the contribution along the wire surface. Evaluating A_z at the wire surface (where $x = s$ and $y = h_w - r_w$), making the approximation that $r_w \ll s, h_w$ and multiplying by the length of the wire (l) we obtain

$$L_{clamp} = -\frac{\mu_0 l}{4\pi} \left[\ln \left(\frac{2s}{\sqrt{(2s)^2 + (2h_w)^2}} \right) + \ln \left(\frac{r_w}{2h_w} \right) \right] \tag{15}$$

Typical parameters for clamps of this style are $r_w = 1.5$ mm, $s = 15$ mm, $h_w = 15$ mm and $l = 40$ mm so that $L_{clamp} = 13.4$ nH. In this case the inductance of the terminating clamp is actually larger than $L_{tot}h$.

2.5 Varying the Slot Cross Section

This subsection indicates how to proceed if the width of the slot varies as a function of depth, which might occur in order to accommodate a gasket, for example. Figure 13 shows the side view of a slot having three different widths. Two different gaskets are employed in the slot.

The analysis proceeds exactly as before except that L_{gap} consists of three parallel inductances so that

$$\frac{1}{L_{gap}} = \frac{1}{L_{gap1}} + \frac{1}{L_{gap2}} + \frac{1}{L_{gap3}} \tag{16}$$

where

$$L_{gap1} = \mu_0 \frac{w_1}{d_1}$$
$$L_{gap3} = \mu_0 \frac{w_3}{d_3}$$

as previously defined, but L_{gap2} needs correction terms to account for the vertical surfaces in the gap 2 region. The correction terms take the form of inductances in parallel to the original gap inductance so the

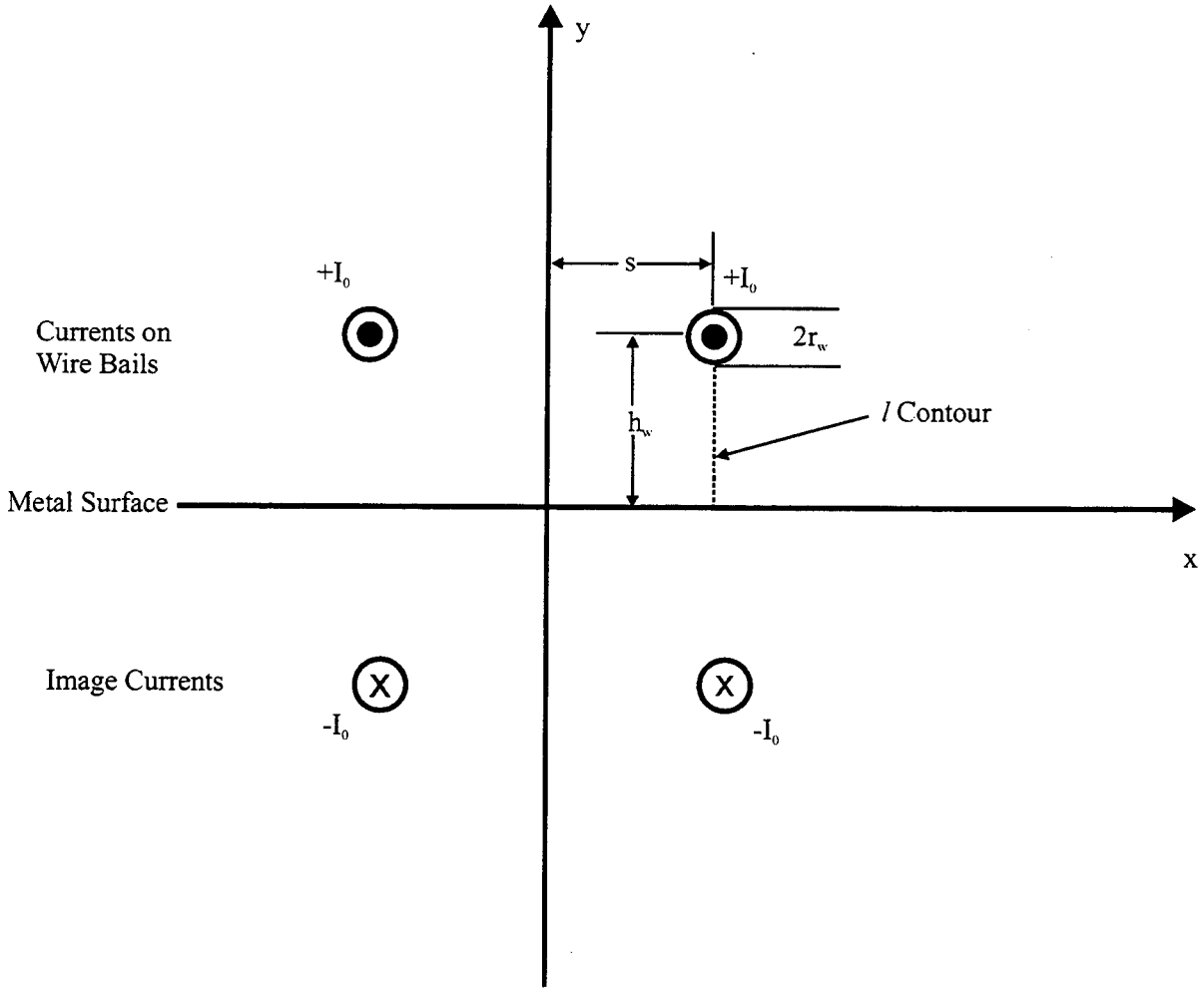

Figure 12. End View of Wire Bail

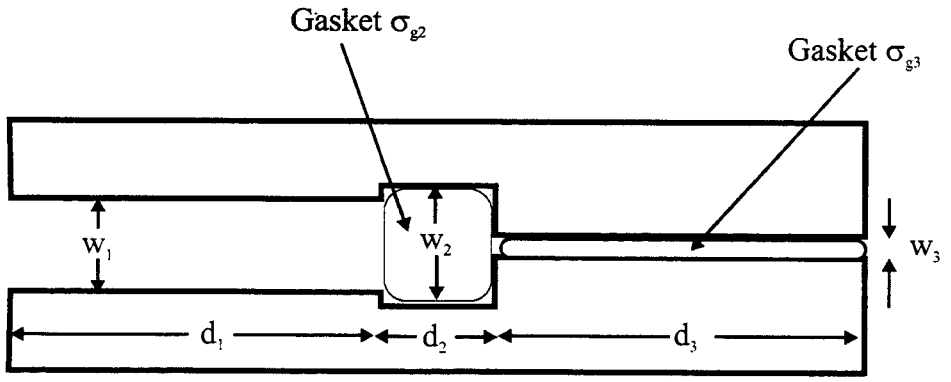

Figure 13. Variable Width Slot

correction lowers the original inductance value.

$$\frac{1}{L_{gap2}} = \frac{d_2}{\mu_0 w_2} + \frac{1}{L_{v21}} + \frac{1}{L_{v23}}$$

Assuming that there is negligible interaction between the vertical surfaces on the left side and the vertical surfaces on the right side,

$$\begin{aligned}
\frac{1}{L_{v21}} &= \frac{1}{2\pi\mu_0}\left[\frac{w_2}{w_1}\left(1+\frac{w_1}{w_2}\right)^2 \ln\left(1+\frac{w_1}{w_2}\right) - \frac{w_2}{w_1}\left(1-\frac{w_1}{w_2}\right)^2 \ln\left(1-\frac{w_1}{w_2}\right) - 2\ln\left(4\frac{w_1}{w_2}\right)\right] \\
&\approx \frac{1}{\pi\mu_0}\ln\left(\frac{e}{4}\frac{w_2}{w_1}\right) \qquad \text{when } w_2 >> w_1
\end{aligned}$$

where $e = 2.71828$. Similarly,

$$\begin{aligned}
\frac{1}{L_{v23}} &= \frac{1}{2\pi\mu_0}\left[\frac{w_2}{w_3}\left(1+\frac{w_3}{w_2}\right)^2 \ln\left(1+\frac{w_3}{w_2}\right) - \frac{w_2}{w_3}\left(1-\frac{w_3}{w_2}\right)^2 \ln\left(1-\frac{w_3}{w_2}\right) - 2\ln\left(4\frac{w_3}{w_2}\right)\right] \\
&\approx \frac{1}{\pi\mu_0}\ln\left(\frac{e}{4}\frac{w_2}{w_3}\right) \qquad \text{when } w_2 >> w_3
\end{aligned}$$

The gasket conductance becomes

$$G = G_2 + G_3 \tag{17}$$

where

$$G_3 = \sigma_{g3}\frac{d_3}{w_3}$$

as previously defined, but like L_{gap2}, G_2 also needs a correction to account for the vertical surfaces in the gap 2 region. The correction takes the form of a conductance in parallel so it increases the original conductance value.

$$G_2 = \sigma_{g2}\frac{d_2}{w_2} + G_{v21} + G_{v23}$$

$$\begin{aligned}
G_{v21} &= \frac{\sigma_{g2}}{2\pi}\left[\frac{w_2}{w_1}\left(1+\frac{w_1}{w_2}\right)^2 \ln\left(1+\frac{w_1}{w_2}\right) - \frac{w_2}{w_1}\left(1-\frac{w_1}{w_2}\right)^2 \ln\left(1-\frac{w_1}{w_2}\right) - 2\ln\left(4\frac{w_1}{w_2}\right)\right] \\
&\approx \frac{\sigma_{g2}}{\pi}\ln\left(\frac{e}{4}\frac{w_2}{w_1}\right) \qquad \text{when } w_2 >> w_1 \\
G_{v23} &= \frac{\sigma_{g2}}{2\pi}\left[\frac{w_2}{w_3}\left(1+\frac{w_3}{w_2}\right)^2 \ln\left(1+\frac{w_3}{w_2}\right) - \frac{w_2}{w_3}\left(1-\frac{w_3}{w_2}\right)^2 \ln\left(1-\frac{w_3}{w_2}\right) - 2\ln\left(4\frac{w_3}{w_2}\right)\right] \\
&\approx \frac{\sigma_{g2}}{\pi}\ln\left(\frac{e}{4}\frac{w_2}{w_3}\right) \qquad \text{when } w_2 >> w_3
\end{aligned}$$

3 Circular Viewing Apertures

3.1 Uniform Magnetic Field Coupling

A second type of aperture commonly found in Faraday cages is the circular aperture. These apertures are typically used to view the contents of the Faraday cage as seen in Figure 1. Let us ignore the effect of the cover or content geometry on the $\vec{H}$ field and simplify the problem to that of a circular aperture in an infinite ground plane as shown in Figure 14. In this section we will conduct several levels of bounding

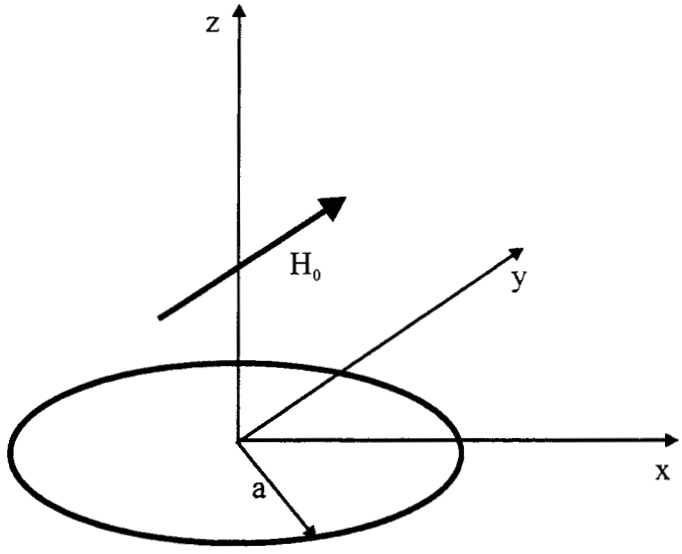

Figure 14. Circular Aperture Driven by H Field

analysis. First, we find the voltage on a conducting loop positioned at the aperture, which intercepts all of the flux entering the Faraday cage through the aperture. The advantage of this analysis is that we need knowledge of only one parameter: the aperture radius. As we consider apertures with larger radii, the above bounding voltage becomes too high to be useful. Therefore, we take into account the distance between the aperture and the actual location of a conducting loop, but we still require that the loop intercepts all of the flux passing through a surface surrounding the aperture at this given distance. This analysis requires knowledge of two parameters: aperture radius and distance. The distance and radius may be such that this bound is also too high to be useful, so finally, we calculate the voltage on a conducting loop accounting for both the distance between the conducting loop and the aperture and the area of the loop.

Before we begin the analysis, let us examine what is happening physically. Figure 15 shows the top view of a circular aperture illuminated by a $\hat{y}$-directed, uniform $\overrightarrow{H}$ field. Because the electric current flows around the aperture symmetrically, $y = 0$ is a plane of symmetry for the $\overrightarrow{H}$ field. The $\overrightarrow{H}$ field enters the Faraday cage through the bottom half of the aperture ($y < 0$) and leaves through the top half ($y > 0$).

We begin the analysis by solving for the magnetic scalar potential ϕ_m when a uniform H field (H_0) exists on one side of a circular aperture. ϕ_m is related to the H field by the equation.

$$\vec{H} = -\nabla\phi_m \tag{18}$$

and satisfies Laplace's equation ($\nabla^2\phi_m = 0$).

In order to model a circular aperture having the radius of a, we use the oblate spheroidal coordinate system (ξ, ζ, φ) shown in Figure 16, where $(0 \leq \xi \leq 1)$, $(-\infty < \zeta < \infty)$, and $(-\pi \leq \varphi < \pi)$ [6]. These choices for the ranges of coordinates are appropriate for the aperture problem because the coordinates are continuous throughout the region where the field exists. The oblate spheroidal coordinates are related to the Cartesian coordinates by the following equations:

$$x = a\sqrt{1+\zeta^2}\sqrt{1-\xi^2}\cos\varphi \tag{19}$$

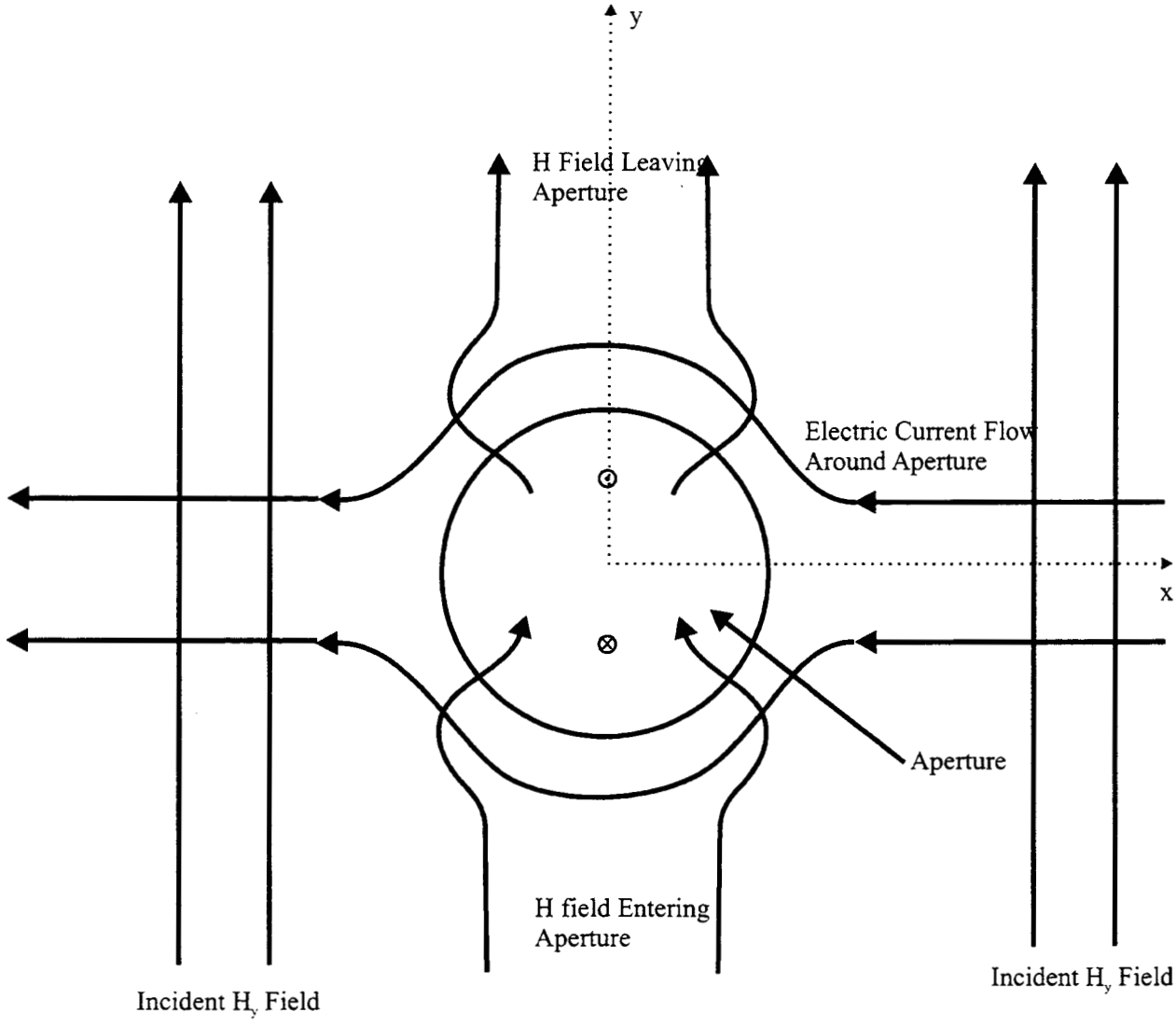

Figure 15. Physical Picture of Uniform H Field Near Circular Aperture

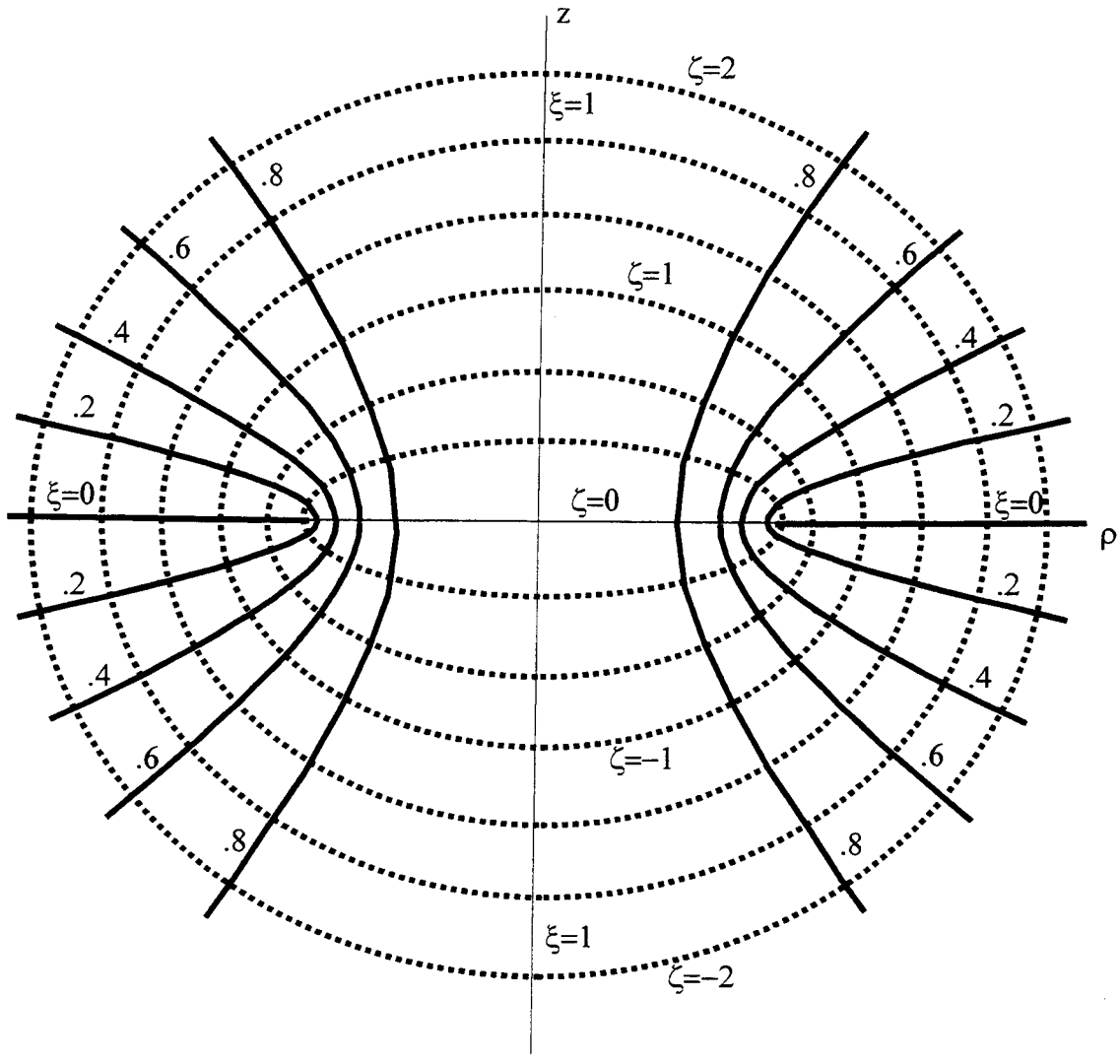

Figure 16. Oblate Spheroidal Coordinate System

$$y = a\sqrt{1+\zeta^2}\sqrt{1-\xi^2}\sin\varphi$$
$$z = a\zeta\xi$$

The solution of Laplace's equation in this coordinate system takes the form of

$$\phi_m = \sum_m \sum_n \left(A' P_n^m(\xi) + B' Q_n^m(\xi)\right)\left(A P_n^m(j\zeta) + B Q_n^m(j\zeta)\right)\left(C\sin(m\varphi) + D\cos(m\varphi)\right) \tag{20}$$

Where P_n^m and Q_n^m are the associated Legendre functions of the first and second kind respectively, and j is $\sqrt{-1}$.

In the upper half-plane, far away from the aperture, $\vec{H} = \hat{y}H_0$. Therefore, using equation 18, we find by inspection that

$$\phi_m(\zeta = +\infty) = -H_0 y$$

where y is the Cartesian coordinate. Converting to oblate spheroidal coordinates using equation 19, we obtain

$$\phi_m(\zeta = +\infty) = -H_0 a[(1-\xi^2)(1+\zeta^2)]^{\frac{1}{2}}\sin\varphi$$

In the lower half-plane, far away from the aperture, $\vec{H} = 0$. Therefore,

$$\phi_m(\zeta = -\infty) = 0$$

First we note, that because of symmetry exhibited by the circular aperture, and in order to match the incident field in the upper half-plane, only the $m = 1$ and $n = 1$ modes have non-zero coefficients in equation 20. Further, the coefficient of $\cos(m\varphi)$ must be zero. The potential must be finite at $\xi = 1$, which means that the coefficient B' must be zero. We are left with

$$\phi_m = P_1^1(\xi)\left(A P_1^1(j\zeta) + B Q_1^1(j\zeta)\right)\sin\varphi$$

Substituting the actual expressions for the associated Legendre functions, we obtain

$$\phi_m = (1-\xi^2)^{\frac{1}{2}}\left[jA(1+\zeta^2)^{\frac{1}{2}} + B(1+\zeta^2)^{\frac{1}{2}}\left(\operatorname{arccot}\zeta - \frac{\zeta}{1+\zeta^2}\right)\right]\sin\varphi$$

Letting $\zeta \to +\infty$, we find that $jA = -H_0 a$. Letting $\zeta \to -\infty$, and using the proper branch cut so that $\operatorname{arccot}(-\zeta) = \pi - \operatorname{arccot}(+\zeta)$ we find that $B = -jA/\pi$. Therefore,

$$\phi_m = (1-\xi^2)^{\frac{1}{2}}\left[-H_0 a(1+\zeta^2)^{\frac{1}{2}} + \frac{H_0 a}{\pi}(1+\zeta^2)^{\frac{1}{2}}\left(\operatorname{arccot}\zeta - \frac{\zeta}{1+\zeta^2}\right)\right]\sin\varphi$$

In order to use the formulas found in [7] for gradient, we make the substitutions $\zeta = \sinh\eta$, where $(-\infty < \eta < +\infty)$, and $\xi = \cos\theta$, where $(0 \le \theta \le \pi/2)$, to obtain

$$\phi_m = -H_0 a\sin\theta\cosh\eta\sin\varphi\left[1 - \frac{1}{\pi}\operatorname{arccot}(\sinh\eta) + \frac{1}{\pi}\frac{\sinh\eta}{\cosh^2\eta}\right] \tag{21}$$

To find the maximum voltage that could appear on a conducting loop within the container, we postulate that a conducting loop positioned at the aperture intercepts all of the $\vec{H}$ field flowing through half the aperture. Using equation 18 to find the $\hat{\eta}$ directed H field gives

$$H_\eta(\eta,\theta,\varphi) = -\frac{1}{a(\cosh^2\eta - \sin^2\theta)^{\frac{1}{2}}}\frac{\partial\phi_m}{\partial\eta} \tag{22}$$

$$= \frac{H_0 a\sin\theta\sin\varphi}{a(\cosh^2\eta - \sin^2\theta)^{\frac{1}{2}}}\left[\sinh\eta - \frac{1}{\pi}\sinh\eta\operatorname{arccot}(\sinh\eta) + \frac{1}{\pi} + \frac{1}{\pi\cosh^2\eta}\right] \tag{23}$$

Letting $\eta \to 0$, we find that H_η in the aperture is

$$H_\eta(0,\theta,\phi) = \frac{2H_0\sin\theta\sin\varphi}{\pi\cos\theta}$$

In cylindrical coordinates, $\rho = a\cosh\eta\sin\theta$. In the aperture, therefore, where $\eta = 0$, $\rho = a\sin\theta$. Substituting, in order to convert H_η to cylindrical coordinates we obtain

$$H_z(\rho,\phi,0) = \frac{2H_0}{\pi}\frac{\rho}{\sqrt{a^2-\rho^2}}\sin\varphi$$

Next we find the magnetic flux (Φ) flowing into the Faraday cage through the aperture by integrating $B_z = \mu_0 H_z$ over the bottom half of the aperture.

$$\begin{aligned}\Phi &= (-\hat{z}\cdot\hat{z})\mu_0\int_0^a\int_{-\pi}^{0} H_z\rho d\varphi d\rho \\ &= \mu_0 H_0 a^2\end{aligned}$$

The maximum voltage is

$$\begin{aligned}V_{max} &= \frac{\partial\Phi}{\partial t} \\ &= \frac{\partial H_0}{\partial t}\mu_0 a^2\end{aligned} \tag{24}$$

Equation 24 can be used if lightning attaches to the cart more than an aperture diameter away from the aperture. The $\overrightarrow{H}$ field due to the lightning current can be averaged over the aperture area to determine H_0.

3.2 Lightning Attaches to Aperture Edge

The worst-case scenario involving lightning alone is if the lightning arc attaches to the edge of the circular aperture, as shown in Figure 17. Later, we will discuss a case even worse than this one, but which requires that a wire be present to conduct lightning current across the aperture. If the aperture is filled with a dielectric plunger so that a wire cannot fall across the aperture, or if there is some other reason that the wire scenario cannot occur, then this is the appropriate worst-case for the circular aperture.

Physically, the current and magnetic field behaves as shown in Figure 18. We assume the direction of current flow to be from the attachment point toward the lightning source along the arc channel. Therefore, current flows on the ground plane around the aperture and toward the attachment point. The H field enters the Faraday cage through the bottom half of the aperture ($y < 0$) and leaves through the top half ($y > 0$). For this case, the $\vec{H}$ field cannot be averaged across the aperture, since in the vicinity of a current source I, the field behaves as

$$\vec{H} = \hat{\varphi}\frac{I}{2\pi\rho}$$

(we have temporarily assumed that the origin is at the arc position on the edge of the circular aperture) [1]. In Appendix C, however, we show that by restricting the analysis to include only the $m = 1$ mode, we can use uniform field results if we replace H_0 by $\overrightarrow{H}$ due to the lightning current evaluated at the center of the aperture, namely,

$$H_0 \rightarrow \frac{I}{2\pi a}$$

Making this replacement in equation 24 we obtain

$$V_{\max} = \frac{\mu_0 a}{2\pi}\frac{\partial I}{\partial t}$$

If we include all of the modes, using equation C-4, we obtain

[1] In previous memorandums we averaged H_y over the aperture diameter. Averaging requires knowledge of the arc radius, it over-estimates $V_{\max}$ and it cannot be rigorously justified. We therefore, changed the analysis to the methods outlined in Appendices C and D.

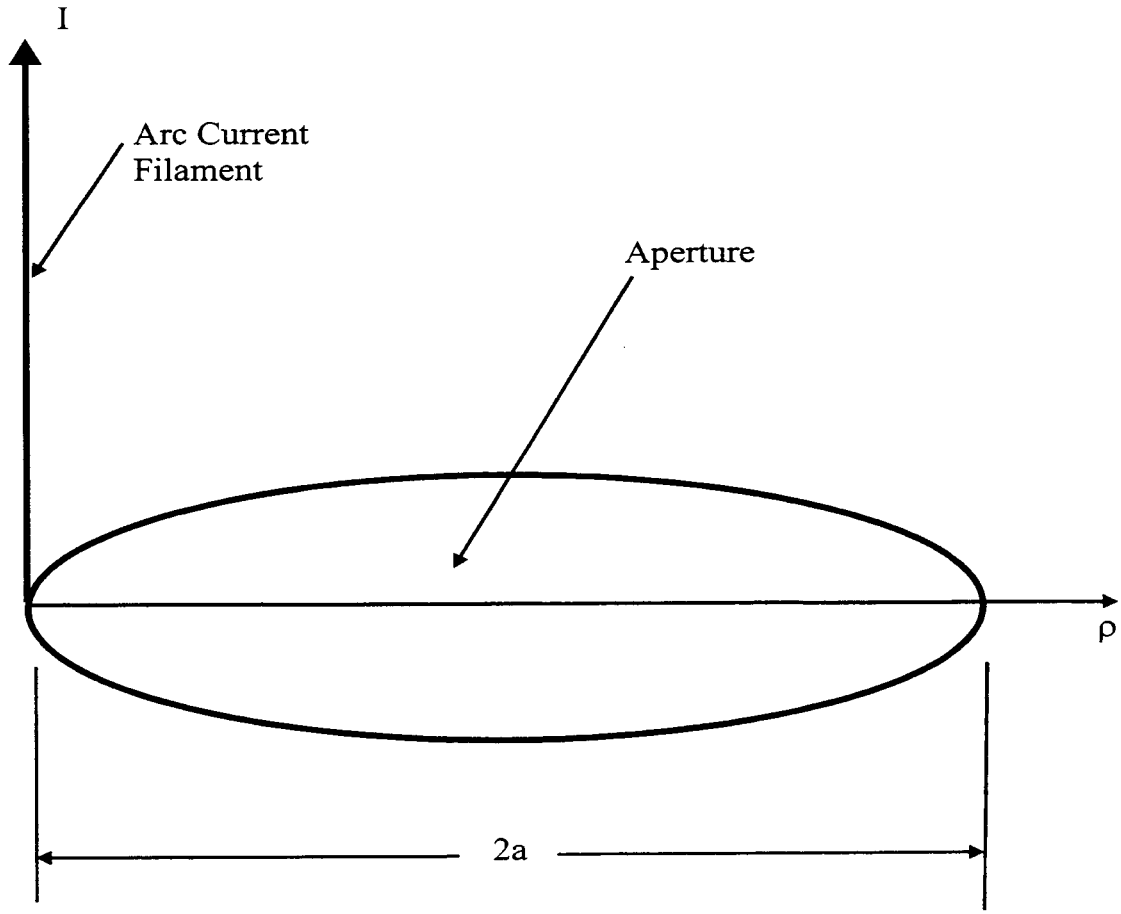

Figure 17. Lightning Striking Edge of Aperture

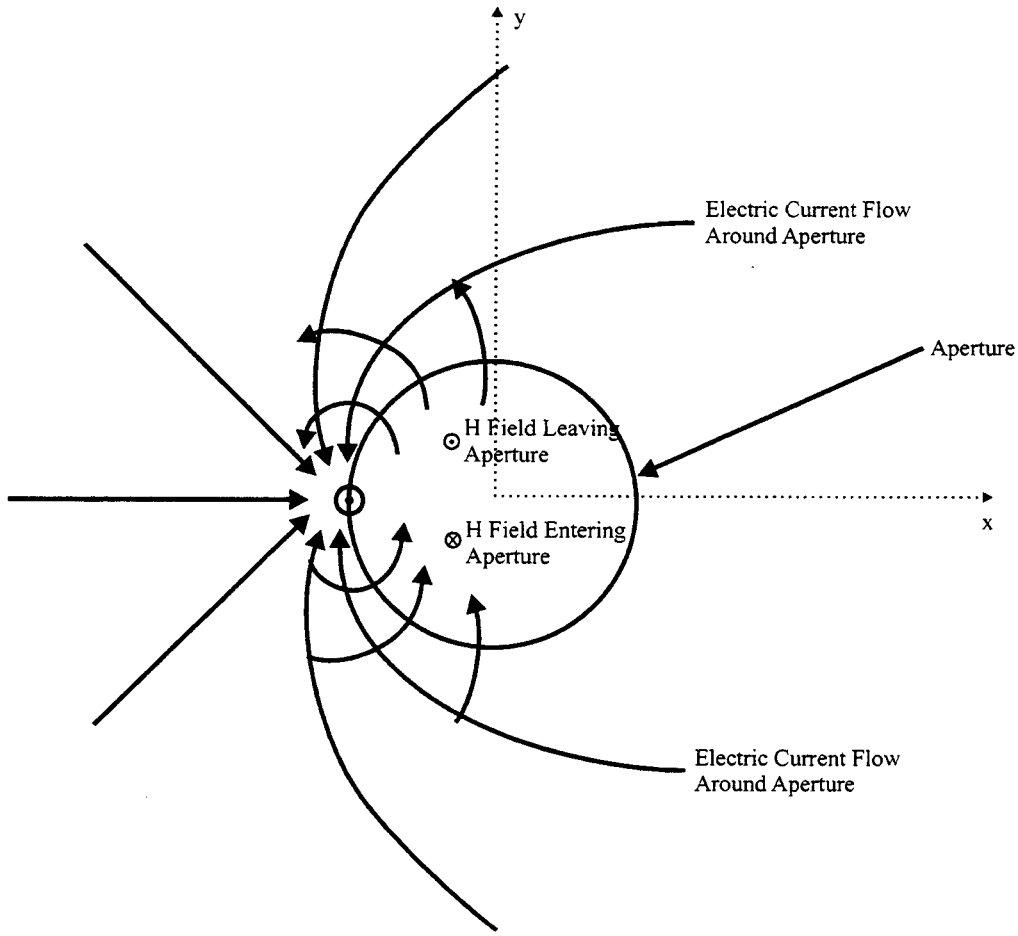

Figure 18. Physical Picture of H Field due to Current Attached to Aperture Edge

$$V_{\max} = \frac{\mu_0 a}{\pi}(0.6478)\frac{\partial I}{\partial t} \tag{25}$$

Therefore, in the aperture, including only the $m = 1$ mode underestimates the voltage by 23%. As we move away from the aperture, this error becomes smaller. Because the uniform field excitation with the above substitution yields good results and is probably more familiar to the reader we will continue to develop the uniform field results in the main body of this report to demonstrate the procedure, but will use equations from Appendix C as appropriate. As an example calculation, if we assume an aperture having a radius of $a = 5$ cm, then substituting in equation 25, $V_{\max} = 0.6478 \times 8.0$ kV $= 5.2$ kV when worst-case lightning strikes the edge of the aperture.

If the conducting loops inside the cage were physically constrained so they were guaranteed to be some distance from the aperture, we could take this distance into account when calculating $V_{\max}$. Assume that the conducting loops are constrained so they cannot break the surface $\eta = \eta_0$ where $\eta_0 < 0$. The $\overline{H}$ field enters the aperture and crosses the $\eta = \eta_0$ surface as shown in Figure 19. Revisiting equation 23 when $\eta = \eta_0$ we obtain

$$\begin{aligned} H_\eta(\eta_0, \theta, \varphi) &= -\frac{1}{a(\cosh^2\eta_0 - \sin^2\theta)^{\frac{1}{2}}}\frac{\partial \phi_m}{\partial \eta} \\ &= \frac{H_0 \sin\theta \sin\varphi}{(\cosh^2\eta_0 - \sin^2\theta)^{\frac{1}{2}}}\left[\sinh\eta_0 - \frac{1}{\pi}\sinh\eta_0 \operatorname{arccot}(\sinh\eta_0) + \frac{1}{\pi} + \frac{1}{\pi\cosh^2\eta_0}\right] \end{aligned}$$

Assume that the conducting loop is large enough to intercept all of the flux passing through the η_0 surface. We calculate this flux by integrating over half of the $\eta = \eta_0$ surface

$$\begin{aligned} \Phi &= (-\widehat{\eta}\cdot\widehat{\eta})\mu_0 \int_0^{\frac{\pi}{2}}\int_{-\pi}^{0} H_\eta(\eta_0,\theta,\varphi)a^2\sqrt{\cosh^2\eta_0 - \sin^2\theta}\cosh\eta_0 \sin\theta d\varphi d\theta \\ &= \mu_0 H_0 a^2 \frac{\pi}{2}\cosh\eta_0\left[\sinh\eta_0 - \frac{1}{\pi}\sinh\eta_0 \operatorname{arccot}(\sinh\eta_0) + \frac{1}{\pi} + \frac{1}{\pi\cosh^2\eta_0}\right] \end{aligned}$$

Substituting for H_0, and converting back to the (ξ, ζ, φ) coordinates to be consistent with the appendices

$$\Phi = \mu_0 a \frac{I}{4\pi}\sqrt{1+\zeta_0^2}\left[\pi\zeta_0 - \zeta_0 \operatorname{arccot}(\zeta_0) + 2 - \frac{\zeta_0^2}{(1+\zeta_0^2)}\right]$$

We note that the ζ coordinate in the appendices range over positive values in the region of interest, while here the ζ coordinate ranges over negative values. We re-write the above changing the sign of ζ and remembering the branch cut definition $\operatorname{arccot}(-\zeta) = \pi - \operatorname{arccot}(+\zeta)$

$$\Phi(-\zeta_0) = -\mu_0 a \frac{I}{4\pi}\sqrt{1+\zeta_0^2}\left[\zeta_0 \operatorname{arccot}(\zeta_0) - 2 + \frac{\zeta_0^2}{(1+\zeta_0^2)}\right] \tag{26}$$

which is the same as equation C-3.

In our example, we will assume that the conducting loop is constrained so that it never gets closer than $z_{top} = 10$ cm from the aperture. Therefore, using equation 19, $(-\zeta_0) = z_{top}/a = 2.00$ and substituting in equation 26, we obtain

$$V_{\max} = \frac{\mu_0 a}{\pi}[0.152]\frac{\partial I}{\partial t}$$

So for the most-likely case of the arc attaching to the edge of the $a = 5$ cm aperture, $V_{max} = 0.152 \times 8.0\,\text{kV} =$ 1.2 kV. For convenience, however, whenever we are calculating the total flux through a quarter spheroid in the future, we will use the fit function (equation C-5), which is

$$V_{\max} = \frac{\mu_0 a}{\pi}\left[(0.4124)\operatorname{arccot}\zeta_0 - \frac{\zeta_0}{1+\zeta_0^2}(0.07907)\right]\frac{\partial I}{\partial t} \tag{27}$$

One question that arises is that the above analysis was conducted in free-space, while the Faraday cages

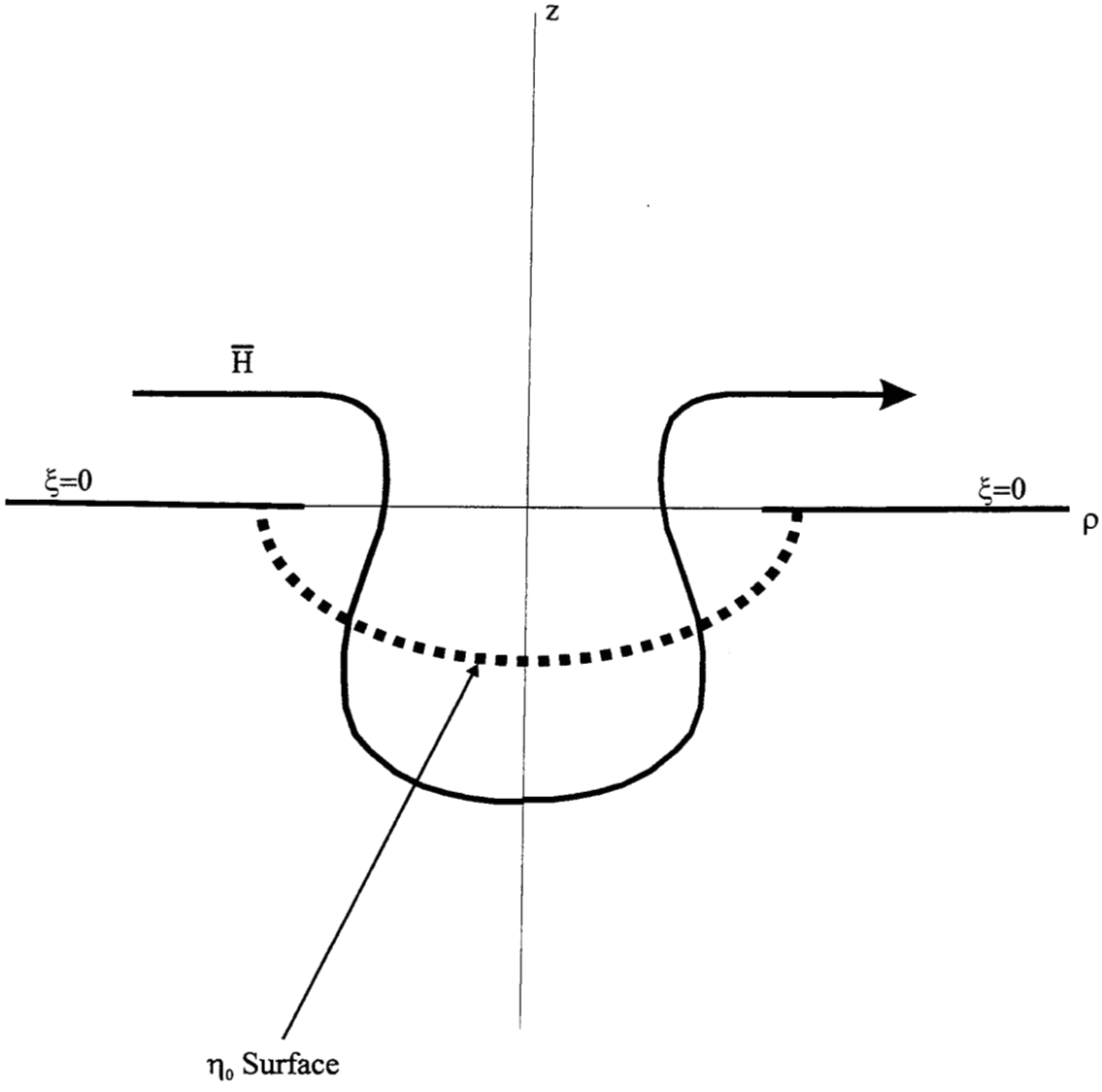

Figure 19. Magnetic Flux Crossing η_0 Surface

are usually filled with parts made of metal. If the metal pieces are highly conductive, such as aluminum, or steel and are oriented such that the normal of the metal surface is parallel to the ζ_0 surface normal, the metal will tend to prevent the $\overrightarrow{H}$ field from crossing the ζ_0 surface. The free-space analysis will be a bound for this situation. If, on the other hand, the metal pieces have a high permeability, such as the soft, laminated, iron used in transformer cores or ferrites, or if they are conducting as before, but are oriented such that the normal of the metal is perpendicular to the ζ_0 normal, the metal will tend to increase the amount of $\overrightarrow{H}$ field crossing the surface. The free-space analysis will not bound this situation. It is possible to do analysis for this situation by imposing a perfect magnetic conductor (PMC) boundary condition at ζ_0, but thought to be unnecessary, since we have never seen this second situation in practice.

Finally, we consider specifics of the loop geometry. Far away from the aperture – at least the aperture diameter ($2a$) away – we can approximate ϕ_m in terms of the magnetic dipole moment m_y.

$$\begin{aligned} \phi_m &= \frac{m_y y}{4\pi r^3} \\ &= \frac{m_y r \sin\theta \sin\varphi}{4\pi r^3} \end{aligned}$$

where $m_y = -2\alpha_{yy} H_y^{sc}$, $\alpha_{yy} = 4a^3/3$ for a circular aperture, $H_y^{sc} = H_0$ (the short circuit $\vec{H}$ field on the interior side of the aperture, anticipating that we will eventually replace H_0 with the term $I/2\pi a$) and r, θ and φ are the spherical coordinates. The $\hat{r}$ directed H field is calculated by applying equation 18.

$$\begin{aligned} H_r &= -\frac{\partial \phi_m}{\partial r} \\ &= +\frac{m_y \sin\theta \sin\varphi}{2\pi r^3} \\ H_r^{\max} &= \frac{4a^3 H_0}{3\pi r^3} \end{aligned}$$

The $\widehat{\theta}$ and $\widehat{\varphi}$ components of H are similarly computed:

$$\begin{aligned} H_\theta &= -\frac{1}{r}\frac{\partial \phi_m}{\partial \theta} \\ &= -\frac{m_y \cos\theta \sin\varphi}{4\pi r^3} \\ H_\theta^{\max} &= \frac{2a^3 H_0}{3\pi r^3} \end{aligned}$$

$$\begin{aligned} H_\varphi &= -\frac{1}{r\sin\theta}\frac{\partial \phi_m}{\partial \varphi} \\ &= -\frac{m_y \cos\varphi}{4\pi r^3} \\ H_\varphi^{\max} &= \frac{2a^3 H_0}{3\pi r^3} \end{aligned}$$

The largest component is $H_r^{\max}$, so we will orient the loop to maximize this component. If the loop is in the vicinity of a piece of metal, we must double this value because the H field from the image in the conductor will add to the direct field. If it is in a corner formed by two pieces of metal we must quadruple the value. As shown in Figure 20, we will assume the loop is in the vicinity of a single piece of metal.

The magnetic flux is, therefore,

$$\begin{aligned} \Phi &= \mu_0 2 H_r^{\max} A_{loop} \\ &= \mu_0 2 \frac{4a^3 H_0}{3\pi r^3} A_{loop} \end{aligned}$$

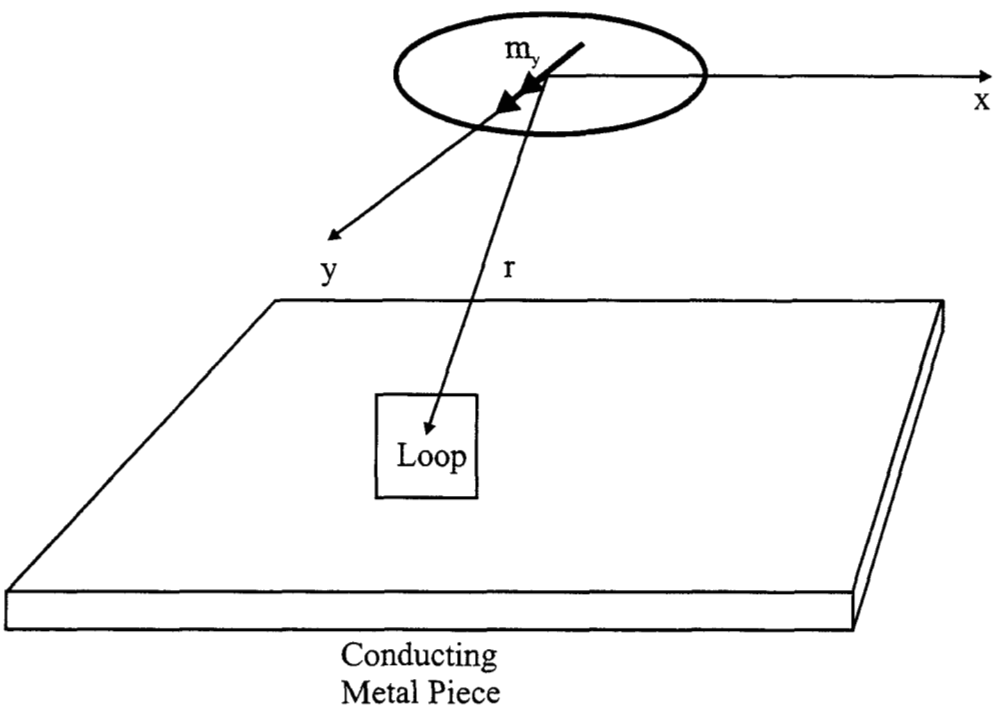

Figure 20. Aperture Approximated by Magnetic Dipole

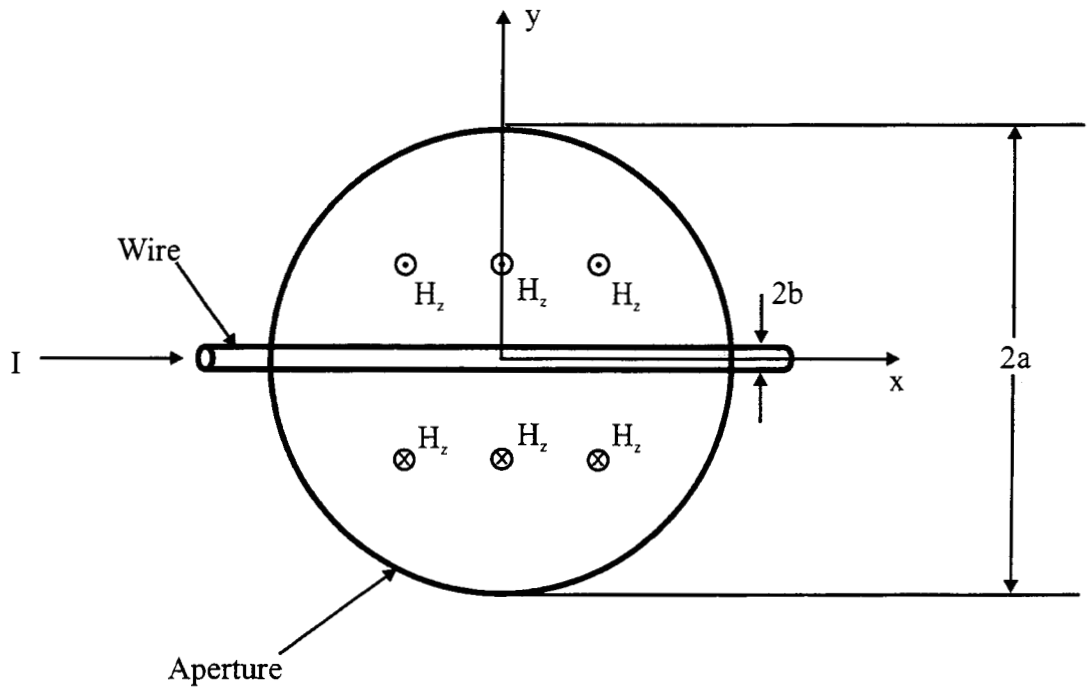

Figure 21. Lightning Current Guided Across Circular Aperture by Wire

Substituting for H_0 we obtain

$$V_{\max} = \frac{\mu_0 a}{\pi} \frac{4}{3\pi} \frac{a}{r^3} A_{loop} \frac{\partial I}{\partial t} \tag{28}$$

assuming, as before, that the loop is 10 cm below the aperture ($a = 0.05$ m, $r = 0.1$ m) and, additionally, that the loop area is $A_{loop} = 0.0025$ m^2, $V_{\max} = 8.0$ kV $\times$ 0.424 $\times$ 50 m$^{-2}\times$ 0.0025 m^2 = 0.424 kV.

3.3 Lightning Guided By Wire Across Aperture

The worst-case, but highly-unlikely, scenario is shown in Figure 21. It requires the presence of both a wire, which has fallen across the aperture, and worst-case lightning, which strikes the wire. The wire guides the lightning current across the aperture and causes an H_z field in the plane of the aperture.

$$H_z \approx \left\{ \frac{I}{2\pi|y|} \qquad \text{if } |y| \to b \right.$$

Using equation D-2:

$$\Phi = \frac{\mu_0 I a}{\pi} \left[\ln\left(\frac{8a}{b}\right) - 1 \right]$$

We can get an expression for the voltage on a conducting loop located at the aperture and intercepting all flux entering half the aperture.

$$V_{\max} = \frac{\mu_0 a}{\pi} \left[\ln\left(\frac{8a}{b}\right) - 1 \right] \frac{\partial I}{\partial t} \tag{29}$$

As an example let us again assume that $a = 5$ cm and $b = 1$ mm.(the radius of a typical wire), then $V_{\max} = 8$ kV $\times(5.0) = 40$ kV, which is large compared to the result when the lightning current attaches to the edge (5 kV).

If we now take distance between the conductor loop and the aperture into account, but allowing the loop to integrate all of the flux crossing a ζ_0 surface we can use the fit function of equation D-3 to obtain

$$V_{\max} = \frac{\mu_0 a}{\pi}\left[\ln\left(\frac{\sqrt{1+\zeta_0^2}}{\zeta_0 + (1.436)b/a}\right) + (0.9199)\,\mathrm{arccot}\,\zeta_0 + \frac{\zeta_0}{1+\zeta_0^2}(0.6509)\right]\frac{\partial I}{\partial t} \tag{30}$$

As an example let us assume that $a = 5$ cm, that $z_{top} = 10$ cm from the aperture so $\zeta_0 = 2.00$ and that the wire is a filament of zero radius ($b = 0$). $V_{\max} = 8$ kV $\times [0.112 + 0.427 + 0.260] = 6.4$ kV.

Finally, at sufficient distance away from the aperture, we can use the dipole moment and equation 18 to calculate the $\overrightarrow{H}$ field at the loop location and take the area of the loop into account.

$$\begin{aligned}\phi_m &= \frac{m_y y}{4\pi r^3} \\ &= \frac{m_y r \sin\theta \sin\varphi}{4\pi r^3}\end{aligned}$$

From equation D-1,

$$m_y = -2Ia^2 \tag{31}$$

Therefore,

$$\begin{aligned}H_r &= -\frac{\partial \phi_m}{\partial r} \\ &= \frac{m_y \sin\theta \sin\varphi}{2\pi r^3} \\ H_r^{\max} &= \frac{a^2 I}{\pi r^3}\end{aligned}$$

and allowing the field to double inside due to the presence of metal pieces

$$\begin{aligned}\Phi &= \mu_0 2 H_r^{\max} A_{loop} \\ &= \mu_0 2 \frac{a^2 I}{\pi r^3} A_{loop}\end{aligned}$$

$$V_{\max} = \frac{\mu_0 a}{\pi} 2 \frac{a}{r^3} A_{loop} \frac{\partial I}{\partial t} \tag{32}$$

As before if we assume that the loop is 10 cm below the aperture ($a = 0.05$ m, $r = 0.1$ m) and, additionally, that the loop area is $A_{loop} = 0.0025$ m^2, $V_{\max} = 8.0$ kV $\times$ 2 $\times$ 50 m$^{-2}\times$ 0.0025 m^2 = 2 kV.

The equations developed in this section can also be used to analyze the type of sensor shown in Figure 2. Since the plunger is made of a non-metallic material, we can ignore its effects and analyze the hole through which the plunger fits as a circular aperture. Typically, $a = 1.0$ cm for these types of sensors, so using equation 25, (because the presence of the plunger prevents the worst-case scenario of a wire falling across the aperture), we obtain $V_{\max} = 1.04$ kV, without needing to take loop position or geometry into account.

3.4 Uniform Electric Field Coupling

Only magnetic field can couple through a narrow slot – there is no significant electric field coupling. Electric field can couple through the circular aperture, however, and we will examine electric field coupling in this section. The analysis of this section has many similarities with Section 3.1 and uses the method outlined in [6]. We ignore the effect of the cover or content geometry on the $\overrightarrow{E}$ field and simplify the problem to that of a circular aperture in an infinite ground plane as shown in Figure 22.Figure .23. shows what is happening physically. An $\overrightarrow{E}$ field normal to the aperture enters the Faraday cage and induces voltage on a wire inside.We begin the analysis by solving for the electric scalar potential ϕ when a uniform

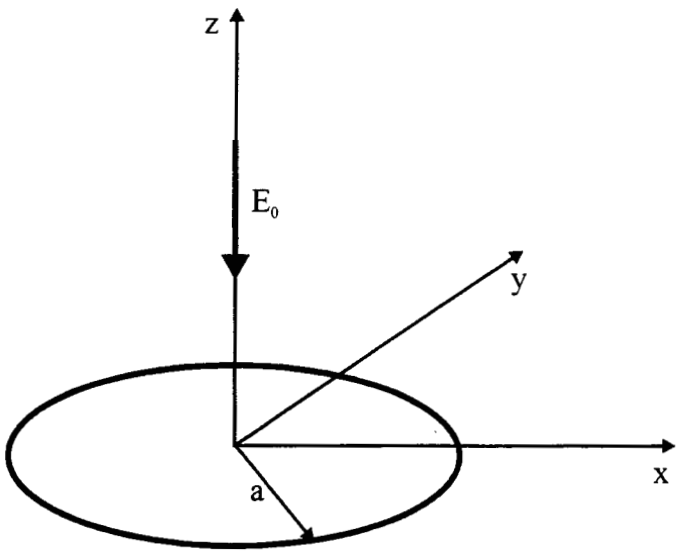

Figure 22. Circular Aperture Driven by E Field

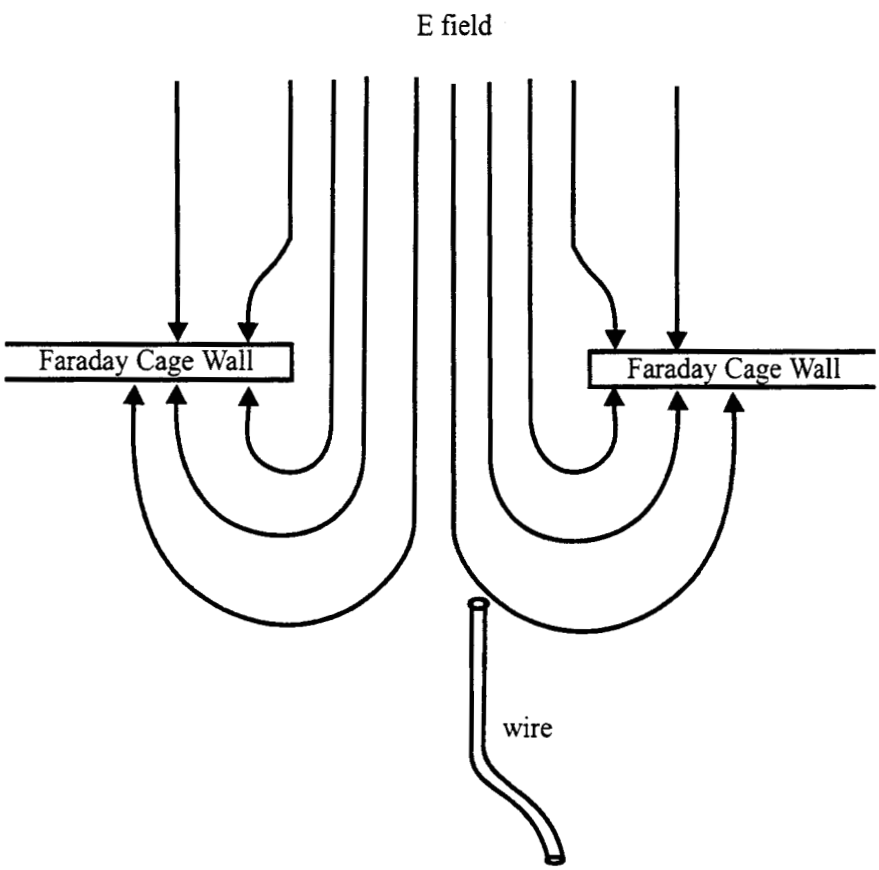

Figure 23. E field Coupling Through Aperture

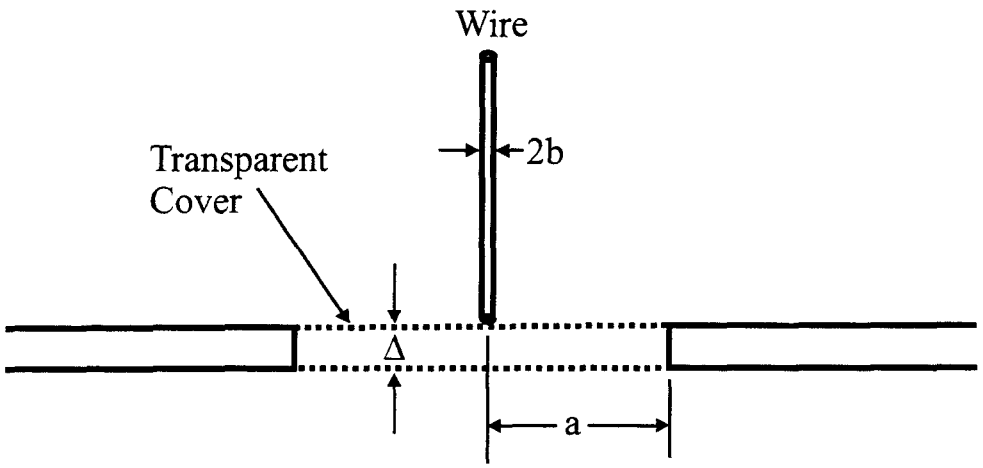

Figure 24. Wire Touching Center of Aperture

E field (E_0), exists on one side of the aperture. ϕ is related to the E field by the equation

$$\vec{E} = -\nabla\phi \tag{33}$$

and satisfies Laplace's equation. We can again use the oblate spheroidal coordinate system shown in Figure 16. . Symmetry of the geometry and the form of the incident field makes the coefficients of all modes in the general series solution (the same type of series as shown in equation 20) to be zero except for the coefficients of m=0, n=1. Matching the potential at $z = +\infty$, where $\phi = Er\cos\theta$ and at $z = -\infty$, where $\phi = 0$ yields

$$\phi = aE_0\xi\left[\zeta - \frac{1}{\pi}\left(\zeta\,\mathrm{arccot}\,\zeta - 1\right)\right] \tag{34}$$

Note that in the $-z$ region, ζ is negative and the branch cut definition is $\mathrm{arccot}(-\zeta) = \pi - \mathrm{arccot}(+\zeta)$. We imagine that lightning strikes the building where the Faraday cage is located causing a voltage difference between floor and ceiling and immersing the cage in a uniform E field. In order to calculate the E field, therefore, we need specifics of the enclosing structure. This is markedly different than the H field penetration, where we only needed the characteristics of the lightning current itself.

To obtain a solution for the potential without having to account for building characteristics, Appendix E examines the case where a wire touches the center of a circular aperture and lightning strikes the wire. The wire is prevented from entering the aperture by a sheet of transparent material that covers the aperture. This case is shown in Figure 24.

Manipulating equation E-6, we obtain

$$V_{\max} \approx \frac{E_b a}{\ln(2a/b)} \ln\left(\frac{a}{\Delta}\right)$$

Returning to our example where $a = 5$ cm and $b = 1$ mm, we assume that $\Delta = 3$ mm, which is a typical thickness for a transparent viewing port cover. We note from Figure 26 that for gaps of approximately 5 cm, $E_b = 10$ kV/cm, so $E_b a = 50$ kV. $V_{\max}$ then is 30.5 kV, which is large, but is bounded by the wire-across-aperture case (40 kV) discussed previously.

Next we use equation E-10 to obtain

$$V_{\max} \approx \frac{E_b a}{\ln(2a/b)} \frac{1}{2} \ln\left(\frac{1+\zeta_0^2}{\zeta_0^2 + \Delta^2/a^2}\right) \tag{35}$$

If we take our observation point to be 10 cm below the aperture as in previous examples ($\zeta_0 = z_{top}/a = 2.00$) and substitute in equation 35 we obtain $V_{\max} = 1.2$ kV. This is a smaller voltage than the wire-across-aperture case (6.4 kV) discussed previously.

It is interesting to note that in equation 34, if we set

$$E_0 = E_b \frac{3\pi/2}{\ln(2a/b)}$$

(where the quantities on the right hand side are defined in Appendix E), we find that the uniform field solution preserves the far field dipole solution found in equation E-7.

4 Diffusion

A low-frequency, magnetic field can penetrate a finitely-conducting wall of a Faraday cage by means of diffusion. Usually, when the conductivity of the wall is high, like that of aluminum, the voltage due to diffusion is negligible, even if the wall is thin. We include the effect here to document the equation and demonstrate that the voltage is small.

The worst-case situation for diffusion is if lightning current flows near a conducting wall, on the other side of which is a cable loop having a length along the wall of l as shown in Figure 25. Note that the loop could be formed by a cable in combination with the wall, so the voltage induced between the cable and the wall due to the magnetic field diffusing through the thickness of the wall is calculated in accordance to the following formula for non-magnetic wall materials:

$$V \approx \frac{4lI}{\pi\sigma\Delta^2}\left[e^{-T}\left\{T + \frac{3}{2}\left(1+\frac{1}{T}\right) - \left(2+\frac{3}{T}\right)\sqrt{T/\pi}\right\} - \frac{3}{2T}\,\mathrm{erf\,c}\left(\sqrt{T}\right)\right]$$

where $T = t_s/(4t)$, $t_d = \mu\sigma\Delta^2$. The peak voltage is

$$V_d = \frac{4lI}{\pi e\sigma\Delta^2}(0.54) \tag{36}$$

where σ is the conductivity of the wall, Δ is the thickness of the wall, I is the peak lightning current and e is the base of the natural logarithm (2.718).

Let us assume that the wall of the Faraday cage is made of 6061 aluminum ($\sigma = 2.6 \times 10^7\ (\Omega - \mathrm{m})^{-1}$) and has a thickness of 1.5 mm. Assume that the length of the cable l is approximately 0.3 meters. With the above parameters $V_d = 260$ V. This is much smaller than the kilovolt range of the other effects.

5 Standoff

Once the voltage available on the inside of the Faraday cage is calculated, we must determine if the electrical insulation that exists inside the Faraday cage, such as air gaps and insulation around wires, will hold off the voltage and keep current from flowing onto the sensitive contents. Because there is a wide variety of insulating material present inside the Faraday cages, the only insulation that we will discuss here is that provided by an air gap because that type of insulation is common to all. In determining the amount of voltage that an air gap will hold off, we use the information provided in [8] for needlepoints because needlepoints require the least amount of voltage to breakdown, and therefore, provide a worst-case estimate; in other words, if the needlepoint gap won't breakdown, other types of gaps won't breakdown either. The data from [8] is shown in Figure 26 for convenience.

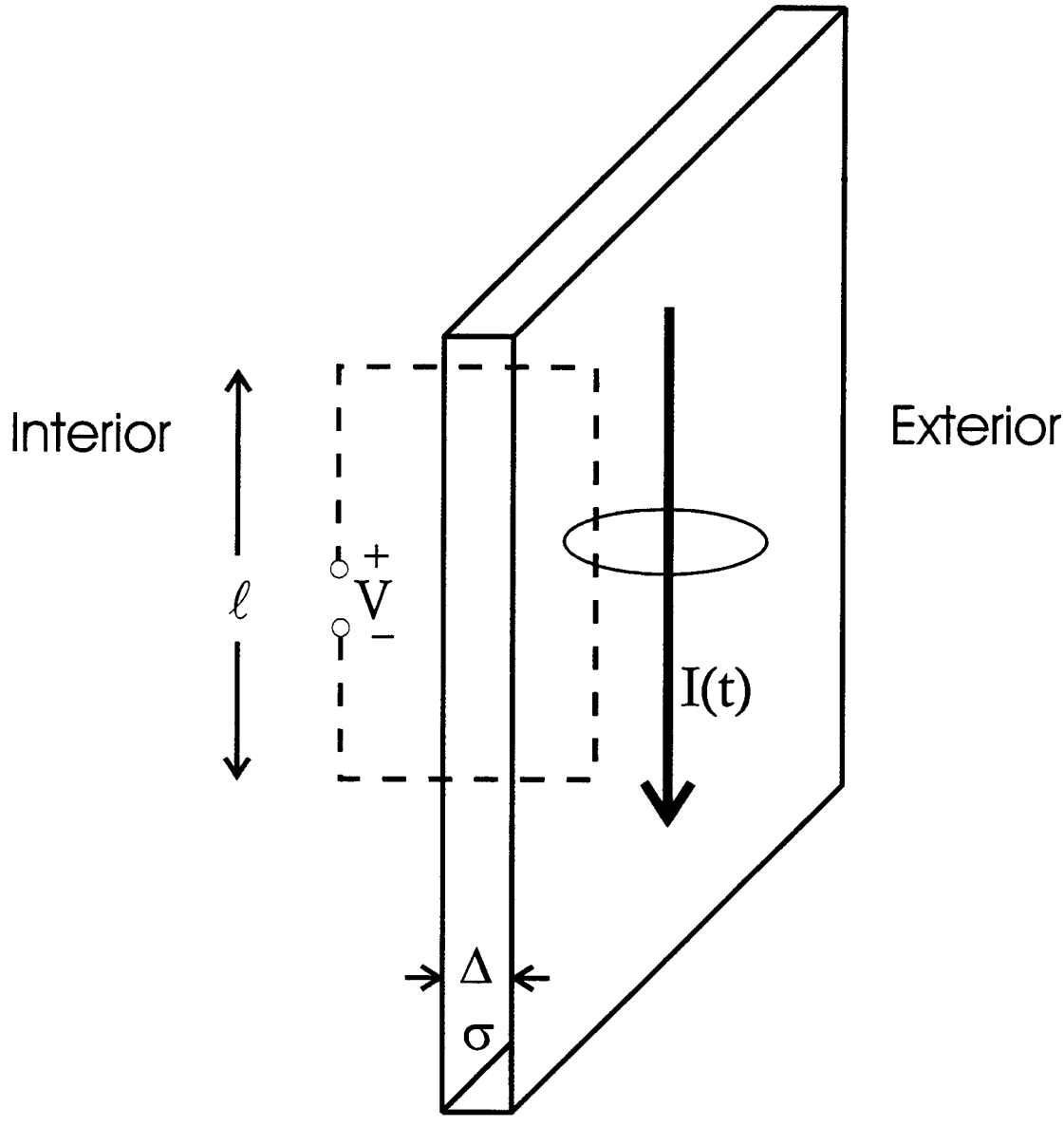

Figure 25. Geometry Details of the Diffusion Calculation

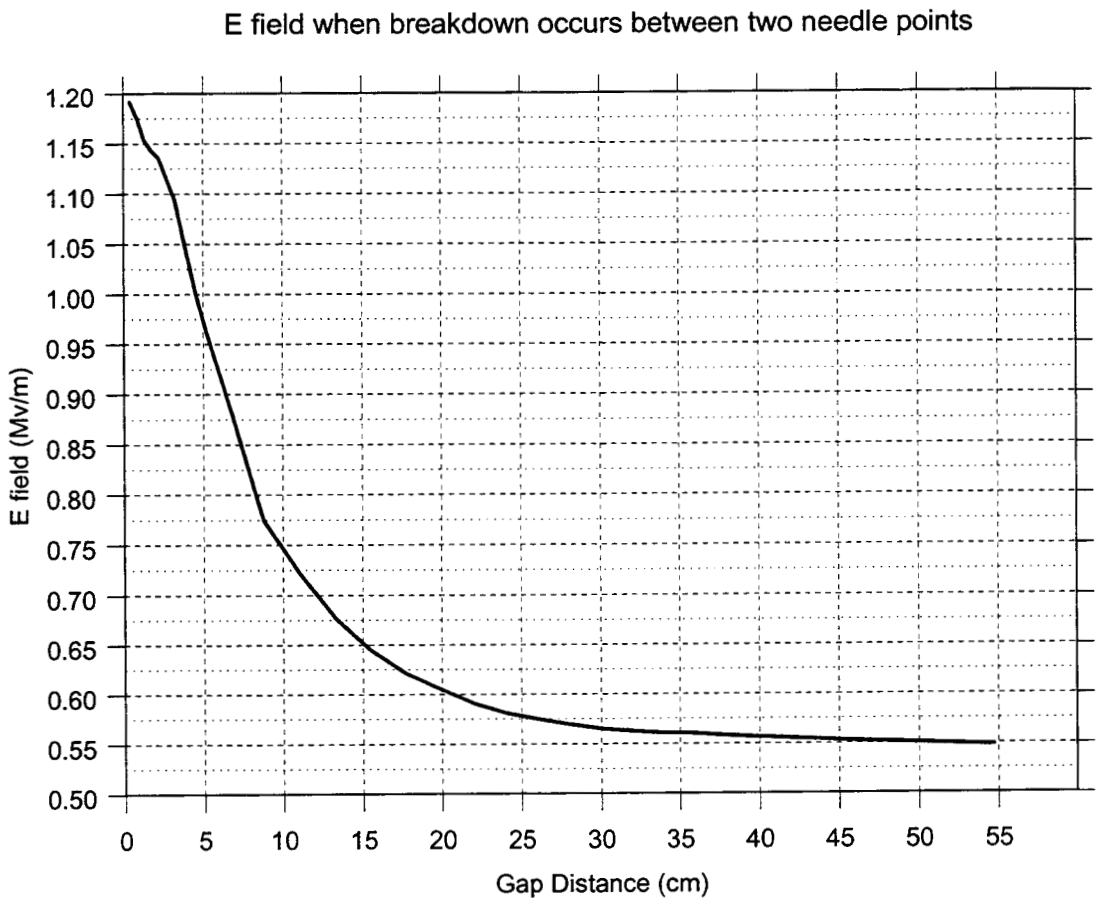

Figure 26. E field Required to Breakdown a Needle Point Gap

As an example, if the maximum voltage inside a Faraday cage is determined to be 3 kV and a critical air gap is measured to be 15 cm, we see from Figure 26 that the air gap is expected to stand off 0.65 MV/m or 97 kV (0.65 MV/m $\times$ 0.15m) so we don't expect the air gap to break down.

6 Burnthrough

Burnthrough is associated with the continuing current component of lightning that occurs in late time after the leading edge of the lightning waveform. The lightning arc becomes so hot that it melts the metal at the attachment point and forms a hole. The lightning increases the size of the hole by moving around the hole edge and continuing to melt the metal. Unpublished tests performed for Sandia by the Bundeswehr Universität München (German Armed Forces University in Munich) where worst-case continuing current was attached to plates of various metals indicate that lightning will not burn through a 0.1875 inch thick steel plate, but it will burn through a 0.1875 inch thick aluminum plate quite easily. The burnthrough holes are on the order of 1 cm in diameter. Fortunately, a standoff distance imposed around the sensitive contents helps in this situation since it is unlikely that lightning will detach from the edge of the burnthrough hole, pass through the hole and attach to contents several hole diameters behind. If standoff is not imposed and the sensitive contents lie directly behind the hole, it is not clear what will happen. A single test on a flat cable lying 0.2 inches behind a burnthrough hole indicates that the voltage induced on the cable is less than 50 volts [9].

7 References

[1] R. J. Fisher and M. A. Uman, *Recommended Baseline Direct-Strike Lightning Environment for Stockpile-to-Target Sequences*, Sandia Report SAND89-0192, UC-13, May 1989, p. 11.

[2] W. C. Hart and E. W. Malone, *Lightning and Lightning Protection,* EEC, Inc., Gainesville, Virginia, 1988, p.3.19.

[3] L. K. Warne and K.C. Chen, "A simple transmission line model for narrow slot apertures having depth and losses," *IEEE Trans. Electromagnetic Compatibility*, vol. 34, no. 3, Aug. 1992, pp. 173-182.

[4] K. O. Merewether, "Analysis of W84, W70 and W79 nuclear weapon shipping and storage containers in response to nearby lightning," Sandia Technical Memorandum to M.E. Morris, Sandia National Laboratories, Albuquerque, May 1, 1990.

[5] L. K. Warne, K. O. Merewether and R. E. Jorgenson, "Nonlinear Diffusion and Slot Voltages", to be published.

[6] W. R. Smythe, *Static and Dynamic Electricity*, Hemisphere Publishing Corp., New York, 1989, pp. 168-177.

[7] P. Moon and D. E. Spencer, *Field Theory Handbook,* Springer-Verlag, New York, 1988, pp. 31-34.

[8] R. C. Weast, *Handbook of Chemistry and Physics, 55th edition*, CRC Press, Cleveland OH, 1974, p. E-55.

[9] G. H. Schnetzer, R. J. Fisher and M. A. Dinallo, *Measured Responses of Internal Enclosures and Cables due to Burnthrough Penetration of Weapon Cases by Lightning*, Sandia Report SAND94-0312, UC-706, Aug. 1994.

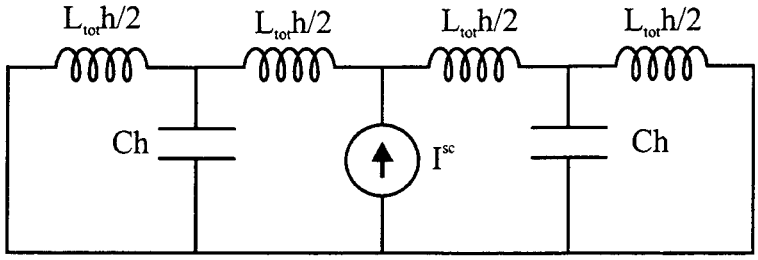

Figure 1. Lumped Circuit Model of Transmission Line

Appendix A. Transmission Line Model

In this appendix we will examine approximations of the transmission line models in various limits in order to show how simplified circuits follow naturally from more complex analysis. Using techniques described in [A-1] we can obtain an expression for the voltage along a transmission line, which is driven by a current source I at $z = 0$ and is shorted at $z = h$ and $z = -h$. A time dependency of $e^{j\omega t}$ is assumed.

$$V(z) = \frac{Z_0 I}{\sinh(2\gamma h)} \sinh(\gamma h) \sinh \gamma(h + z) \qquad \text{where } -h < z < 0 \qquad \text{(A-1)}$$

$$V(z) = \frac{Z_0 I}{\sinh(2\gamma h)} \sinh(\gamma h) \sinh \gamma(h - z) \qquad \text{where } 0 < z < +h$$

If the transmission line is lossless, $\gamma = j\omega\sqrt{L_{tot}C}$, which is the propagation constant and $Z_0 = \sqrt{L_{tot}/C}$, which is the characteristic impedance. C, the capacitance per unit length, is expressed in terms of the slot parameters as

$$C = \epsilon\frac{d}{w} + \epsilon\frac{2}{\pi}\left[\ln\left(\frac{8h}{w}\right) + \ln 2 - \frac{7}{3}\right]$$

where ϵ is the permittivity of the material filling the slot (8.854×10^{-12} Farads/meter for free space). Let us calculate some of the above parameters at $\omega = 2 \times 10^6$ radians/second for a slot having the following dimensions: $w = 1.0$ mm, $d = 25.0$ mm and $2h = 500.0$ mm. $C = 0.255$ nF/m, and $L_{tot} = 43.6$ nH/m so $\gamma = .0067$ radians/m. Since γ is so small, the $\sinh(\gamma x)$ terms in equation A-1 can be replaced by their small argument approximation (γx) yielding

$$V(z) = \frac{Z_0 I}{2}\gamma(h + z) \qquad \text{where } -h < z < 0 \qquad \text{(A-2)}$$

$$V(z) = \frac{Z_0 I}{2}\gamma(h - z) \qquad \text{where } 0 < z < +h$$

These equations state that the voltage is zero at $z = -h$, increases linearly to the value of $j\omega I L_{tot}h/2$ (substituting for Z_0 and γ), and then decreases linearly to zero at $z = +h$. Recognizing that the expression $j\omega I$ in the frequency domain is equivalent to $\partial I/\partial t$ in the time domain, we have obtained

$$V_{pec} = L_{slot}\frac{\partial I}{\partial t} \qquad \text{(A-3)}$$

where $L_{slot} = L_{tot}h/2$.

From a circuit point of view, if we replace the transmission line by the lumped circuit shown in Figure 1, we note that at $\omega = 2 \times 10^6$ radians/second we have the impedance of the capacitance ($-j7.84$ kΩ) in parallel with the impedance of the inductance ($+j0.011$ Ω). Over five orders of magnitude difference between the two impedances implies that the shunting capacitance can be ignored without affecting the results.

If the transmission line is lossy (accounting for the conductive gasket), since γ has a large, real part, we

can replace the $\sinh(\gamma x)$ terms in the equation A-1 by $e^{\gamma x}/2$ yielding

$$\begin{aligned} V(z) &= \frac{Z_0 I}{e^{2\gamma h}} e^{\gamma h} \frac{e^{\gamma(h+z)}}{2} && \text{where } -h/2 < z < 0 \\ &= \frac{Z_0 I}{2} e^{\gamma z} \end{aligned} \tag{A-4}$$

$$\begin{aligned} V(z) &= \frac{Z_0 I}{e^{2\gamma h}} e^{\gamma h} \frac{e^{\gamma(h-z)}}{2} && \text{where } 0 < z < +h/2 \\ &= \frac{Z_0 I}{2} e^{-\gamma z} \end{aligned}$$

where we have changed the upper and lower range of z to ensure that we stay away from $\pm h$ where our approximation of $\sinh(\gamma x)$ doesn't hold. These equations state that the voltage at the current source is $Z_0 I/2$ and that the voltage falls off exponentially in each direction toward the teminating bolts.

A.1 References

[A-1]P. E. Mayes, *Electromagnetics for Engineers,* Edwards Brothers, Inc., Ann Arbor, Michigan, 1965, pp.1-103.

Appendix B. Voltage with Lossy Gasket

Here we assume that a lossy gasket fills the slot and that the decay length in the gasket is sufficiently short that we can ignore the ends of the slot when it is driven at the center with current I_0. We treat the problem as two dimensional in the slot interior and it is thus convenient in this section to take the x coordinate along the slot length, the y coordinate in the slot depth direction, and the z coordinate in the slot width direction. The fields are taken as independent of z in the slot interior. The problem is set up with $-\infty < x < \infty$, $0 < y < d$, and $0 < z < w$. We symmetrize about $y = 0$ and extend the region to $-d < y < d$. This symmetrization requires us to double the drive current $I = 2I_0$. In the interior region there is only E_z, H_x, and H_y. Maxwell's equations with time dependence $e^{j\omega t}$ are

$$\nabla \times \underline{E} = -j\omega\mu_g \underline{H}$$

$$\nabla \times \underline{H} = \underline{J} + (\sigma_g + j\omega\varepsilon_g)\,\underline{E}$$

where μ_g is the magnetic permeability of the gasket, σ_g is the electric conductivity of the gasket, and ε_g is the electric permittivity of the gasket. Eliminating the magnetic field gives

$$\nabla \times \nabla \times \underline{E} = \nabla(\nabla \cdot \underline{E}) - \nabla^2 \underline{E} = -j\omega\mu_g \underline{J} - j\omega\mu_g(\sigma_g + j\omega\varepsilon_g)\,\underline{E}$$

Taking the divergence of the field to vanish ($\partial E_z/\partial z = 0$), with only a z component, gives

$$\left(\nabla^2 + k_g^2\right) E_z = j\omega\mu_g J_z$$

where the complex gasket wavenumber is found from

$$k_g^2 = -j\omega\mu_g(\sigma_g + j\omega\varepsilon_g)$$

Note that $\mathrm{Im}(k_g) < 0$. The current is taken as a zero radius filament at the origin in the z direction

$$\left(\frac{\partial^2}{\partial x^2} + \frac{\partial^2}{\partial y^2} + k_g^2\right) E_z = \left[\frac{1}{\rho}\frac{\partial}{\partial\rho}\rho\frac{\partial}{\partial\rho} + \frac{1}{\rho}\frac{\partial^2}{\partial\varphi^2} + k_g^2\right] E_z = j\omega\mu_g I\delta(x)\,\delta(y) = j\omega\mu_g I\frac{\delta(\rho)}{2\pi\rho}$$

The electric field radiated by the filament (two dimensional Green's function), without boundary conditions is

$$E_z^i = \left(-j\omega\mu_g I\right)\frac{-j}{4}H_0^{(2)}(k_g\rho) = -\omega\mu_g I_0\frac{1}{2}H_0^{(2)}\left(k_g\sqrt{x^2+y^2}\right)$$

where $H_0^{(2)}(z) = J_0(z) - jY_0(z)$ is the Hankel function of the second kind. The $y = \pm d$ edges of the symmetrized slot interior are taken as open circuits. This implies the boundary conditions

$$H_x(x, \pm d) = 0$$

The magnetic field is found from the electric field by means of

$$-j\omega\mu_g H_x = \frac{\partial E_z}{\partial y}$$

Thus we want

$$\frac{\partial E_z}{\partial y}(x, \pm d) = 0$$

and

$$E_z(x,y) \to 0\,,\; x \to \pm\infty$$

The total field can thus be expanded in the modal series

$$E_z = \sum_{n=0}^{\infty} A_n e^{-j|x|\sqrt{k_g^2 - n^2\pi^2/d^2}} \cos(n\pi y/d)$$

Substituting into the Helmholtz equation gives

$$\sum_{n=0}^{\infty} A_n \left(\frac{\partial^2}{\partial x^2} + k_g^2 - n^2\pi^2/d^2\right) e^{-j|x|\sqrt{k_g^2 - n^2\pi^2/d^2}} \cos(n\pi y/d) = j\omega\mu_g I\delta(x)\,\delta(y)$$

Using the orthogonality relation

$$\int_{-d}^{d} \cos(n\pi y/d)\cos(n'\pi y/d)\,dy = \frac{2d}{\varepsilon_n}\delta_{nn'}$$

where $\varepsilon_n = 2$ for $n \geq 1$, but equals unity for $n = 0$, gives

$$\frac{2d}{\varepsilon_n} A_n \left(\frac{\partial^2}{\partial x^2} + k_g^2 - n^2\pi^2/d^2\right) e^{-j|x|\sqrt{k_g^2 - n^2\pi^2/d^2}} = j\omega\mu_g I\delta(x)$$

Integrating over a small distance about the origin

$$\int_{-\Delta}^{\Delta} dx\,,\; \Delta \to 0$$

gives

$$-j\frac{2d}{\varepsilon_n} A_n 2\sqrt{k_g^2 - n^2\pi^2/d^2} = j\omega\mu_g I$$

or

$$A_n = \frac{-\omega\mu_g I\varepsilon_n}{4\sqrt{k_g^2 d^2 - n^2\pi^2}}$$

Now we want the value of the voltage

$$V = -E_z w$$

at $x = 0$, $y = d$. This is given by

$$V = \frac{1}{2}\omega\mu_g I_0 w \sum_{n=0}^{\infty} \frac{\varepsilon_n (-1)^n}{\sqrt{k_g^2 d^2 - n^2\pi^2}}$$

$$= \frac{1}{2}\omega\mu_g I_0 w \left[\frac{1}{k_g d} + 2\sum_{n=1}^{\infty}(-1)^n \left\{\frac{1}{\sqrt{k_g^2 d^2 - n^2\pi^2}} - \frac{1}{(-jn\pi)}\right\} - j\frac{2}{\pi}\ln 2\right] \qquad \text{(B-1)}$$

where the sum

$$\sum_{n=1}^{\infty} \frac{(-1)^n}{n} = -\ln 2$$

has been used. Note that the asymptotic form for $k_g d \to 0$ is

$$V/(I_0/2) \sim \frac{\omega \mu_g w}{k_g d} - j\omega\mu_g w \frac{2}{\pi} \ln 2$$

$$\sim Z_0 - j\omega\mu_g w \frac{2}{\pi} \ln 2 \tag{B-2}$$

where $Z_0 = (w/d)\sqrt{j\omega\mu_g/(\sigma_g + j\omega\varepsilon_g)}$ is the characteristic impedance of the gasket filled stripline and the reactive term results from the characteristics of the filament drive..

When $k_g d >> 1$ we can take the solution to be asymptotically the sum of the incident field and a reflection in the $y = d$ boundary

$$E_z \sim 2E_z^i = -\omega\mu_g I_0 H_0^{(2)}(k_g d)$$

and

$$V \sim w\omega\mu_g I_0 H_0^{(2)}(k_g d)$$

We can also add the remaining images in the $y = -d$ boundary to obtain and alternative representation for V

$$V = w\omega\mu_g I_0 \sum_{n=0}^{\infty} H_0^{(2)}(k_g(2n+1)d) \tag{B-3}$$

Figure 1 shows a comparison of equations B-1 and B-2. As the conductivity becomes large, equation B-2 overestimates the voltage.

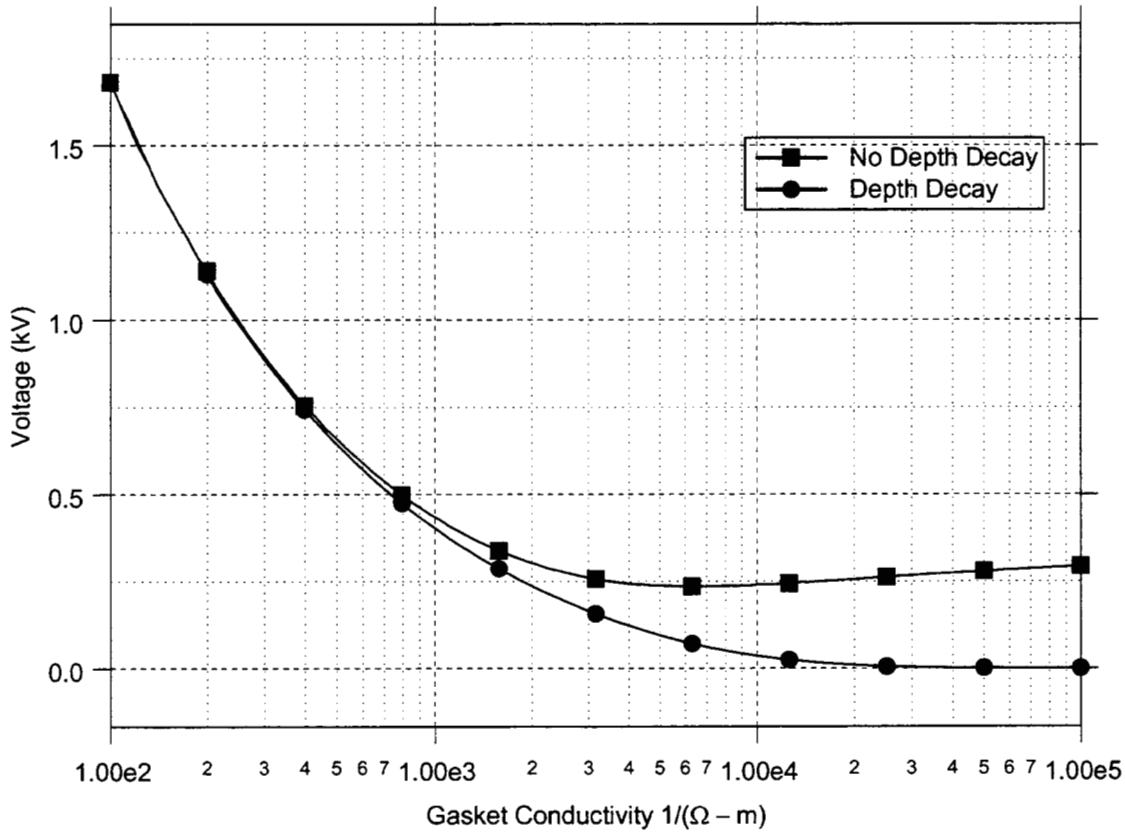

Figure 1. Comparison of Equations (B-1) and (B-2), d=25mm, w=3mm

Appendix C. Electric Current Filament Normal to Plane at Hole Edge

The lightning current I is positive z directed, it is attached to the edge of a circular hole of radius a, and is normal to the plane containing the hole. The problem is to find the fields penetrating the hole. The magnetic field is represented in terms of the scalar potential

$$\overrightarrow{H} = -\nabla\phi_m$$

where in regions free of current

$$\nabla^2\phi_m = 0$$

Here we will first use cylindrical coordinates to represent the short circuit field (the field with the hole shorted), then transition to oblate spheroidal coordinates to solve the actual problem. The short circuit drive can be taken as

$$\phi_m^{sc} = -\frac{I}{2\pi}\varphi' = -\frac{I}{2\pi}\arctan\left(\frac{y'}{x'}\right) = -\frac{I}{2\pi}\arctan\left(\frac{y}{x+a}\right)$$

$$= -\frac{I}{2\pi}\arctan\left(\frac{\rho\sin\varphi}{\rho\cos\varphi + a}\right) = -\frac{I}{2\pi}\arctan\left[\frac{(\rho/a)\sin\varphi}{1+(\rho/a)\cos\varphi}\right]$$

where $-\pi < \varphi' < \pi$ is the cylindrical coordinate with origin at the wire, $0 < \rho < \infty$ and $-\pi < \varphi < \pi$ are cylindrical coordinates with origin at the aperture center. The relations between the Cartesian (x, y, z) and cylindrical (ρ, φ, z) systems are

$$x = \rho\cos\varphi$$

$$y = \rho\sin\varphi$$

$$z = z$$

Expanding in cylindrical coordinates we can write

$$\phi_m^{sc} = -\frac{I}{2\pi}\left[-\sum_{m=1}^{\infty}\frac{1}{m}(-\rho/a)^m\sin(m\varphi)\right], \; 0 < \rho/a < 1$$

$$= -\frac{I}{2\pi}\left[\varphi + \sum_{m=1}^{\infty}\frac{1}{m}(-\rho/a)^{-m}\sin(m\varphi)\right], \; \rho/a > 1$$

The total potential is taken as

$$\phi_m^{tot} = \phi_m^{sc} + \phi_m \,, \; z > 0$$

$$= \phi_m \,, \; z < 0$$

where ϕ_m is the potential scattered by the hole. Continuity of the normal magnetic field at the aperture, the fact that it vanishes on the conducting plane, and the vanishing of the normal component of the short circuit field, means that

$$\frac{\partial \phi_m}{\partial z} \text{ continuous at } z = 0$$

$$\frac{\partial \phi_m}{\partial z}(\rho, \varphi, z) = 0\,,\ a < \rho < \infty$$

Continuity of the tangential component of the magnetic field in the hole means that

$$\phi_m^{sc}(\rho, \varphi) + \phi_m(\rho, \varphi, +0) = \phi_m(\rho, \varphi, -0)\ ,\ 0 < \rho < a$$

Noting that ϕ_m is odd in z gives

$$\phi_m(\rho, \varphi, +0) = -\frac{1}{2}\phi_m^{sc}(\rho, \varphi)\ ,\ 0 < \rho < a$$

If we immerse a PMC (perfect magnetic conductor) disc of radius a in a potential field

$$\phi_m^i(\rho, \varphi) = \frac{1}{2}\phi_m^{sc}(\rho, \varphi)$$

we will find the same scattered potential as the hole problem in the upper half space $z > 0$ and negative the scattered potential of the hole problem in the lower half space $z < 0$ (the incident and scattered potentials in the disc problem are even in z). We will, therefore, solve the PMC disc problem and use the results for the hole problem.

C.1 PMC Disc Solution in Oblate Spheroidal Coordinate System

The incident potential is taken as

$$\phi_m^i(\rho, \varphi) = \frac{1}{2}\phi_m^{sc}(\rho, \varphi) = -\frac{I}{4\pi}\left[-\sum_{m=1}^{\infty}\frac{1}{m}(-\rho/a)^m \sin(m\varphi)\right]\ ,\ 0 < \rho/a < 1$$

$$= -\frac{I}{4\pi}\left[\varphi + \sum_{m=1}^{\infty}\frac{1}{m}(-\rho/a)^{-m}\sin(m\varphi)\right]\ ,\ \rho/a > 1$$

The relation between the Cartesian system (x, y, z) and the oblate spheroidal system (ξ, ζ, φ) shown in Figure 1 is [C-1]

$$x = a\sqrt{1+\zeta^2}\sqrt{1-\xi^2}\cos\varphi$$

$$y = a\sqrt{1+\zeta^2}\sqrt{1-\xi^2}\sin\varphi$$

$$z = a\zeta\xi$$

where $-1 < \xi < 1$, $0 < \zeta < \infty$, and $-\pi < \varphi < \pi$. (Note the differences in the coordinate ranges shown in Figures 16 and 1). The relation between this system and the cylindrical system is

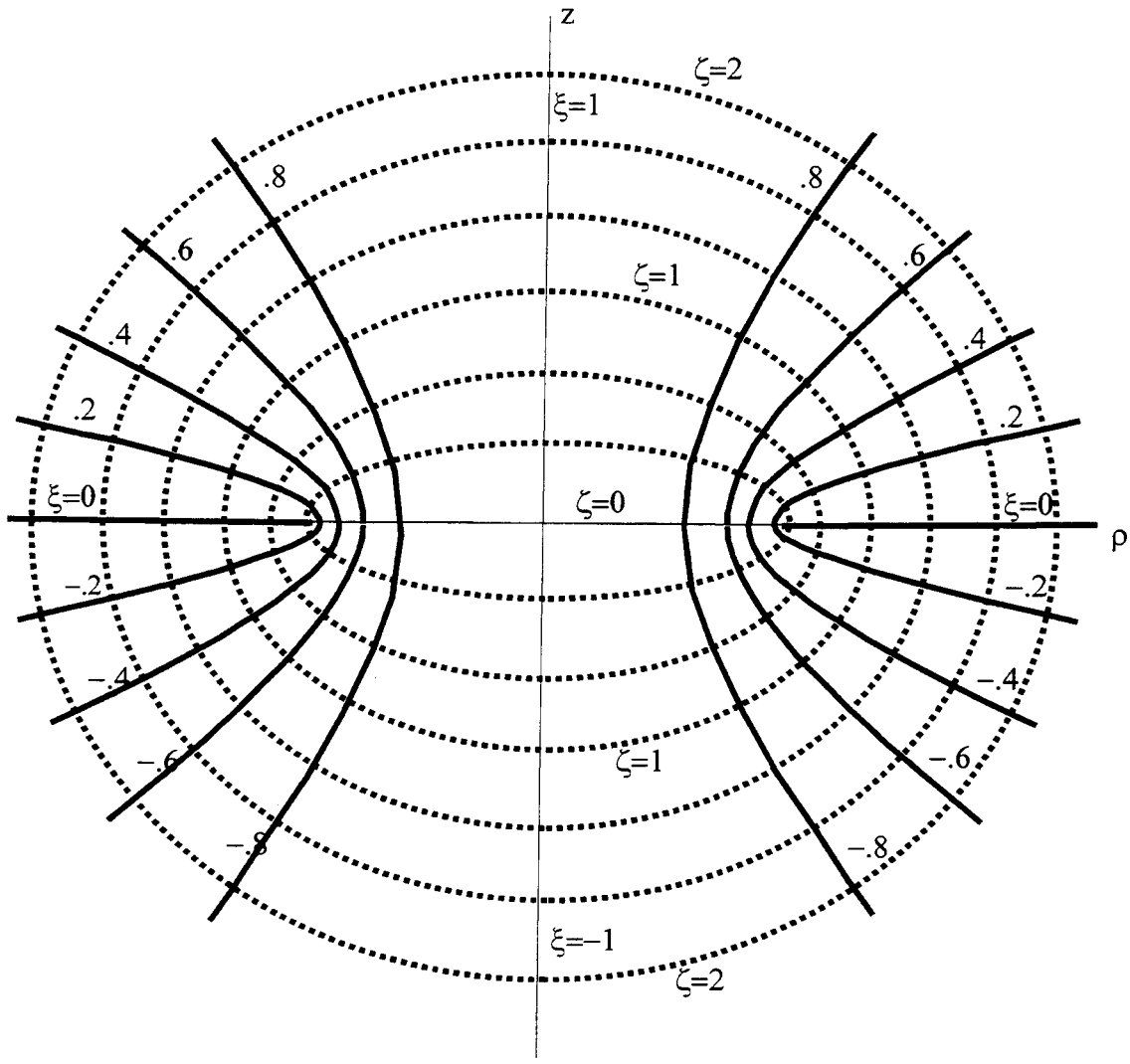

Figure 1. Oblate Spheroidal Coordinate System Used in Appendix

$$\rho = a\sqrt{1+\zeta^2}\sqrt{1-\xi^2}$$

$$\varphi = \varphi$$

$$z = a\zeta\xi$$

Note that

$$r = \sqrt{\rho^2+z^2} = a\sqrt{1+\zeta^2-\xi^2} \sim a\zeta\,,\ \zeta \to \infty$$

The general solution of Laplace's equation in this system is

$$\begin{aligned}\phi_m(\zeta,\xi,\varphi) &= \sum_n\sum_m \left[A_{mn}P_n^m(j\zeta) + B_{mn}Q_n^m(j\zeta)\right]\left[C_{mn}P_n^m(\xi) + D_{mn}Q_n^m(\xi)\right]\times \\ &\quad \left[E_{mn}\sin(m\varphi) + F_{mn}\cos(m\varphi)\right]\end{aligned}$$

where $j = \sqrt{-1}$ is the imaginary unit and P_n^m and Q_n^m are associated Legendre functions. The definitions of the special functions corresponds to that given in [C-2] and [C-3]. We eliminate A_{mn} so the scattered potential decays as $\zeta \to \infty$. We eliminate D_{mn} so the scattered potential remains finite along the z axis $\xi = 1$. We eliminate F_{mn} by symmetry and thus

$$\phi_m(\zeta,\xi,\varphi) = \sum_{n=1}^{\infty}\sum_{m=1}^{n} B_{mn}Q_n^m(j\zeta)\,P_n^m(\xi)\sin(m\varphi)$$

where $P_n^m(\xi) = 0$ for $m > n$ has been used. The boundary condition on the disc for the scattered potential is

$$\phi_m(0,\xi,\varphi) = -\phi_m^i(\xi,\varphi)$$

As a result of symmetry in the disc problem, the boundary condition $\frac{\partial\phi_m}{\partial z}(\rho,\varphi,0) = 0$ for $a < \rho < \infty$, is automatically satisfied. We need to expand the incident potential in the aperture in order to match the boundary condition. Letting $\zeta = 0$ and $\rho/a = \sqrt{1-\xi^2}$ in the cylindrical coordinate expression gives

$$\phi_m^i(\xi,\varphi) = \frac{I}{4\pi}\sum_{m=1}^{\infty}\frac{1}{m}\left(-\sqrt{1-\xi^2}\right)^m \sin(m\varphi)\,,\ -1 < \xi < 1$$

Noting that [C-4]

$$P_n(\xi) = \frac{(2n)!}{2^n(n!)^2}\left[\xi^n + O\left(\xi^{n-2}\right)\right]\,,\ \xi \to 0$$

and [C-2]

$$P_n^m(\xi) = \left(-\sqrt{1-\xi^2}\right)^m \frac{d^m}{d\xi^m}P_n(\xi)$$

gives

$$P_m^m(\xi) = \frac{(2m)!}{2^m m!}\left(-\sqrt{1-\xi^2}\right)^m$$

and thus

$$\phi_m^i(\xi,\varphi) = \frac{I}{4\pi}\sum_{m=1}^{\infty}\frac{2^m m!}{m(2m)!}P_m^m(\xi)\sin(m\varphi)\ ,\ -1<\xi<1$$

Applying the boundary condition on the disc and noting the orthogonality relations

$$\int_{-\pi}^{\pi}\sin(m\varphi)\sin(m'\varphi)\,d\varphi = \pi\delta_{mm'}$$

$$\int_{-\pi}^{\pi}\sin(m\varphi)\cos(m'\varphi)\,d\varphi = 0$$

and [C-2]

$$\int_{-1}^{1}P_n^m(\xi)\,P_{n'}^m(\xi)\,d\xi = \frac{(n+m)!}{\left(n+\frac{1}{2}\right)(n-m)!}\delta_{nn'}$$

gives

$$B_{mn}Q_n^m(j0) = -\frac{I}{4\pi}\frac{2^m m!}{m(2m)!}\delta_{mn}$$

Reversing the sign of the scattered potential to find the result appropriate to the hole problem yields

$$\phi_m(\zeta,\xi,\varphi) = \frac{I}{4\pi}\sum_{m=1}^{\infty}\frac{2^m m!}{m(2m)!}\frac{Q_m^m(j\zeta)}{Q_m^m(j0)}P_m^m(\xi)\sin(m\varphi)\ ,\ 0<\zeta<\infty\,,\ -1<\xi<0\,,\ -\pi<\varphi<\pi \qquad \text{(C-1)}$$

C.2 Dipole Moment

The field far from the aperture is found from the dipole moment of the aperture. The asymptotic form of the Legendre function is [C-2]

$$Q_n^m(j\zeta) \sim \frac{(-1)^m 2(n+m)!}{\left(\frac{3}{2}\right)_n(2j\zeta)^{n+1}},\ \zeta\to\infty$$

where $(u)_n = \Gamma(u+n)/\Gamma(u) = u\cdot(u+1)\cdots(u+n-1)$, $(u)_0 = 1$, and $\Gamma(x)$ is the gamma function [C-2]. Therefore, the $n=m=1$ term is dominant far from the aperture. The values of the denominator Legendre functions are given by [C-2]

$$Q_n^m(j0) = \sqrt{\pi}\frac{(-1)^m 2^{m-1}\Gamma\left(\frac{1+n+m}{2}\right)}{j^{n+1}\Gamma\left(1+\frac{n-m}{2}\right)}$$

The function for $n=m=1$ is actually

$$Q_1^1(j\zeta) = \sqrt{1+\zeta^2}\left(\operatorname{arccot}\zeta - \frac{\zeta}{1+\zeta^2}\right)$$

where $\pi/2 > \operatorname{arccot}\zeta > 0$ for $0 < \zeta < \infty$. Thus

$$Q_1^1(j0) = \frac{\pi}{2}$$

$$Q_1^1(j\zeta) \sim \frac{2}{3\zeta^2}, \zeta \to \infty$$

and we can write

$$\phi_m \sim \frac{I}{4\pi}\frac{Q_1^1(j\zeta)}{Q_1^1(j0)}P_1^1(\xi)\sin\varphi \sim \frac{I}{4\pi}\frac{4}{3\pi\zeta^2}\left(-\sqrt{1-\xi^2}\right)\sin\varphi$$

$$\sim -\frac{Ia^2y}{3\pi^2r^3}$$

where we have used $y \sim a\zeta\sqrt{1-\xi^2}\sin\varphi$ and $r \sim a\zeta$ as $\zeta \to \infty$. The potential of a magnetic dipole is

$$\phi_m \sim \frac{\vec{m}\cdot\vec{r}}{4\pi r^3}$$

Thus the dipole moment in this case is

$$\underline{m} = -\frac{4a^2}{3\pi}\hat{y} \tag{C-2}$$

It is interesting that for a plane exciting field the dipole moment of an aperture is [C-5]

$$\vec{m} = -2\overleftrightarrow{\alpha}_m \cdot \vec{H}^{sc}$$

The polarizability for a circular aperture is a diagonal tensor

$$\vec{m} = -2\alpha_m \vec{H}^{sc}$$

and has the value [C-5]

$$\alpha_m = \frac{4}{3}a^3$$

This implies that

$$\vec{H}^{sc} = -\frac{I}{2\pi a}\hat{y}$$

which is the value of the field exactly at the middle of the circular aperture.

C.3 Magnetic Flux Through Quarter Spheroid

The magnetic flux crossing one quarter of an oblate spheroid is now found. The magnetic flux crossing

a quarter spheroid with surface at $\zeta = \zeta_0$ is [C-1]

$$\Phi = -\mu_0 \int_{-1}^{0} a\sqrt{\frac{\xi^2+\zeta_0^2}{1-\xi^2}}d\xi \int_{-\pi}^{0} a\sqrt{\left(1+\zeta_0^2\right)\left(1-\xi^2\right)}d\varphi \frac{1}{a}\sqrt{\frac{1+\zeta_0^2}{\xi^2+\zeta_0^2}}\frac{\partial \phi_m}{\partial \zeta}\left(\zeta_0,\xi,\varphi\right)$$

$$= -\mu_0 a\left(1+\zeta_0^2\right)\int_{-1}^{0} d\xi \int_{-\pi}^{0} d\varphi \frac{\partial \phi_m}{\partial \zeta}\left(\zeta_0,\xi,\varphi\right)$$

Using the above eigenfunction expansion and noting that [C-2] $P_n^m(-\xi) = (-1)^{m+n} P_n^m(\xi)$ gives

$$\Phi = -\mu_0 a \frac{I}{4\pi}\sum_{m=1}^{\infty}\frac{2^m m!}{m\,(2m)!}\left(1+\zeta_0^2\right)\frac{jQ_m^{m\prime}\left(j\zeta_0\right)}{Q_m^m\left(j0\right)}\int_{-1}^{0} P_m^m\left(\xi\right)d\xi \int_{-\pi}^{0}\sin\left(m\varphi\right)d\varphi$$

$$= \mu_0 a \frac{I}{4\pi}\sum_{m=1}^{\infty}\frac{2^m m!}{m\,(2m)!}\left(1+\zeta_0^2\right)\frac{jQ_m^{m\prime}\left(j\zeta_0\right)}{Q_m^m\left(j0\right)}\int_{0}^{1} P_m^m\left(\xi\right)d\xi \frac{1}{m}\left[1-\cos\left(m\pi\right)\right]$$

$$= -\mu_0 a \frac{I}{2\pi}\sum_{m,odd}^{\infty}\frac{1}{m^2}\left(1+\zeta_0^2\right)\frac{jQ_m^{m\prime}\left(j\zeta_0\right)}{Q_m^m\left(j0\right)}\int_{0}^{1}\left(\sqrt{1-\xi^2}\right)^m d\xi$$

The integral can be carried out as

$$\int_0^1\left(\sqrt{1-\xi^2}\right)^m d\xi = \frac{1}{2}\int_0^1 (1-u)^{m/2}\,u^{-1/2}du$$

$$= \frac{1}{2}B\left(\frac{m}{2}+1,\frac{1}{2}\right) = \frac{\Gamma\left(\frac{m+2}{2}\right)\Gamma\left(\frac{1}{2}\right)}{2\Gamma\left(\frac{m+3}{2}\right)}$$

where $B\left(p,q\right)$ is the beta function [C-2]. Note that for m odd

$$\int_0^1\left(\sqrt{1-\xi^2}\right)^m d\xi = \frac{\pi}{2}\frac{\left(\frac{1}{2}\right)_{(m+1)/2}}{\left(\frac{m+1}{2}\right)!}$$

The recurrence relation for the derivative of the Legendre function is [C-2]

$$\left(1+\zeta_0^2\right)jQ_n^{m\prime}\left(j\zeta_0\right) = (m+n)\,(n-m+1)\sqrt{1+\zeta_0^2}Q_n^{m-1}\left(j\zeta_0\right) - m\zeta_0 Q_n^m\left(j\zeta_0\right)$$

This yields the expression for the magnetic flux through the half spheroid

$$\Phi = -\mu_0 a\frac{I}{4}\sum_{m,odd}^{\infty}\frac{\left(\frac{1}{2}\right)_{(m+1)/2}}{m\left(\frac{m+1}{2}\right)!}\left[\frac{2\sqrt{1+\zeta_0^2}Q_m^{m-1}\left(j\zeta_0\right)-\zeta_0 Q_m^m\left(j\zeta_0\right)}{Q_m^m\left(j0\right)}\right]$$

Note that for $m = 1$ only we use

$$\left(1+\zeta_0^2\right)\frac{jQ_1^{1\prime}\left(j\zeta_0\right)}{Q_1^1\left(j0\right)} = \frac{2}{\pi}\left[\zeta_0\,\mathrm{arccot}\,\zeta_0 - 2 + \zeta_0^2/\left(1+\zeta_0^2\right)\right]\sqrt{1+\zeta_0^2}$$

to find

$$\Phi \approx -\mu_0 a \frac{I}{8}\left[\frac{\left(1+\zeta_0^2\right) jQ_1^{1\prime}\left(j\zeta_0\right)}{Q_1^1\left(j0\right)}\right] = -\mu_0 a \frac{I}{4\pi}\left[\zeta_0 \operatorname{arccot}\zeta_0 - 2 + \zeta_0^2/\left(1+\zeta_0^2\right)\right]\sqrt{1+\zeta_0^2} \qquad \text{(C-3)}$$

The limit $\zeta_0 \to \infty$ is the flux through a quarter sphere by the dipole field

$$\Phi/\left(\mu_0 Ia/\pi\right) \approx \frac{1}{3\zeta_0} \sim \frac{a}{3r}$$

C.4 Magnetic Flux Through Half Aperture

Taking $\zeta_0 = 0$ in the preceding formula gives the magnetic flux through half the aperture

$$\Phi = -\mu_0 a \frac{I}{2} \sum_{m,odd} \frac{\left(\frac{1}{2}\right)_{(m+1)/2}}{m\left(\frac{m+1}{2}\right)!} \frac{Q_m^{m-1}\left(j0\right)}{Q_m^m\left(j0\right)}$$

The relation for the ratio

$$\frac{jQ_n^{m\prime}\left(j0\right)}{Q_n^m\left(j0\right)} = \left(m+n\right)\left(n-m+1\right)\frac{Q_n^{m-1}\left(j0\right)}{Q_n^m\left(j0\right)} = -\left(m+n\right)\left(n-m+1\right)\frac{\Gamma\left(\frac{n+m}{2}\right)\Gamma\left(1+\frac{n-m}{2}\right)}{2\Gamma\left(1+\frac{n-m+1}{2}\right)\Gamma\left(\frac{n+m+1}{2}\right)}$$

gives

$$\frac{jQ_m^{m\prime}\left(j0\right)}{Q_m^m\left(j0\right)} = 2m\frac{Q_m^{m-1}\left(j0\right)}{Q_m^m\left(j0\right)} = -2\frac{\Gamma\left(m+1\right)}{\Gamma\left(\frac{1}{2}\right)\Gamma\left(m+\frac{1}{2}\right)} = -\frac{2}{\pi}\frac{m!}{\left(\frac{1}{2}\right)_m}$$

Therefore

$$\Phi = \mu_0 a \frac{I}{2\pi} \sum_{m,odd}^{\infty} \frac{m!\left(\frac{1}{2}\right)_{(m+1)/2}}{m^2\left(\frac{m+1}{2}\right)!\left(\frac{1}{2}\right)_m}$$

To accelerate the sum we note that the asymptotic form of the summand is

$$\frac{m!\left(\frac{1}{2}\right)_{(m+1)/2}}{m^2\left(\frac{m+1}{2}\right)!\left(\frac{1}{2}\right)_m} = \frac{\Gamma\left(m\right)\Gamma\left(\frac{m}{2}\right)}{\left(m+1\right)\Gamma\left(\frac{m+1}{2}\right)\Gamma\left(m+\frac{1}{2}\right)}$$

$$\sim \frac{\sqrt{2}}{m^2}\left(1-\frac{5}{8m}\right), \; m \to \infty$$

Using the known sum [C-2]

$$\sum_{m,odd} \frac{1}{m^2} = \frac{\pi^2}{8}$$

we can write

$$\Phi = \frac{a\mu_0 I}{\pi}\left[\sum_{m,odd}^{\infty}\left\{\frac{m!\left(\frac{1}{2}\right)_{(m+1)/2}}{2m^2\left(\frac{m+1}{2}\right)!\left(\frac{1}{2}\right)_m} - \frac{1}{m^2\sqrt{2}}\right\} + \frac{\pi^2}{8\sqrt{2}}\right]$$

Numerical evaluation yields

$$\Phi \approx \frac{a\mu_0 I}{\pi}(0.6478) \tag{C-4}$$

It is interesting that the $m = 1$ term of the original sum (without the subtraction of the asymptotic form) gives

$$\Phi \approx \frac{a\mu_0 I}{\pi}(0.5)$$

This is the result of the plane field term ($m = 1$).

C.5 Fit Function for Magnetic Flux Through Quarter Spheroid

It is useful to have a simple fit to the flux through the quarter spheroid as a function of ζ_0. Using the distant dipole moment behavior (along with $\arctan\zeta_0 \sim 1/\zeta_0$, $\zeta_0 \to \infty$) and the flux in the aperture limit (along with $\arctan(0) = \pi/2$) we can write

$$\Phi \approx \frac{a\mu_0 I}{\pi}\left[F_0\frac{2}{\pi}\operatorname{arccot}\zeta_0 - \frac{\zeta_0}{1+\zeta_0^2}\left(\frac{2}{\pi}F_0 - \frac{1}{3}\right)\right] \tag{C-5}$$

where

$$F_0 \approx 0.6478$$

The various approximation discussed in the paragraphs above are summarized in Figure 2. Note the asymptotes shown by dotted lines on the left side of the plot indicate the flux integrated over half the aperture taking into account only the m=1 mode (0.5) and taking into account the higher order modes (0.6478). Note also how well the fit function of equation C-5 (solid line tagged with open squares) approximates the exact flux of the more-complicated equation C-1 (solid line).

C.6 References

[C-1] W. R. Smythe, *Static and Dynamic Electricity*, Hemisphere Publishing Corp., New York, 1989, pp. 168-177.

[C-2] M. Abramowitz and I. A. Stegun, *Handbook of Mathematical Functions*, Dover Pub., Inc., New York, pp. 258, 332-339, 808.

[C-3] I. S. Gradshteyn and I. M. Ryzhik, *Tables of Integrals, Series, and Products*, Academic Press, New York, pp. 147, 366, 796, 799, 998-1000.

[C-4] H. Bateman (Bateman Manuscript Project), *Higher Transcendental Functions*, Volume 1, McGraw-Hill Book Co., Inc., 1953, p. 151.

[C-5] K. S. H. Lee, *EMP Interaction: Principles, Techniques, and Reference Data*, Hemisphere Pub. Corp., New York, 1986, pp. 439, 441.

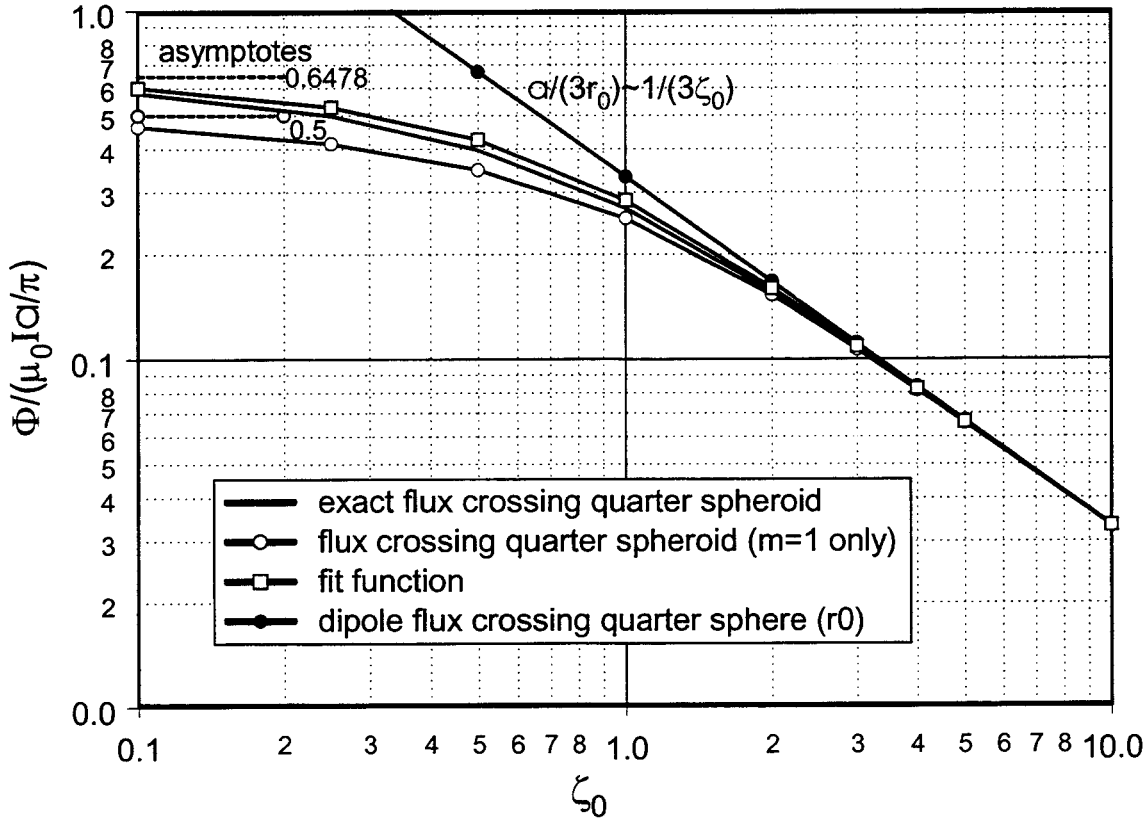

Figure 2. Plot of Various Flux Approximations When Arc is Normal to Aperture

Appendix D. Electric Current on Wire Across Aperture

The current I is now taken to be positive x directed and bisects the aperture along the x axis. We first assume the current exists on a zero radius filament. Later to find the flux passing through half the aperture the actual radius of the wire will be required.

D.1 Filament Solution on Polarized Magnetic Disc

There is a discontinuity in magnetic potential introduced at the zero radius filament. In the actual problem the z directed field is even in z (the magnetic potential is thus odd in z). The boundary conditions can be taken as

$$\frac{\partial \phi_m}{\partial z} \text{ continuous at } z = 0$$

$$\frac{\partial \phi_m}{\partial z} = 0\,,\; a < \rho < \infty$$

$$\phi_m(\rho, \varphi, -0) = (I/4) - (I/4)\operatorname{sgn}(\varphi)\;,\; 0 < \rho < a$$

$$\phi_m(\rho, \varphi, +0) = -(I/4) + (I/4)\operatorname{sgn}(\varphi)\;,\; 0 < \rho < a$$

It is convenient to change the symmetry of the problem in a way similar to the preceding section by taking the potential to be even in z

$$\phi_m(\rho, \varphi, \pm 0) = (I/4)\operatorname{sgn}(\varphi)\;,\; 0 < \rho < a$$

This is the problem of a PMC disc of radius a, charged to two different magnetic potentials. The boundary conditions on the actual surrounding plane are obeyed via symmetry. The field in the upper half plane $z > 0$ is the same as the original filament problem. The field in the lower half plane is minus the filament problem. The solution to Laplace's equation in oblate spheroidal coordinates is again

$$\phi_m(\zeta, \xi, \varphi) = \sum_{n=1}^{\infty} \sum_{m=1}^{n} B_{mn} Q_n^m(j\zeta)\, P_n^m(\xi) \sin(m\varphi)$$

Applying the disc boundary condition on the potential

$$\phi_m(0, \xi, \varphi) = (I/4)\operatorname{sgn}(\varphi)\;,\; -1 < \xi < 1\,,\; -\pi < \varphi < \pi$$

and using orthogonality, gives

$$B_{mn} Q_n^m(j0)\, \frac{2(n+m)!}{(2n+1)(n-m)!}\pi = \frac{I}{2}\int_{-1}^{1} P_n^m(\xi)\, d\xi \int_0^{\pi} \sin(m\varphi)\, d\varphi$$

$$= I\int_0^1 P_n^m(\xi)\, d\xi \frac{1}{m}\left[1 - \cos(m\pi)\right]\;,\; m+n \text{ even}$$

$$= I\frac{2}{m}\int_0^1 P_n^m(\xi)\,d\xi\,,\ m \text{ and } n \text{ odd}$$

$$= 0\,,\ \text{otherwise}$$

The integral can be carried out by means of the identity [D-1]

$$\int_0^1 P_\nu^m(\xi)\,d\xi = \frac{(-1)^m \pi 2^{-2m-1}\Gamma(1+\nu+m)}{\Gamma\left(\frac{1}{2}+\frac{m}{2}\right)\Gamma\left(\frac{3}{2}+\frac{m}{2}\right)\Gamma(1-m+\nu)}\,{}_3F_2\left(\frac{m+\nu+1}{2},\frac{m-\nu}{2},\frac{m}{2}+1;m+1,\frac{3+m}{2};1\right)$$

where the generalized hypergeometric series

$${}_3F_2(a_1,a_2,a_3;b_1,b_2;z) = \sum_{k=0}^{\infty}\frac{(a_1)_k(a_2)_k(a_3)_k}{(b_1)_k(b_2)_k}\frac{z^k}{k!}$$

terminates when any one of the first three arguments is zero or a negative integer (for integer order and degree). The result for odd integer degree and order is

$$\int_0^1 P_n^m(\xi)\,d\xi = -\frac{\pi(n+m)!m!\left(\frac{n-m}{2}\right)!}{2^{2m+1}\left(\frac{m-1}{2}\right)!(n-m)!}\sum_{k=0}^{(n-m)/2}\frac{(-1)^k\left(\frac{m+n+1}{2}\right)_k\left(\frac{m}{2}+1\right)_k}{(m+k)!\left(k+\frac{m+1}{2}\right)!k!\left(\frac{n-m}{2}-k\right)!}$$

The potential in the filament problem for $z<0$ is thus

$$\phi_m(\zeta,\xi,\varphi) = -\frac{I}{\pi}\sum_{n,odd}^{\infty}\sum_{m,odd}^{n}\frac{(2n+1)(n-m)!}{m(n+m)!}\frac{Q_n^m(j\zeta)}{Q_n^m(j0)}P_n^m(\xi)\sin(m\varphi)\int_0^1 P_n^m(\xi)\,d\xi$$

D.1.1 dipole moment

The dipole moment contribution to the potential is found by retaining only the $n=m=1$ term

$$\phi_m \sim -\frac{I}{\pi}\frac{3}{2}\frac{Q_1^1(j\zeta)}{Q_1^1(j0)}P_1^1(\xi)\sin\varphi\int_0^1 P_1^1(\xi)\,d\xi$$

$$\sim -\frac{I}{2\pi}\frac{1}{\zeta^2}\sqrt{1-\xi^2}\sin\varphi \sim -\frac{Ia^2y}{2\pi r^3}$$

Thus the dipole moment is

$$\vec{m} = -2Ia^2\hat{y} \tag{D-1}$$

D.1.2 magnetic flux through quarter spheroid

The magnetic flux through one quarter of a spheroid at $\zeta=\zeta_0$ is

$$\Phi = -\mu_0 a\left(1+\zeta_0^2\right)\int_{-1}^{0}d\xi\int_{-\pi}^{0}d\varphi\frac{\partial\phi_m}{\partial\zeta}(\zeta_0,\xi,\varphi)$$

$$= -\frac{2}{\pi}\mu_0 aI \sum_{n,odd}^{\infty}\sum_{m,odd}^{n} \frac{(2n+1)(n-m)!}{m^2(n+m)!}\left(1+\zeta_0^2\right)\frac{jQ_n^{m\prime}(j\zeta_0)}{Q_n^m(j0)}\left[\int_0^1 P_n^m(\xi)\,d\xi\right]^2$$

$$= -\frac{2}{\pi}\mu_0 aI \sum_{n,odd}^{\infty}\sum_{m,odd}^{n} \frac{(2n+1)(n-m)!}{m^2(n+m)!}\frac{(m+n)(n-m+1)\sqrt{1+\zeta_0^2}Q_n^{m-1}(j\zeta_0) - m\zeta_0 Q_n^m(j\zeta_0)}{Q_n^m(j0)}$$
$$\times\left[\int_0^1 P_n^m(\xi)\,d\xi\right]^2$$

Note that the $n = m = 1$ term gives

$$\Phi \approx -\mu_0 aI\frac{3}{8}\left[\zeta_0 \operatorname{arccot}\zeta_0 - 2 + \zeta_0^2/\left(1+\zeta_0^2\right)\right]\sqrt{1+\zeta_0^2}$$

The $\zeta_0 \to \infty$ limit is the flux through a quarter sphere by the dipole field

$$\Phi/\left(\mu_0 Ia/\pi\right) \approx \frac{\pi}{2\zeta_0} \sim \frac{\pi a}{2r}$$

D.2 Extension for Small Values of ζ_0

As the aperture is approached $\zeta_0 \to 0$ it is very difficult to sum the series for the flux. As an alternative we assume that for small ζ_0 flux changes occur as a result of proximity to the current filament along the x axis. The field about the filament in the $y = 0$ plane, for $-a < x < a$, ignoring perturbations caused by the boundary of the hole, is

$$H_y(y=0) \sim \frac{I}{2\pi z}$$

In spheroidal coordinates for $\varphi = 0$ $(x > 0)$ this becomes

$$H_\varphi(\zeta,\xi,0) \sim \frac{I}{2\pi a\zeta\xi}$$

If we consider the amount of magnetic flux between two spheroid surfaces ζ_0 and ζ_1, along the length of the wire $-a < x < a$ on $y = 0$, we have

$$\Phi_f(\zeta_1,\zeta_0) = 2\mu_0\int_{\zeta_0}^{\zeta_1}\int_{\xi_0}^{1} H_\varphi(\zeta,\xi,0)\,a\sqrt{\frac{\xi^2+\zeta^2}{1-\xi^2}}d\xi\, a\sqrt{\frac{\xi^2+\zeta^2}{1+\zeta^2}}d\zeta$$

where $\xi = \xi_0$ when $x = a$ (the wire end)

$$\xi_0 = \frac{\zeta}{\sqrt{1+\zeta^2}}$$

For small values of ζ (as the spheroid surface approaches the aperture) this flux change should be approximately the same as the flux change crossing surface of the spheroid. Thus we should be able to write

$$\Phi(\zeta_0) \sim \Phi_f(\zeta_1,\zeta_0) + \Phi(\zeta_1)$$

We take ζ_1 to be the smallest value of ζ for which the flux can be computed reliably from the series solution. For example, the value of the series including terms up to $N = 21$ is

$$\Phi(0.5) \approx \frac{\mu_0 Ia}{\pi}(2.0178)$$

The value including terms up to $N = 11$ is (2.0092). Carrying out the indicated integration in

$$\Phi_f(\zeta_1, \zeta_0) = \frac{\mu_0 Ia}{\pi} \int_{\zeta_0}^{\zeta_1} \frac{d\zeta}{\zeta\sqrt{1+\zeta^2}} \int_{\xi_0}^{1} (\xi + \zeta^2/\xi) \frac{d\xi}{\sqrt{1-\xi^2}}$$

gives

$$\int_{\xi_0}^{1} (\xi + \zeta^2/\xi) \frac{d\xi}{\sqrt{1-\xi^2}} = \sqrt{1-\xi_0^2} + \zeta^2 \ln\left(\frac{1+\sqrt{1-\xi_0^2}}{\xi_0}\right)$$

$$= \frac{1}{\sqrt{1+\zeta^2}} + \zeta^2 \ln\left(\frac{1+\sqrt{1+\zeta^2}}{\zeta}\right)$$

and thus

$$\Phi_f(\zeta_1, \zeta_0) = \frac{\mu_0 Ia}{\pi} \int_{\zeta_0}^{\zeta_1} \left[\frac{1}{\zeta(1+\zeta^2)} + \frac{\zeta}{\sqrt{1+\zeta^2}} \ln\left(\frac{1+\sqrt{1+\zeta^2}}{\zeta}\right)\right] d\zeta$$

or

$$\Phi_f(\zeta_1, \zeta_0) / (\mu_0 Ia/\pi) = \left[\ln\left(\frac{\zeta}{\sqrt{1+\zeta^2}}\right) + \left(1+\sqrt{1+\zeta^2}\right)\left\{\ln\left(1+\sqrt{1+\zeta^2}\right) - 1\right\}\right.$$

$$\left. + (1 - \ln\zeta)\sqrt{1+\zeta^2} + \frac{1}{2}\ln\left(\frac{\sqrt{1+\zeta^2}-1}{\sqrt{1+\zeta^2}+1}\right)\right]_{\zeta_0}^{\zeta_1}$$

If we take $\zeta_1 = 0.5$ and $\zeta_0 = 0.25$ we find

$$\Phi(0.25) / (\mu_0 Ia/\pi) \approx 0.7599 + 2.0178 \approx 2.7777$$

The value determined from the series at $\zeta_0 = 0.25$, for $N = 21$, is (2.7282). The value determined from the series for $N = 11$ is (2.6777).

Note that the asymptotic form of the flux as $\zeta_0 \to 0$, predicted from the above formula, is

$$\Phi / (\mu_0 Ia/\pi) \sim -\ln(2\zeta_0) + 1 + 1.13398$$

$$\sim -\ln(\zeta_0) + 1.4408\,,\ \zeta_0 \to 0$$

D.3 Displaced Wire Across Aperture

The actual wire with radius b is taken to be displaced upward from the aperture by distance b (so that its bottom surface is flush with the aperture). The field below the aperture for $y = 0$ and $-a < x < a$, is thus

$$H_y\,(y=0) = \frac{I}{2\pi\,(z+b)}$$

In spheroidal coordinates for $\varphi = 0$ $(x > 0)$ this becomes

$$H_\varphi\,(\zeta,\xi,0) \sim \frac{I}{2\pi\,(a\zeta\xi + b)}$$

The amount of magnetic flux between two spheroid surfaces ζ_0 and ζ_1, along the length of the wire $-a < x < a$ on $y = 0$, is

$$\Phi_b\,(\zeta_1,\zeta_0) = \frac{\mu_0 I a}{\pi}\int_{\zeta_0}^{\zeta_1}\frac{d\zeta}{\sqrt{1+\zeta^2}}\int_{\xi_0}^{1}\frac{1}{(\zeta\xi + b/a)}\frac{\xi^2+\zeta^2}{\sqrt{1-\xi^2}}d\xi$$

where again $\xi = \xi_0$ when $x = a$ (the wire end). Using the result

$$\int_{\xi_0}^{1}\frac{1}{(\zeta\xi + b/a)}\frac{\xi^2+\zeta^2}{\sqrt{1-\xi^2}}d\xi = \int_{\arcsin\xi_0}^{\pi/2}\frac{\sin^2\theta+\zeta^2}{(\zeta\sin\theta + b/a)}d\theta$$

$$= \frac{1}{\zeta^2}\int_{\arcsin\xi_0}^{\pi/2}\left[\zeta\sin\theta - b/a + \frac{b^2/a^2+\zeta^4}{(\zeta\sin\theta + b/a)}\right]d\theta$$

$$= \frac{1}{\zeta}\sqrt{1-\xi_0^2} - \frac{1}{\zeta^2}\,(b/a)\,(\pi/2 - \arcsin\xi_0) + \frac{b^2/a^2+\zeta^4}{\zeta^2}\int_{\arcsin\xi_0}^{\pi/2}\frac{d\theta}{(\zeta\sin\theta + b/a)}$$

and the identity from [D-1]

$$\int\frac{d\theta}{(\zeta\sin\theta + b/a)} = \frac{2}{\sqrt{b^2/a^2-\zeta^2}}\arctan\left[\frac{(b/a)\tan(\theta/2)+\zeta}{\sqrt{b^2/a^2-\zeta^2}}\right],\ b^2/a^2 > \zeta^2$$

$$= \frac{1}{\sqrt{\zeta^2-b^2/a^2}}\ln\left[\frac{(b/a)\tan(\theta/2)+\zeta-\sqrt{\zeta^2-b^2/a^2}}{(b/a)\tan(\theta/2)+\zeta+\sqrt{\zeta^2-b^2/a^2}}\right],\ b^2/a^2 < \zeta^2$$

as well as

$$\tan\left(\frac{1}{2}\arcsin\xi_0\right) = \frac{\xi_0}{1+\sqrt{1-\xi_0^2}} = \frac{\zeta}{1+\sqrt{1+\zeta^2}}$$

gives

$$\int_{\arcsin\xi_0}^{\pi/2} \frac{d\theta}{(\zeta\sin\theta + b/a)}$$

$$= \frac{2}{\sqrt{b^2/a^2-\zeta^2}}\left\{\arctan\left(\sqrt{\frac{b/a+\zeta}{b/a-\zeta}}\right) - \arctan\left(\frac{\zeta}{\sqrt{b^2/a^2-\zeta^2}}\frac{1+\sqrt{1+\zeta^2}+b/a}{1+\sqrt{1+\zeta^2}}\right)\right\}, \; b^2/a^2 > \zeta^2$$

$$= \frac{1}{\sqrt{\zeta^2-b^2/a^2}}\ln\left[\frac{\sqrt{\zeta+b/a}-\sqrt{\zeta-b/a}}{\sqrt{\zeta+b/a}+\sqrt{\zeta-b/a}}\frac{\zeta b/a+\left(1+\sqrt{1+\zeta^2}\right)\left(\zeta+\sqrt{\zeta^2-b^2/a^2}\right)}{\zeta b/a+\left(1+\sqrt{1+\zeta^2}\right)\left(\zeta-\sqrt{\zeta^2-b^2/a^2}\right)}\right], \; b^2/a^2 < \zeta^2$$

$$= \frac{1}{\sqrt{\zeta^2-b^2/a^2}}\ln\left[2\frac{\left\{\zeta b/a+\left(1+\sqrt{1+\zeta^2}\right)\left(\zeta+\sqrt{\zeta^2-b^2/a^2}\right)\right\}\left(\zeta+\sqrt{\zeta^2-b^2/a^2}\right)}{\left(\sqrt{\zeta+b/a}+\sqrt{\zeta-b/a}\right)^2\left\{\zeta\left(\zeta+\sqrt{\zeta^2-b^2/a^2}\right)+\left(1+\sqrt{1+\zeta^2}\right)b/a\right\}}\right], \; b^2/a^2 < \zeta^2$$

Taking $\zeta_0 \geq b/a$ we obtain

$$\Phi_b(\zeta_1,\zeta_0) = \frac{\mu_0 Ia}{\pi}\int_{\zeta_0}^{\zeta_1}\frac{d\zeta}{\sqrt{1+\zeta^2}}G(\zeta)$$

where

$$\int_{\xi_0}^{1}\frac{1}{(\zeta\xi+b/a)}\frac{\xi^2+\zeta^2}{\sqrt{1-\xi^2}}d\xi = G(\zeta) = \frac{1}{\zeta\sqrt{1+\zeta^2}} - \frac{1}{\zeta^2}(b/a)\left[\pi/2 - \arcsin\left(\zeta/\sqrt{1+\zeta^2}\right)\right]$$

$$+\frac{b^2/a^2+\zeta^4}{\zeta^2\sqrt{\zeta^2-b^2/a^2}}\ln\left[2\frac{\left\{\zeta b/a+\left(1+\sqrt{1+\zeta^2}\right)\left(\zeta+\sqrt{\zeta^2-b^2/a^2}\right)\right\}\left(\zeta+\sqrt{\zeta^2-b^2/a^2}\right)}{\left(\sqrt{\zeta+b/a}+\sqrt{\zeta-b/a}\right)^2\left\{\zeta\left(\zeta+\sqrt{\zeta^2-b^2/a^2}\right)+\left(1+\sqrt{1+\zeta^2}\right)b/a\right\}}\right], \; \zeta_0 \geq b/a$$

The flux $\Phi_b(\zeta_1,\zeta_0)$ was evaluated by numerical integration. The extrapolated flux through the quarter spheroid was taken to be

$$\Phi(\zeta_0) \sim \Phi_b(\zeta_1,\zeta_0) + \Phi(\zeta_1)$$

where again $\zeta_1 = 0.5$ with

$$\Phi(0.5) \approx \frac{\mu_0 Ia}{\pi}(2.0178)$$

was used.

D.4 Potential for Assumed Charge On Polarized Magnetic Disc

The flux for the filament solution will exhibit a logarithmic singularity if we attempt to take $\zeta_0 \to 0$. To overcome this problem we first subtract an assumed solution that has the same singularity then take the

limit. The flux associated with the assumed solution can then be added back for a finite radius wire.

First we determine the potential for this assumed solution. We take the magnetic disc to have fixed magnetic charge with assumed density (on each side of the disc)

$$\sigma_m^a = \frac{\mu_0 I}{2\pi y}$$

In the oblate spheroidal coordinate system this condition is

$$-\mu_0 \frac{1}{a}\sqrt{\frac{1+\zeta_0^2}{\xi^2+\zeta_0^2}}\frac{\partial \phi_m^a}{\partial \zeta}(\zeta_0,\xi,\varphi) = \frac{\mu_0 I}{2\pi a\sqrt{1+\zeta_0^2}\sqrt{1-\xi^2}\sin\varphi}$$

where we take $\zeta_0 \to 0$

$$-\frac{\partial \phi_m^a}{\partial \zeta}(0,\xi,\varphi) = \frac{I}{2\pi \sin\varphi}\frac{|\xi|}{\sqrt{1-\xi^2}}\,,\ -1<\xi<1\,,\ -\pi<\varphi<\pi$$

Again the Laplace solution is taken as

$$\phi_m^a(\zeta,\xi,\varphi) = \sum_{n=1}^{\infty}\sum_{m=1}^{n} B_{mn}^a Q_n^m(j\zeta)\,P_n^m(\xi)\sin(m\varphi)$$

Inserting this into the assumed magnetic charge condition, using orthogonality, gives

$$-B_{mn}^a jQ_n^{m\prime}(j0)\frac{2(n+m)!}{(2n+1)(n-m)!}\pi = \frac{I}{2\pi}\int_{-1}^{1} P_n^m(\xi)\frac{|\xi|\,d\xi}{\sqrt{1-\xi^2}}\int_{-\pi}^{\pi}\frac{\sin(m\varphi)}{\sin\varphi}d\varphi$$

$$= \frac{2I}{\pi}\int_0^1 P_n^m(\xi)\frac{\xi d\xi}{\sqrt{1-\xi^2}}\int_0^{\pi}\frac{\sin(m\varphi)}{\sin\varphi}d\varphi\,,\ m+n \text{ even}$$

Using the result [D-1]

$$\int_0^{\pi}\frac{\sin(m\varphi)}{\sin\varphi}d\varphi = \pi\,,\ m \text{ odd}$$

$$= 0\,,\ m \text{ even}$$

we have

$$-B_{mn}^a jQ_n^{m\prime}(j0)\frac{2(n+m)!}{(2n+1)(n-m)!}\pi = 2I\int_0^1 P_n^m(\xi)\frac{\xi d\xi}{\sqrt{1-\xi^2}}\,,\ m \text{ and } n \text{ odd}$$

Using the result [D-1]

$$\int_0^1 P_\nu^\mu(\xi)\frac{\xi d\xi}{\sqrt{1-\xi^2}} = \frac{2^{\mu-1}\Gamma\left(\frac{1-\mu}{2}\right)}{\Gamma(1-\mu)\Gamma\left(\frac{3-\mu}{2}\right)}\,{}_3F_2\left(\frac{\nu-\mu+1}{2},-\frac{\nu+\mu}{2},\frac{1-\mu}{2};1-\mu,\frac{3-\mu}{2};1\right)$$

as a guide, we find in the limit for degree and order as odd integers gives

$$\int_0^1 P_n^m(\xi)\frac{\xi d\xi}{\sqrt{1-\xi^2}} = 2^{m-1}\left(\frac{n+m}{2}\right)!\sum_{k=m}^{(n+m)/2}(-1)^k\frac{\left(\frac{n-m+1}{2}\right)_k}{(k-m)!\left(\frac{1-m}{2}+k\right)k!\left(\frac{n+m}{2}-k\right)!}$$

The potential in the filament problem for $z<0$ is thus

$$\phi_m^a(\zeta,\xi,\varphi) = \frac{I}{\pi}\sum_{n,odd}^{\infty}\sum_{m,odd}^{n}\frac{(2n+1)(n-m)!}{(n+m)!}\frac{Q_n^m(j\zeta)}{jQ_n^{m\prime}(j0)}P_n^m(\xi)\sin(m\varphi)\int_0^1 P_n^m(\xi)\frac{\xi d\xi}{\sqrt{1-\xi^2}}$$

D.4.1 dipole moment

It is interesting to calculate the dipole potential in this case. The $n=m=1$ term is

$$\phi_m^a \sim \frac{3I}{2\pi}\frac{Q_1^1(j\zeta)}{jQ_1^{1\prime}(j0)}P_1^1(\xi)\sin\varphi\int_0^1 P_1^1(\xi)\frac{\xi d\xi}{\sqrt{1-\xi^2}}$$

$$\sim -\frac{I}{4\pi}\frac{1}{\zeta^2}\sqrt{1-\xi^2}\sin\varphi \sim -\frac{Ia^2y}{4\pi r^3}$$

where we have used the fact that $jQ_1^{1\prime}(j0)=-2$. The dipole moment is thus

$$\vec{m}^a = -Ia^2\hat{y}$$

It is interesting that this is exactly half the true result for the filament problem.

D.4.2 magnetic flux through quarter spheroid

The magnetic flux through one quarter of the spheroid $\zeta=\zeta_0$ is

$$\Phi^a = -\mu_0 a\left(1+\zeta_0^2\right)\int_{-1}^0 d\xi\int_{-\pi}^0 d\varphi\frac{\partial\phi_m^a}{\partial\zeta}(\zeta_0,\xi,\varphi)$$

$$= \frac{2}{\pi}\mu_0 aI\sum_{n,odd}^{\infty}\sum_{m,odd}^{n}\frac{(2n+1)(n-m)!}{m(n+m)!}\left(1+\zeta_0^2\right)\frac{jQ_n^{m\prime}(j\zeta_0)}{jQ_n^{m\prime}(j0)}\int_0^1 P_n^m(\xi)\,d\xi\int_0^1 P_n^m(\xi)\frac{\xi d\xi}{\sqrt{1-\xi^2}}$$

Note that for $n=m=1$ we have

$$\left(1+\zeta_0^2\right)\frac{jQ_1^{1\prime}(j\zeta_0)}{jQ_1^{1\prime}(j0)} = -\frac{1}{2}\left[\zeta_0\operatorname{arccot}\zeta_0 - 2 + \zeta_0^2/\left(1+\zeta_0^2\right)\right]\sqrt{1+\zeta_0^2}$$

$$\Phi^a \approx -\mu_0 aI\frac{3}{16}\left[\zeta_0\operatorname{arccot}\zeta_0 - 2 + \zeta_0^2/\left(1+\zeta_0^2\right)\right]\sqrt{1+\zeta_0^2}$$

half the previous result.

D.5 Difference Flux Through Half Aperture

Now we take the difference flux

$$\Delta\Phi = \Phi - \Phi^a$$

$$= -\frac{2}{\pi}\mu_0 aI \sum_{n,odd}^{\infty}\sum_{m,odd}^{n} \frac{(2n+1)(n-m)!}{m(n+m)!}\left(1+\zeta_0^2\right) jQ_n^{m\prime}(j\zeta_0)$$

$$\left[\frac{1}{mQ_n^m(j0)}\int_0^1 P_n^m(\xi)\,d\xi + \frac{1}{jQ_n^{m\prime}(j0)}\int_0^1 P_n^m(\xi)\frac{\xi d\xi}{\sqrt{1-\xi^2}}\right]\int_0^1 P_n^m(\xi)\,d\xi$$

and let $\zeta_0 \to 0$

$$\Delta\Phi/(\mu_0 Ia/\pi) = -2\sum_{n,odd}^{\infty}\sum_{m,odd}^{n}\frac{(2n+1)(n-m)!}{m(n+m)!}\left[\frac{jQ_n^{m\prime}(j0)}{mQ_n^m(j0)}\int_0^1 P_n^m(\xi)\,d\xi + \int_0^1 P_n^m(\xi)\frac{\xi d\xi}{\sqrt{1-\xi^2}}\right] \times \int_0^1 P_n^m(\xi)\,d\xi$$

where for both n and m odd we have

$$\frac{jQ_n^{m\prime}(j0)}{Q_n^m(j0)} = -\frac{2}{\pi}(n-m+1)\frac{\left(\frac{n-m}{2}\right)!\left(\frac{n+m}{2}\right)!}{\left(\frac{3}{2}\right)_{(n-m)/2}\left(\frac{1}{2}\right)_{(n+m)/2}}$$

Numerical evaluation of $\Delta\Phi/(\mu_0 Ia/\pi) = S$ has been carried out including terms up to $n = N$. The value for $N = 11$ is 1.345023694. The value for $N = 15$ is 1.355276395. The value for $N = 21$ is 1.363722349. The original logarithmic divergence in Φ corresponds to a $O(1/n)$ term in the series for $\zeta_0 \to 0$. The subtraction of Φ^a cancels this logarithmic divergence and is expected to lead to a $O\left(1/n^2\right)$ term in the summand for $\Delta\Phi$. The infinite sum thus should have the form

$$S = S_N + R_N$$

where the partial sum (to $n = N$) is S_N and the remainder R_N is taken to have the asymptotic form

$$R_N \sim C/(N+1)$$

Using the $N = 11$ and $N = 21$ results we find

$$C \approx 0.493644492$$

$$S \approx 1.386160735$$

(Note that, if we had taken the remainder to have the form $R_N \sim C/N + D/N^2 \sim C/(N - D/C)$, and used all three values $N = 11, 15, 21$ to determine the coefficients, we obtain $S \approx 1.386339736$ and $-D/C \approx 0.9513$). This result produces the value 1.355307954 for $N = 15$, which has an error of 3×10^{-5} from the calculated value. Thus we take

$$\Delta\Phi/\left(\mu_0 Ia/\pi\right) = S \approx 1.3863 \approx 2\ln 2$$

as the approximate value.

It is interesting that if the $n = m = 1$ term is the only one included we obtain

$$\Delta\Phi/\left(\mu_0 Ia/\pi\right) \approx -\frac{3\pi}{16}\left[\zeta_0 \operatorname{arccot}\zeta_0 - 2 + \zeta_0^2/\left(1+\zeta_0^2\right)\right]\sqrt{1+\zeta_0^2}$$

The limit $\zeta_0 = 0$ gives

$$\Delta\Phi/\left(\mu_0 Ia/\pi\right) \approx \frac{3\pi}{8} \approx 1.178$$

D.5.1 half aperture magnetic flux for finite radius wire

To obtain the half aperture magnetic flux for the finite radius wire we first integrate the assumed magnetic charge over the appropriate surface from the wire radius $b << a$ to the edge of the hole

$$\Phi_b^a = \int_b^a \int_{-\sqrt{a^2-y^2}}^{\sqrt{a^2-y^2}} \sigma_m^a dx dy = \frac{\mu_0 I}{\pi}\int_b^a \sqrt{a^2-y^2}\frac{dy}{y}$$

$$= \frac{\mu_0 aI}{\pi}\int_{\arcsin(b/a)}^{\pi/2} \left(\csc\theta - \sin\theta\right) d\theta = \frac{\mu_0 aI}{\pi}\left[\ln\left(\frac{1+\sqrt{1-b^2/a^2}}{b/a}\right) - \sqrt{1-b^2/a^2}\right]$$

$$\sim \mu_0 I\frac{a}{\pi}\left[\ln\left(2a/b\right) - 1\right],\ a >> b$$

Adding the correction gives the total flux through the half aperture

$$\Phi_b = \Phi_b^a + \Delta\Phi = \mu_0 I\frac{a}{\pi}\left[\ln\left(8a/b\right) - 1\right] \tag{D-2}$$

D.6 Fit Function for Magnetic Flux Through Quarter Spheroid

It is again useful to have a simple fit to the flux through the quarter spheroid as a function of ζ_0. Using the distant dipole moment behavior (along with $\arctan\zeta_0 \sim 1/\zeta_0$, $\zeta_0 \to \infty$), the flux in the aperture limit (along with $\arctan(0) = \pi/2$), and the extrapolated asymptotic behavior when the wire radius is zero we choose

$$\Phi/\left(\mu_0 Ia/\pi\right) \approx \ln\left(\frac{\sqrt{1+\zeta_0^2}}{\zeta_0 + \beta_1 b/a}\right) + F_1\frac{2}{\pi}\operatorname{arccot}\zeta_0 - \frac{\zeta_0}{1+\zeta_0^2}\left(\frac{2}{\pi}F_1 - \frac{\pi}{2}\right) \tag{D-3}$$

where the value of the flux crossing the aperture $\Phi_b/\left(\mu_0 Ia/\pi\right) = \ln\left(8a/b\right) - 1$, $\zeta_0 = 0$ is used to set

$$F_1 \approx \ln\left(8\beta_1\right) - 1$$

and the extrapolated asymptotic behavior of the filament $\Phi/\left(\mu_0 Ia/\pi\right) \sim -\ln\left(\zeta_0\right) + 1.4408$, $b = 0$, $\zeta_0 \to 0$

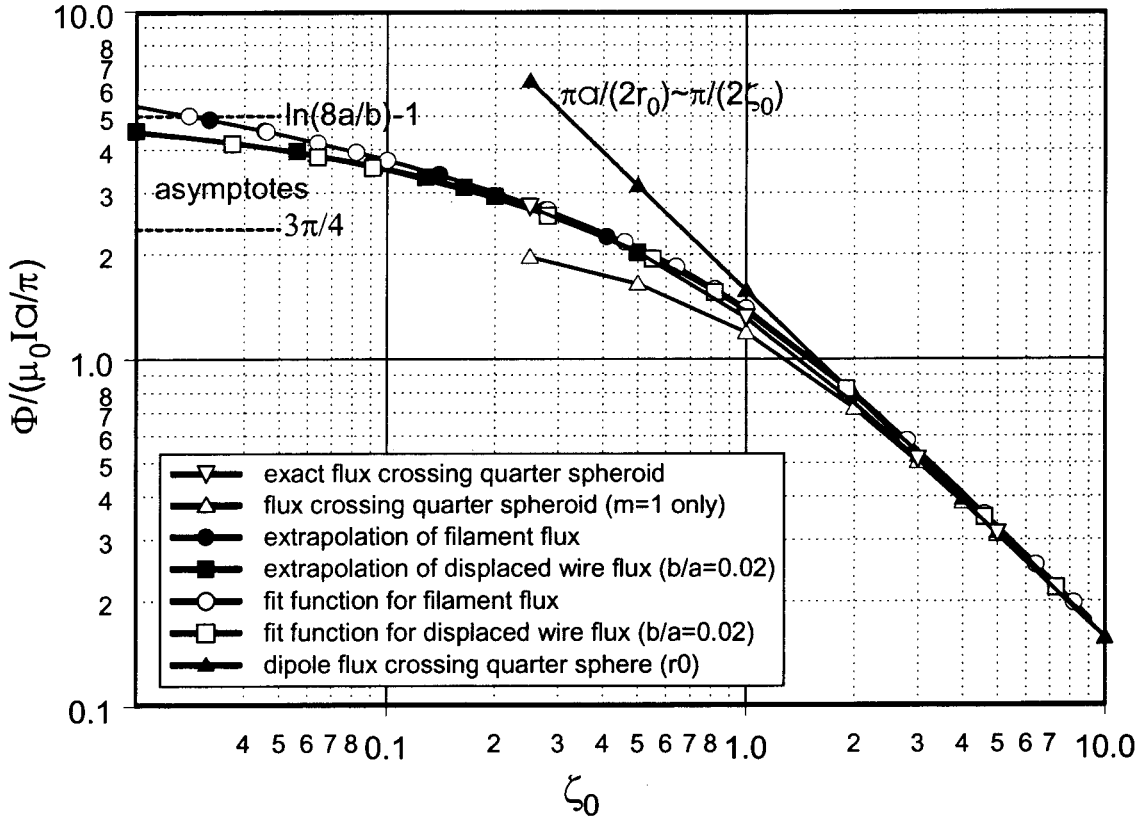

Figure 1. Plot of Various Flux Approximations When Wire Lies Across Aperture

is used to set

$$\beta_1 \approx 1.4446$$

It is curious that we nearly have $F_1 = \ln(8\beta_1) - 1 = \beta_1$, which has solution $\beta_1 \approx 1.4532$. Note that, although the contribution of the logarithm contributes a term $-\beta_1 b/(a\zeta_0)$ as $\zeta_0 \to \infty$, this is taken to be small compared to the remaining contribution $\pi/(2\zeta_0)$. It is believed that this contribution is actually the proper correction for the displaced line source in the hole.

D.7 References

[D-1]I. S. Gradshteyn and I. M. Ryzhik, *Tables of Integrals, Series, and Products*, Academic Press, New York, pp. 147, 366, 796, 799, 998-1000.

Appendix E. Electric Line Charge Normal to Hole

In this section we look at the voltages created interior to a conducting enclosure with a circular hole of radius a when a semi-infinite electric line charge q exists exterior to the enclosure. This model is attempting to address the worst case pre-return-stroke phase of the lightning channel development. The electric field penetrating the hole is found.

E.1 Decomposition of Exciting Potential

The electric field is taken as the gradient of a scalar potential

$$\overrightarrow{E} = -\nabla\phi$$

where

$$\nabla^2\phi = -\rho_v/\varepsilon_0$$

We ignore the presence of a dielectric sheet in the hole and treat the media as free space; $\varepsilon_0 \approx 8.854$ pF/m is the electric permittivity of free space. The electric charge density is ρ_v.

If the aperture is shorted the line source can be imaged in the ground plane. Thus the short circuit potential satisfies

$$\nabla^2\phi^{sc} = -\frac{q}{\varepsilon_0}\frac{\delta(\rho)}{2\pi\rho}\mathrm{sgn}(z)$$

where ρ is the cylindrical coordinate and $\mathrm{sgn}(z) = 1$ for $z > 0$ and $\mathrm{sgn}(z) = -1$ for $z < 0$. Thus the short circuit potential is given by

$$\phi^{sc} = \frac{q}{4\pi\varepsilon_0}\left[\int_0^R \frac{dz'}{\sqrt{\rho^2 + (z-z')^2}} - \int_{-R}^0 \frac{dz'}{\sqrt{\rho^2 + (z-z')^2}}\right]$$

$$= \frac{q}{4\pi\varepsilon_0}\left[\int_{-\mathrm{arcsinh}(z/\rho)}^{\mathrm{arcsinh}\{(R-z)/\rho\}} du - \int_{-\mathrm{arcsinh}\{(R+z)/\rho\}}^{-\mathrm{arcsinh}(z/\rho)} du\right]$$

$$= \frac{q}{4\pi\varepsilon_0}\left[\mathrm{arcsinh}\{(R-z)/\rho\} + \mathrm{arcsinh}(z/\rho) + \mathrm{arcsinh}(z/\rho) - \mathrm{arcsinh}\{(R+z)/\rho\}\right]$$

$$= \frac{q}{2\pi\varepsilon_0}\mathrm{arcsinh}(z/\rho)$$

The total potential is taken as

$$\phi^{tot} = \phi^{sc} + \phi\,,\ z > 0$$

$$= \phi\,,\ z < 0$$

where ϕ is the potential scattered by the hole. Continuity of the tangential electric field at the aperture, the fact that the total potential vanishes on the conducting plane, and the vanishing of the short circuit potential, means that

$$\phi \text{ continuous at } z = 0$$

$$\phi(\rho, z) = 0\,,\ a < \rho < \infty$$

Continuity of the normal component of the electric field in the hole means that

$$-\frac{\partial \phi^{sc}}{\partial z}(\rho, +0) - \frac{\partial \phi}{\partial z}(\rho, +0) = -\frac{\partial \phi}{\partial z}(\rho, -0)\ ,\ 0 < \rho < a$$

Noting that $-\frac{\partial \phi}{\partial z}$ is odd in z gives

$$-\frac{\partial \phi}{\partial z}(\rho, +0) = \frac{1}{2}\frac{\partial \phi^{sc}}{\partial z}(\rho, +0)\ ,\ 0 < \rho < a$$

If we immerse a PMC (perfect magnetic conductor) disc of radius a in a potential field

$$\phi^{i}(\rho, z) = \frac{1}{2}\phi^{sc}(\rho, z)$$

we will find the same scattered potential in the upper half space $z > 0$ and negative the scattered potential of the hole problem in the lower half space $z < 0$ (the incident and scattered potentials in the disc problem are even in z).

The aperture potential then satisfies

$$\nabla^2 \phi = 0$$

in the upper or lower half spaces. The boundary conditions are

The boundary condition on the disc for the scattered potential is

$$-\frac{\partial \phi}{\partial z}(\rho, \pm 0) = \frac{\partial \phi^{i}}{\partial z}(\rho, \pm 0) = \frac{q}{4\pi\varepsilon_0 \rho}$$

To obtain the aperture potential in the lower half space $z < 0$ we reverse the sign of the disc potential $\phi \rightarrow -\phi$.

E.2 Oblate Spheroidal Coordinate Solution

The aperture potential ϕ is now expanded in oblate spheroidal coordinates

$$\phi = \sum_{n} A_n P_n(\xi)\, Q_n(j\zeta)$$

where the functions $P_n(j\zeta)$ are not included since this potential decays at infinity. Also the functions $Q_n(\xi)$ are not included since it must be finite at $\xi = \pm 1$. Now using orthogonality [E-2]

$$\int_{-1}^{1} P_n(\xi) P_{n'}(\xi) d\xi = \frac{\delta_{nn'}}{\left(n+\frac{1}{2}\right)}$$

and the above boundary condition

$$-\frac{1}{|\xi|}\frac{\partial\phi}{\partial\zeta}(\xi,0) = \frac{q\,\mathrm{sgn}(\xi)}{4\pi\varepsilon_0\sqrt{1-\xi^2}}$$

gives

$$-A_n\frac{jQ_n'(j0)}{n+1/2} = \frac{q}{4\pi\varepsilon_0}\int_{-1}^{1} P_n(\xi)\frac{\xi d\xi}{\sqrt{1-\xi^2}}$$

Thus for n even the coefficients vanish and for n odd

$$-A_n\frac{jQ_n'(j0)}{n+1/2} = \frac{q}{2\pi\varepsilon_0}\int_{0}^{1} P_n(\xi)\frac{\xi d\xi}{\sqrt{1-\xi^2}}$$

The identity [E-3]

$$\int_{-1}^{1} P_{2n+1}(x)\frac{xdx}{\sqrt{1-x^2}} = \frac{\Gamma\left(\frac{1}{2}+n\right)\Gamma\left(\frac{3}{2}+n\right)}{n!\,(n+1)!}$$

yields

$$A_n = -\frac{q}{4\pi\varepsilon_0}\frac{(n+1/2)}{jQ_n'(j0)}\frac{4}{n(n+1)}\left[\frac{\Gamma\left(1+\frac{n}{2}\right)}{\Gamma\left(\frac{n+1}{2}\right)}\right]^2$$

The values of the denominator Legendre functions are given by [E-2]

$$\frac{jQ_n'(j0)}{Q_n(j0)} = -2\left[\frac{\Gamma\left(1+\frac{n}{2}\right)}{\Gamma\left(\frac{n+1}{2}\right)}\right]^2$$

$$= -2\pi\left[\frac{\left(\frac{1}{2}\right)_{(n+1)/2}}{\left(\frac{n-1}{2}\right)!}\right]^2, \; n \text{ odd}$$

$$Q_n(j0) = \sqrt{\pi}\frac{\Gamma\left(\frac{1+n}{2}\right)}{j^{n+1}2\Gamma\left(1+\frac{n}{2}\right)}$$

$$jQ_n'(j0) = -j^{-1-n}\frac{\Gamma\left(1+\frac{n}{2}\right)}{\Gamma\left(\frac{n+1}{2}\right)}\sqrt{\pi}$$

Thus

$$A_n = \frac{q}{\pi\varepsilon_0}\frac{n+1/2}{n(n+1)}\frac{\Gamma\left(1+\frac{n}{2}\right)}{\Gamma\left(\frac{n+1}{2}\right)}\frac{j^{n+1}}{\sqrt{\pi}}$$

E.3 Potential in Aperture

The potential in the aperture is

$$\phi = \sum_{n,odd} A_n P_n(\xi) Q_n(j0)$$

where

$$A_n Q_n(j0) = \frac{q}{2\pi\varepsilon_0} \frac{(n+1/2)}{n(n+1)}$$

Using

$$\frac{2n+1}{n(n+1)} = \frac{1}{n} + \frac{1}{n+1}$$

we can write

$$A_n Q_n(j0) = \frac{q}{4\pi\varepsilon_0} \left[\frac{1}{n} + \frac{1}{n+1}\right]$$

Using the identities [E-1]

$$\sum_{n=1}^{\infty} \frac{1}{n} P_n(\cos\theta) = -\ln\left[\sin(\theta/2)\left\{\sin(\theta/2)+1\right\}\right]$$

$$\sum_{n=1}^{\infty} \frac{1}{n+1} P_n(\cos\theta) = \ln\left[1+\csc(\theta/2)\right]$$

we find

$$\sum_{n,odd} \frac{1}{n} P_n(\cos\theta) = -\frac{1}{2}\ln\left[\frac{\sin(\theta/2)\left\{\sin(\theta/2)+1\right\}}{\sin(\pi/2-\theta/2)\left\{\sin(\pi/2-\theta/2)+1\right\}}\right]$$

$$\sum_{n,odd} \frac{1}{n+1} P_n(\cos\theta) = \frac{1}{2}\ln\left[\frac{1+\csc(\theta/2)}{1+\csc(\pi/2-\theta/2)}\right]$$

Therefore we find

$$\sum_{n,odd} \left[\frac{1}{n} + \frac{1}{n+1}\right] P_n(\cos\theta) = \ln\left|\cot(\theta/2)\right| = \ln\left|\frac{1+\cos\theta}{\sin\theta}\right|$$

Using $\cos\theta = \xi$

$$\phi = \frac{q}{4\pi\varepsilon_0} \sum_{n,odd} \left[\frac{1}{n} + \frac{1}{n+1}\right] P_n(\xi) = \frac{q}{4\pi\varepsilon_0} \ln\left(\frac{1+\xi}{\sqrt{1-\xi^2}}\right)$$

or

$$\phi(\rho, \pm 0) = \frac{q}{4\pi\varepsilon_0} \ln\left(\frac{a \pm \sqrt{a^2 - \rho^2}}{\rho}\right)$$

where we have used $\xi = \pm\sqrt{1 - \rho^2/a^2}$. The actual potential in the aperture problem for $z = -0$ is the negative of this result $\phi \to -\phi$ and thus

$$\phi(\rho, 0) = \frac{q}{4\pi\varepsilon_0} \ln\left(\frac{a + \sqrt{a^2 - \rho^2}}{\rho}\right) \tag{E-1}$$

Note that as $\rho \to 0$ we have

$$\phi(\rho, 0) \sim \frac{q}{4\pi\varepsilon_0} \ln\left(\frac{2a}{\rho}\right)$$

E.4 Local Geometry at Wire End

Now we must consider how a finite potential is obtained as $\rho \to 0$ when more realistic local geometry is taken into account. The nonzero wire radius b could be taken into account, along with the geometry of the wire end (rounded or flat), or we can take into account the fact that the aperture has a dielectric window of some thickness Δ. Either approach involves evaluation of the potential a small distance from the end of the line charge. Using the above positive semi-infinite line charge potential representation, we can write in the vicinity of the line source end

$$\phi \sim \frac{q}{4\pi\varepsilon_0} \left[\operatorname{arcsinh}\left\{(R - z)/\rho\right\} + \operatorname{arcsinh}(z/\rho) + \text{constant}\right]$$

We take the constant to be $-2\ln R + \ln(2a)$ and thus write

$$\phi \sim \frac{q}{4\pi\varepsilon_0} \left[\ln\left(R - z + \sqrt{\rho^2 + (R - z)^2}\right) + \ln\left(z + \sqrt{\rho^2 + z^2}\right) - 2\ln\rho - 2\ln R + \ln(2a)\right]$$

$$\approx -\frac{q}{4\pi\varepsilon_0} \ln\left(\frac{\rho^2/(2a)}{z + \sqrt{\rho^2 + z^2}}\right) = -\frac{q}{4\pi\varepsilon_0} \ln\left(\frac{\sqrt{\rho^2 + z^2} - z}{2a}\right) \tag{E-2}$$

This potential now agrees with the preceding form in the aperture plane $z = 0$ as $\phi \approx q\ln(2a/\rho)/(4\pi\varepsilon_0)$. Alternatively for $\rho = 0$ we have $\phi \approx q\ln(-a/z)/(4\pi\varepsilon_0)$.

Thus for $\rho = b$ and $z = 0$

$$\phi_w \approx \frac{q}{4\pi\varepsilon_0} \ln(2a/b) \tag{E-3}$$

Suppose the average breakdown strength

$$E_b \approx 10 \text{ kV/cm} \tag{E-4}$$

for a rod-to-plane gap is used to set the charge level q (this is taken from Figure 1 for a spacing of 5 cm – a typical aperture radius); the charge is reduced when the field exceeds this level as a result of breakdown. The average field in the gap between the tip of the surface of the wire and the hole edge is

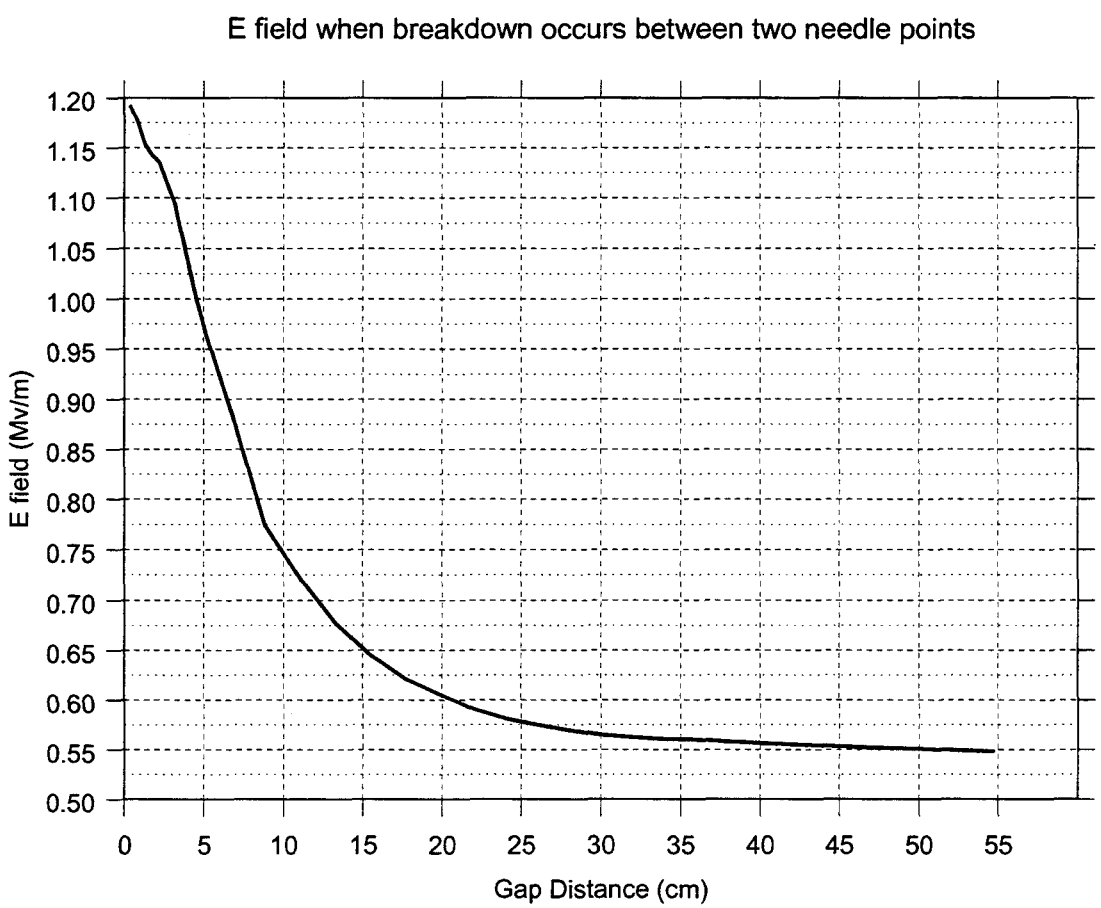

Figure 1. E field Required to Breakdown a Needle Point Gap

$$\langle E\rangle = \frac{1}{b-a}\int_b^a E_\rho(\rho,0)\,d\rho = \phi_w/(a-b) \approx \phi_w/a \approx \frac{q}{4\pi\varepsilon_0 a}\ln(2a/b)$$

since $\phi = 0$ on the conducting plane. If this is set to the average breakdown field

$$q \approx E_b \frac{4\pi\varepsilon_0 a}{\ln(2a/b)} \tag{E-5}$$

Let us now take $z = -\Delta$ and $\rho = 0$

$$\phi_0 \approx \frac{q}{4\pi\varepsilon_0}\ln(a/\Delta) \tag{E-6}$$

as the maximum voltage inside the enclosure. Note that these calculations have not included the effect of the dielectric layer with electric permittivity ε. The effect of this layer is to slightly increase the values of b and Δ. Because of the appearance in the logarithm we do not expect it to be a large effect.

E.5 Dipole Moment

The Legendre functions behave as

$$Q_n(j\zeta) \sim \frac{2n!}{\left(\frac{3}{2}\right)_n (2j\zeta)^{n+1}},\ \zeta \to \infty$$

Therefore the $n = 1$ term is dominant far from the aperture. Using

$$A_1 = -\frac{3q}{8\pi\varepsilon_0}$$

Thus the potential far from the aperture (here we have introduced the minus sign $\phi \to -\phi$ appropriate in the lower half space) is

$$\phi \sim -A_1 P_1(\xi)\,Q_1(j\zeta) = \frac{3q}{8\pi\varepsilon_0}\xi Q_1(j\zeta)$$

The Legendre function is

$$Q_1(j\zeta) = \zeta\,\mathrm{arccot}\,\zeta - 1$$

where $\pi/2 > \mathrm{arccot}\,\zeta > 0$ for $0 < \zeta < \infty$. Thus the $n = 1$ term is

$$\phi \sim \frac{3q}{8\pi\varepsilon_0}\xi(\zeta\,\mathrm{arccot}\,\zeta - 1) \tag{E-7}$$

Note that on the negative z axis (where a maximum magnitude of potential occurs) $\xi = -1$.

Expanding for large ζ

$$\phi \sim -\frac{q}{8\pi\varepsilon_0}\frac{\xi}{\zeta^2}$$

Now using $z = a\xi\zeta$ and $r \sim a\zeta$ as $\zeta \to \infty$ gives

$$\phi \sim -\frac{zqa^2/2}{4\pi\varepsilon_0 r^3} = \frac{\underline{p}\cdot\underline{r}}{4\pi\varepsilon_0 r^3}$$

where the dipole moment is

$$\underline{p} = -\frac{1}{2}qa^2\underline{e}_z \tag{E-8}$$

E.6 Potential at Various Locations

The potential values at various distances from the aperture plane are now discussed.

$$\phi = -\sum_{n,odd} A_n P_n(\xi)\, Q_n(j\zeta) \tag{E-9}$$

where again the minus sign has been introduced in the lower half space. Now on the negative z axis $\xi = -1$ and we let $\zeta = \zeta_0$

$$\phi = \sum_{n,odd} A_n Q_n(j\zeta_0)$$

$$A_n = \frac{q}{4\pi\varepsilon_0} 4 \frac{n+1/2}{n(n+1)} \frac{\left(\frac{1}{2}\right)_{(n+1)/2}}{\left(\frac{n-1}{2}\right)!} j^{n+1}$$

E.7 Fit Function

Note that as $\zeta_0 \to 0$ we expect with $z = -a\zeta_0$ that $(4\pi\varepsilon_0/q)\,\phi \sim -\ln\zeta_0$, $\zeta_0 \to 0$. The actual value approaches $(4\pi\varepsilon_0/q)\,\phi_0 \approx \ln(a/\Delta)$, $\zeta_0 = 0$. The large ζ_0 limit from the dipole moment is $(4\pi\varepsilon_0/q)\,\phi \sim 1/\left(2\zeta_0^2\right)$, $\zeta_0 \to \infty$. Thus as a fit function we try

$$(4\pi\varepsilon_0/q)\,\phi \approx \frac{1}{2}\ln\left(\frac{1+\zeta_0^2}{\zeta_0^2 + \Delta^2/a^2}\right) \tag{E-10}$$

Figure 2 shows a comparison of the series solution and the fit function.

E.8 References

[E-1] V. Mangulis, *Handbook of Series for Scientists and Engineers*, Academic Press, New York, 1965, pp.124, 125.

[E-2] M. Abramowitz and I. A. Stegun, *Handbook of Mathematical Functions*, Dover Pub., Inc., New York, pp. 258, 332-339, 808.

[E-3] I. S. Gradshteyn and I. M. Ryzhik, *Tables of Integrals, Series, and Products*, Academic Press, New York, p. 822

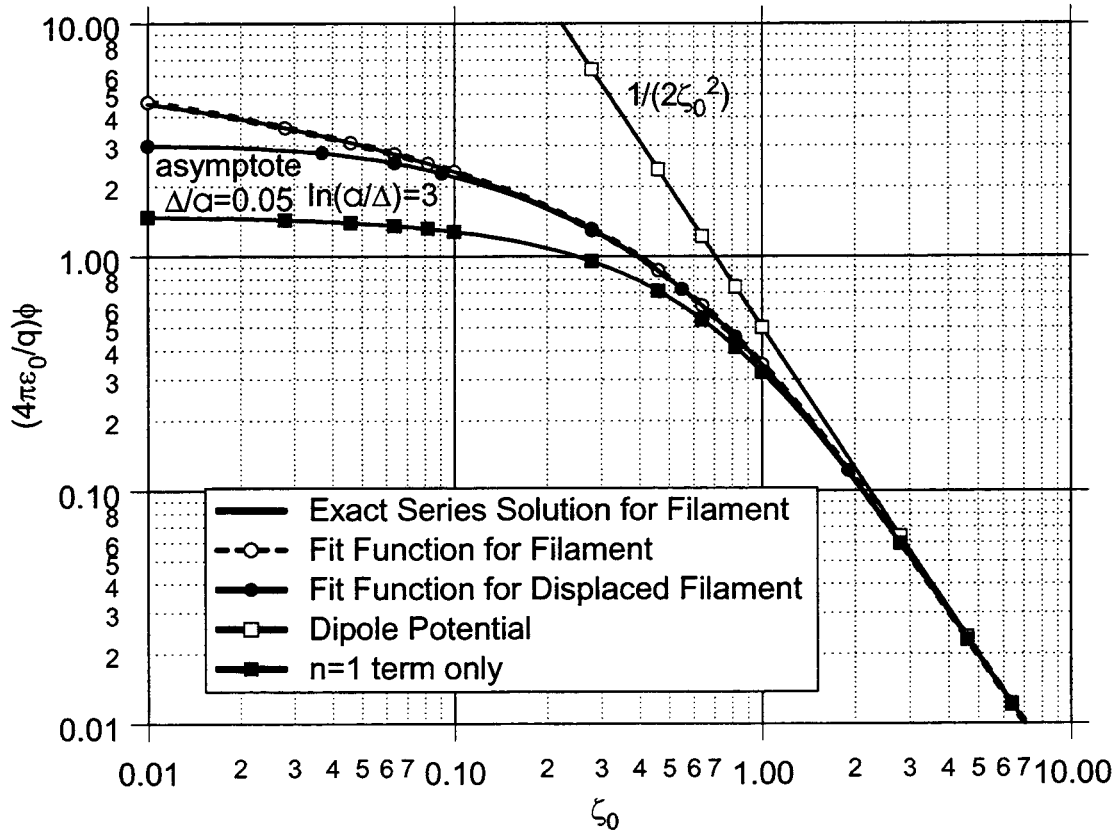

Figure 2. Plot of Various Potential Approximations When Wire Touches Aperture Center

Appendix F. Legendre Functions of Imaginary Argument

We use the expansion [F-1] to evaluate the Legendre function of imaginary argument

$$Q_n^m(j\zeta) = 2^{m+1}(-1)^m \frac{(m+n)!}{\left(\frac{3}{2}\right)_n} \left(\zeta^2+1\right)^{m/2} j^{-n-1} u^{-n-m-1} F\left(\frac{1}{2}+m, n+m+1; n+\frac{3}{2}; \frac{-1}{u^2}\right)$$

$$= 2^{m+1}(-1)^m \frac{(m+n)!}{\left(\frac{3}{2}\right)_n} \left(\zeta^2+1\right)^{m/2} j^{-n-1} u^{-n-m-1} \sum_{k=0}^{\infty} \frac{\left(\frac{1}{2}+m\right)_k (n+m+1)_k}{\left(n+\frac{3}{2}\right)_k k!} (-1)^k u^{-2k}$$

$$u = \zeta + \sqrt{\zeta^2+1}\,, \; 0 < \zeta < \infty$$

where $F(a, b; c; z)$ is the standard hypergeometric function.

F.1 References

[F-1] E. W. Hobson, *The Theory of Spherical and Ellipsoidal Harmonics*, Chelsea Pub. Co., New York, 1965, pp. 113-114.

Distribution:

20	MS1152	R. E. Jorgenson, 01642
20	MS1152	L. K. Warne, 01642
1	MS1152	M. L. Kiefer, 01642
1	MS1152	K. O. Merewether, 01642
1	MS0453	C. L. Knapp, 02820
1	MS0447	J. O. Harrison, 02111
1	MS0479	K. Oishi, 02113
1	MS0479	R. D. Holt, 02113
1	MS0479	M. H. Abt, 02113
1	MS0479	J. P. Atencio, 02113
1	MS1152	M. A. Dinallo, 01643
1	MS0405	T. R. Jones, 12333
1	MS0405	Y. T. Lin, 12333
1	MS0405	M. K. Fuentes, 12333
1	MS0405	T. D. Brown, 12333
1	MS0830	D. H. Loescher, 12335
1	MS0492	K. C. Chen, 12332
1	MS9018	Central Technical files, 8945-1
2	MS0899	Technical Library, 09616
2	MS0612	Review & Approval Desk, 09612 For DOE/OSTI

1 Jim Nunley
BWXT Pantex
P. O. Box 30020
Amarillo, TX 79120-0020